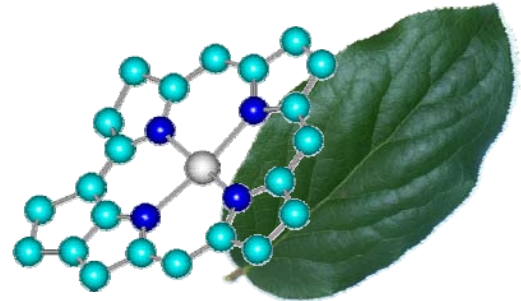
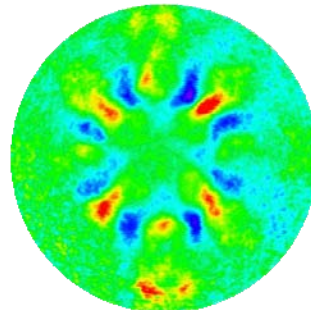
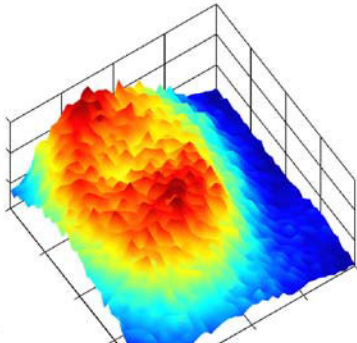
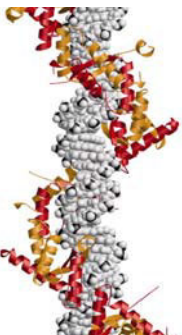


# RESEARCH WITH SYNCHROTRON RADIATION

2000–2005





Freie Universität



Berlin

# RESEARCH WITH SYNCHROTRON RADIATION

2000–2005

This volume summarizes progress and highlights of research with synchrotron radiation at the Freie Universität Berlin. Browsing through the volume shows that a multitude of research projects in physics, chemistry, and the life sciences have profited by the spatial proximity and special scientific ties to the Berlin synchrotron radiation facility BESSY. We thank the Bundesministerium für Bildung and Forschung (BMBF) and the Deutsche Forschungsgemeinschaft (DFG) for their support of the research with synchrotron radiation at the Freie Universität Berlin.

Exciting possibilities for novel research projects have been created by the inauguration of BESSY-II in Berlin-Adlershof. This state-of-the-art research facility enriches and strengthens Berlin as a prime location for excellent science. Due to the intense and efficient utilization of the BESSY, it is foreseeable that also in the future the scientists of the Freie Universität Berlin together with their international partners are going to be at the forefront of research with synchrotron radiation.

Research with synchrotron radiation is an interdisciplinary endeavor. I am looking forward to a continuation and extension. This volume on research with synchrotron radiation in the years 2000-2005 may serve as an encouragement for the upcoming years.

Univ.-Prof. Dr. Helmut Keupp  
Vizepräsident  
Freie Universität Berlin

---

Preface	7
<b>Atomic and Molecular Physics</b>	9
Introduction	11
Doubly excited states in helium: From electron correlation to quantum chaos ( <i>R. Püttner et al.</i> )	13
Probing molecular di-cations and highly excited cations with Auger spectroscopy ( <i>R. Püttner et al.</i> )	17
Chemical mimics for small molecule catalysis by proteins investigated by X-ray absorption spectroscopy ( <i>M. Haumann et al.</i> )	20
Reactions of halogens with surfaces stimulated by VUV light ( <i>V. Ney et al.</i> )	23
Electronic structure of two-dimensional adsorbate layers on transition metal surfaces using VUV and soft X-ray synchrotron radiation ( <i>K. Christmann</i> )	26
<b>Material Science</b>	29
Introduction	31
X-ray magneto-optics and electron structure of lanthanide materials ( <i>K. Starke et al.</i> )	33
Electronic structure of thin films ( <i>E. Weschke et al.</i> )	37
New concept to study magnetic behavior of early 3 <i>d</i> elements ( <i>A. Scherz et al.</i> )	40
Systematics of the induced magnetic moments in 5 <i>d</i> layers and the violation of Hund's third rule ( <i>F. Wilhelm et al.</i> )	43
Direct observation of orbital magnetism in cubic solids ( <i>W. D. Brewer et al.</i> )	45
Monolayer-resolved magnetic moment profile in Ni/Pt multilayers ( <i>F. Wilhelm et al.</i> )	47
Probing the antiferromagnetic spin structure of ultrathin FeMn films by photo- electron emission microscopy ( <i>W. Kuch et al.</i> )	49
Exploring magnetization reversal dynamics in magnetic multilayers with temporal, spatial and layer resolution ( <i>W. Kuch et al.</i> )	52
Magnetic structures and phase transitions in nanostructured materials ( <i>E. Weschke et al.</i> )	55

---

<b>Life Sciences</b>	59
Introduction	61
Digesting conjugated bile acids with the help of bacterial enzymes ( <i>M. Rossocha et al.</i> )	63
Structures of $\omega$ repressors bound to direct and inverted cognate DNA repeats reveal a unique mechanism to modulate transcription ( <i>W. A. Weihofen et al.</i> )	65
Structural studies of the human tethering complex TRAPP involved in vesicular transport ( <i>D. Kümmel et al.</i> )	68
Crystal structure of photosystem II at 3.0 Å resolution ( <i>B. Loll et al.</i> )	72
The oxygen we breathe – photosynthetic O <sub>2</sub> -production followed in X-ray absorption experiments ( <i>M. Haumann et al.</i> )	75
Hydrogen is the fuel: Catalysis at nickel–iron active sites of hydrogenases tracked by X-ray absorption spectroscopy ( <i>S. Löscher et al.</i> )	78
Enigmatic manganese volcanoes at the cell wall of a green alga: Microfocus X-ray spectroscopy relates microscopic and atomic-level structure ( <i>P. Liebisch et al.</i> )	82
Synchrotron radiation circular dichroism reveals structural changes in the photoreceptors phytochrome and photoactive yellow protein ( <i>B. Borucki et al.</i> )	85
 <b>Instrumentation</b>	 89
Introduction	91
VUV and soft X-ray beamline activities of the Freie Universität at BESSY II ( <i>R. Püttner et al.</i> )	93
The Russian–German beamline at BESSY II ( <i>S. L. Molodtsov et al.</i> )	97
Magnetic field pulse creation by synchronized laser pulses for magnetization dynamics studies of multilayered systems ( <i>J. Miguel et al.</i> )	101
X-ray spectroscopy to study catalytic metal centers: A new BioXAS experiment at BESSY beamline KMC-1 ( <i>P. Loja et al.</i> )	104
 Publications	 107
Theses	120

---

---

## Preface

Synchrotron radiation is an invaluable tool for studying physical, chemical and biological problems at the atomic level. Researchers at the Freie Universität Berlin realized early the scientific potential of synchrotron radiation. They promoted and actively contributed to the development of the Berliner Elektronenspeicherring (BESSY), which now is a state-of-the-art facility and a particularly valuable asset of Berlin's research infrastructure.

There is a specific framework of research with synchrotron radiation. More than in other areas, development of and investments in infrastructure and instrumentation is required. The magnitude of the needed resources requires a cooperative effort of a larger circle of research groups. Typically state-of-the-art instrumentation is developed in a joint initiative of several research groups and then used for cutting-edge research by an even larger community. International cooperation plays a prominent role. More than in any other Berlin university, researchers at the Freie Universität are active in both areas, development of novel experimental technology as well as cutting-edge research using synchrotron radiation, as demonstrated by the following collection of articles.

This volume provides an overview of the research with synchrotron radiation at the Freie Universität. In 26 research and review articles, the numerous facets of synchrotron radiation research and its increasing importance, especially in the life and material sciences, are highlighted. The listed publications (more than 200) show the level of international recognition. The 27 PhD theses and four Habilitations illustrate the role in the education, training and promotion of young scientists.

Already in 1984, research groups at the Freie Universität that are actively involved in the synchrotron radiation research successfully started to coordinate their activities. In 1985, the FK (Forschungskommission) of the Freien Universität selected research with synchrotron radiation as a 'Forschungsschwerpunkt' of strategic importance. At different levels and with changes in focus, since 1985 the FK has provided financial support to motivate and strengthen these coordinated research activities. The financial support was accompanied by the hiring of internationally recognized principal investigators that are active in synchrotron radiation research. Thereby the Freie Universität has strengthened further its role in research with synchrotron radiation and the ongoing development of the BESSY.

The importance of synchrotron radiation research for the progress in life and material sciences is increasingly recognized. Nonetheless, the financial resources allocated by the Bundesministerium für Bildung und Forschung (BMBF) for research with synchrotron radiation at German universities has not kept up with the increasing demand. Increasingly fierce competition for dwindling financial resources in conjunction with changes in the funding policies of the BMBF (in the program "Erforschung kondensierter Materie") also have affected researchers at the Freie Universität severely. However, our efforts to compensate for the diminished support by the BMBF by acquisition of grants from other agencies (mostly Deutsche Forschungsgemeinschaft, but also other BMBF programs) had

---

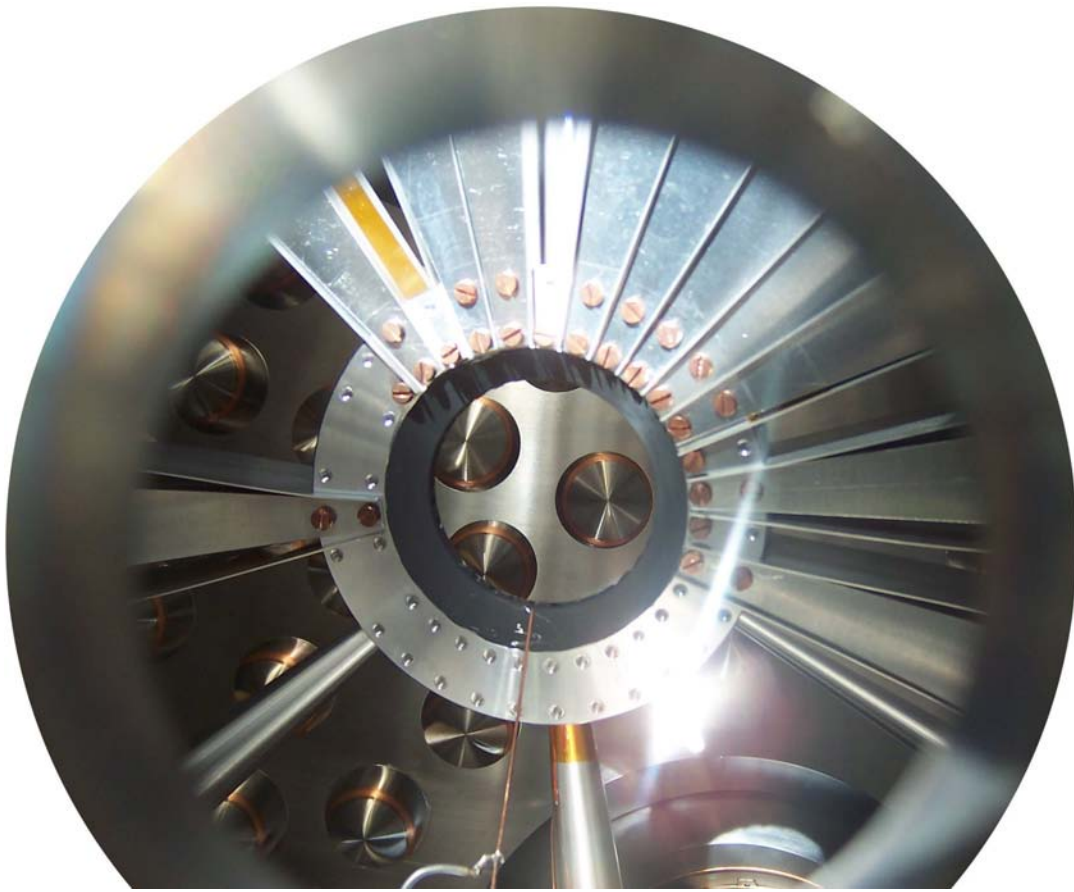
been largely successful. Not only the excellence and perseverance of researchers at the Freie Universität, but also the continued support by the university has played a role. This support has facilitated the proof-of-concept experiments needed for new research or instrumentation initiatives, and it provided the financial resources for the repairs and replacements that are essential for running a state-of-the-art synchrotron experiments. We explicitly thank the Freie Universität Berlin for this special support.

In research with synchrotron radiation, the mere scale of the used scientific instruments requires extensive considerations on research strategies and the allocation of financial resources. However, financial resources only provide the means for exciting science in research fields that will shape the future of our society. We hope that the following collection of articles, which summarize outstanding scientific results and technical progress of the years 2000 to 2005, may provide some enjoyable insights in the broad scope and possibilities of synchrotron-radiation research as well as in the scientific progress recently made at the Freie Universität Berlin.

Prof. Dr. Holger Dau  
*Coordinator  
BESSY user group  
of the FU Berlin*

Prof. Dr. Wolfgang Kuch

Dr. Ralph Püttner



# **Atomic and Molecular Physics**



Previous page: Interior view of the chamber used for measuring the partial cross sections of helium in the region of the doubly excited states. Twelve electron spectrometers on the basis of a time-of-flight technique are mounted around a central ring. The copper needle in the lower part of the picture is the gas inlet, and the propagation direction of synchrotron light is out of the paper plane.

## Atomic and Molecular Physics

Atoms and simple molecules are the building blocks of compound systems over a wide range of complexity from small clusters over solids to living cells. Based on these considerations, studies of single atoms and molecules are of fundamental interest for two different reasons. First, single atoms and molecules consist of only a relatively small number of particles, namely nuclei and electrons. They are, therefore, well suited to serve as model systems for studying complex fundamental properties, like e.g. electron correlation. Second, a wide range of properties of more complex compound systems, like solids, can often readily be derived starting from the properties of single atoms or simple molecules.

However, the properties of isolated atoms and molecules allow to describe only the static properties of larger systems like the electronic structure of solids that determines e.g. the conductivity of a solid. In order to describe a dynamic world including a goal-oriented modification of surfaces or the living world, we need to understand the different aspects of interactions between the building blocks like e.g. surface adsorption or chemical reactions.

Some topics within this broad field of atomic and molecular physics are studied at the Freie Universität Berlin using synchrotron radiation. Fundamental research on electron correlation and quantum chaos has been performed by Püttner *et al.* by studying the doubly excited states in helium, which is the simplest atom that exhibits both of these properties. An Auger process initiated by synchrotron radiation was used in the second contribution by Püttner *et al.* to produce and study stable molecular di-cations. Molecular di-cations are a class of molecules that play an important role in ionized gases like in a plasma or in the ionosphere, but they are difficult to produce and study.

The contribution of Haumann *et al.* deals with the field of life science. These authors applied X-ray absorption spectroscopy on organometallic model complexes in order to elucidate the chemistry of oxygenic photosynthesis and biological hydrogen production.

Two research projects focus on the interaction of atoms and molecules with surfaces. Ney *et al.* studied the light-induced surface reaction between halogens and materials that are relevant in structuring semiconductor devices. In order to shine light on the chemical-analytical processes, the research group of Christmann studied the electronic structure of adsorbate layers on transition metal surfaces.



## Doubly excited states in helium: From electron correlation to quantum chaos

R. Püttner,<sup>1</sup> Y.H. Jiang,<sup>1</sup> R. Hentges,<sup>2</sup> J. Viefhaus,<sup>2</sup> M. Martins,<sup>3</sup>  
J.-M. Rost,<sup>4</sup> D. Delande,<sup>5</sup> U. Becker,<sup>2</sup> and G. Kaindl<sup>1</sup>

<sup>1</sup>*Institut für Experimentalphysik, Freie Universität Berlin, Berlin, Germany*

<sup>2</sup>*Fritz-Haber-Institut Berlin, Berlin, Germany*

<sup>3</sup>*Institut für Experimentalphysik, Universität Hamburg, Hamburg, Germany*

<sup>4</sup>*Max-Planck-Institut für Physik Komplexer Systeme, Dresden, Germany*

<sup>5</sup>*Laboratoire Kastler-Brossel, Université Pierre et Marie Curie, Paris, France*

One very successful approximation for understanding the electronic structure of atoms, molecules, and solids is the independent-electron picture. In this approximation the movement of an electron is assumed to occur in the mean potential created by the nuclei and all other electrons. One consequence of this picture is that only one electron can be excited by one photon; this allows to understand the most intense lines in the spectra of electronic excitations. The direct electron-electron interaction, which is also known as electron correlation, is, however, neglected in this picture and, as a consequence, a number of interesting phenomena cannot be explained. One of these phenomena is the excitation of two or more electrons with one photon, which will be discussed for helium in the present article. Other important phenomena based on the electron correlation are high- $T_c$  superconductivity and the colossal magnetoresistance, with the potential of applications in sensors detecting magnetic fields. These phenomena result in an increased interest in advanced theoretical descriptions of electron-correlation effects.

The helium atom consists of one nucleus and two electrons and is – due to the mutual interaction of all three particles – the simplest atom that exhibits electron-electron interaction. From a more fundamental point of view, it is a three-body system that is

comparable in some respects to the well-known three-body system sun-earth-moon. Since the work of Poincaré a century ago it is well-known that a classical three-body system cannot be solved analytically (it is nonintegrable) and that the dynamics involve a mixture of regularity (as e.g. in the stable system sun-earth-moon) and chaos.

Under normal conditions, tiny objects like atoms have to be described using quantum mechanics. In the process of excitation, however, electrons are promoted into higher orbits resulting in larger sizes of the atoms. The size of an atom can be tailored by continuously varying the energy of the photons used for the excitation process. According to the correspondence principle, with increasing size an atom becomes more and more comparable to a classical object. Therefore, close to the double ionization threshold (which is equivalent to an infinite large size of the atom) the quantum mechanical solution of the helium atom is expected to be strongly influenced by the chaotic dynamics of its classical counterpart. This phenomenon is called quantum chaos.

There is, however, a fundamental difference between classical chaotic dynamics and quantum mechanics: while classical chaotic dynamics has to be described by *nonlinear* equations of motion, the fundamental equation for quantum mechanics – the Schrödinger equation – is

*linear* in time. This fundamental difference rises the question how classical mechanics and quantum mechanics can be reconciled? What are the manifestations of the underlying classical chaos in the quantum spectrum of helium?

Since the interaction of the two electrons is the origin of chaos in the helium atom, quantum chaos can be considered as a consequence of electron correlation. Doubly excited states in helium are particularly well suited to find new descriptions for electron correlation and to study quantum chaos. In this context one can change the main focus of the studies from electron correlation to quantum chaos by increasing the photon energy. Therefore, doubly excited states in helium have been extensively studied by a number of groups since their first observation by Madden and Codling in 1963 [1].

Due to the strong electron correlation in helium, the doubly excited states cannot be assigned using the independent-electron picture. Instead, they have to be assigned using the classification scheme  $N, K_m$ , with  $N$  ( $m$ ) being the quantum number of the inner (outer) electron and  $K$  the angular correlation quantum number that reflects the angle between the two electrons. These excited states decay to  $\text{He}^+(n)$  ions by emitting an electron; here  $n$  describes the principal quantum number of the electron in the helium ion, and the different values of the quantum number  $n$  can be distinguished by the kinetic energies of the emitted electrons.

In the following, two kinds of experiments, which were performed at BESSY II, will be described. In the first experiment we measure the partial cross section (PCS), i.e. we study the decay of doubly excited states  $N, K_m$  to the different final states  $\text{He}^+(n)$  by measuring the kinetic energies of the emitted electrons. These experiments were performed at lower photon

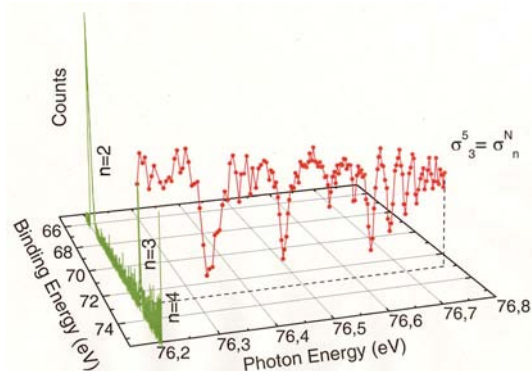


**Fig. 1:** Photoelectron (PE) spectrum taken at  $h\nu=76.2$  eV in green. The PCS to the final state  $\text{He}^+(n=3)$  derived from these PE spectra is given in red.

energies and they aim to confirm experimentally a graphical model for electron correlation that is based on a molecular description [2]. Fig. 1 shows in green a photoelectron (PE) spectrum taken at  $h\nu=76.2$  eV, i.e. in the region of the states with  $N = 5$ . The different peaks labeled by  $n = 2$  to  $4$  indicate the final states in the helium ion subsequent to photoemission. By taking such PE spectra each 3 meV and plotting the integral intensities of the PE peaks, the PCSs are obtained. The PCS leading to the final state  $\text{He}^+(n=3)$  is given in red as an example. Since for a doubly excited state  $N, K_m$  the

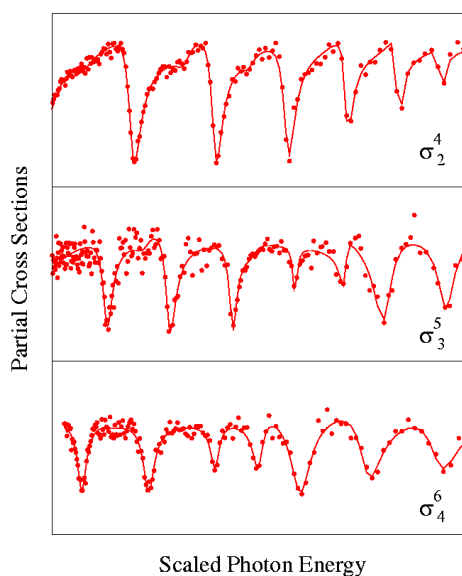


**Fig. 2:** Partial cross sections  $\sigma_n^N$  with  $\Delta N = 2$ .

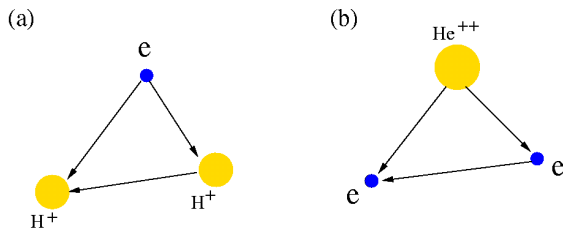


**Fig. 3:** (a) The molecular ion  $H_2^+$  and (b) the helium atom. Figure (b) is obtained from (a) by exchanging the electrons by nuclei and vice versa.

quantum number  $n$  for the electron in  $He^+$  can be  $n = 1, 2, \dots, N-1$  a large number of spectra can be obtained. As can be seen in Fig. 2 for the case of  $\Delta N = N - n = 2$ , there are similarities in the PCSs if  $N$  and  $n$  differ by the same value. These results demonstrate the capability of the graphical model for electron correlation [2, 3], which describes the helium atom in a molecular picture, similar to the molecular ion  $H_2^+$ , by exchanging the functions of the electrons and the nuclei (Fig. 3).

In the second kind of experiments, we measured the total cross section (TCS) of helium, i.e. we did not distinguish between the different final states  $He^+(n)$ . This technique provides higher count rates and is better suited to measure the parts of the spectra with small cross sections. Fig. 4 shows the experimental and theoretical TCS of doubly excited states in helium, with the inner electron being in the states  $N = 9$  to 14. It can be seen that the variations in the cross section decrease with increasing photon energy so that for this energy region, which is higher than for the PCS measurements, the TCS is measured instead of the PCS. The presented energy region is very close to the double ionization threshold and, therefore, signatures of quantum chaos are expected to appear.

One way to study quantum chaos is the analysis of the statistical distribution  $P(s)$  of energy spacings,  $s$ , between neighboring resonances. In the presented analysis, a step

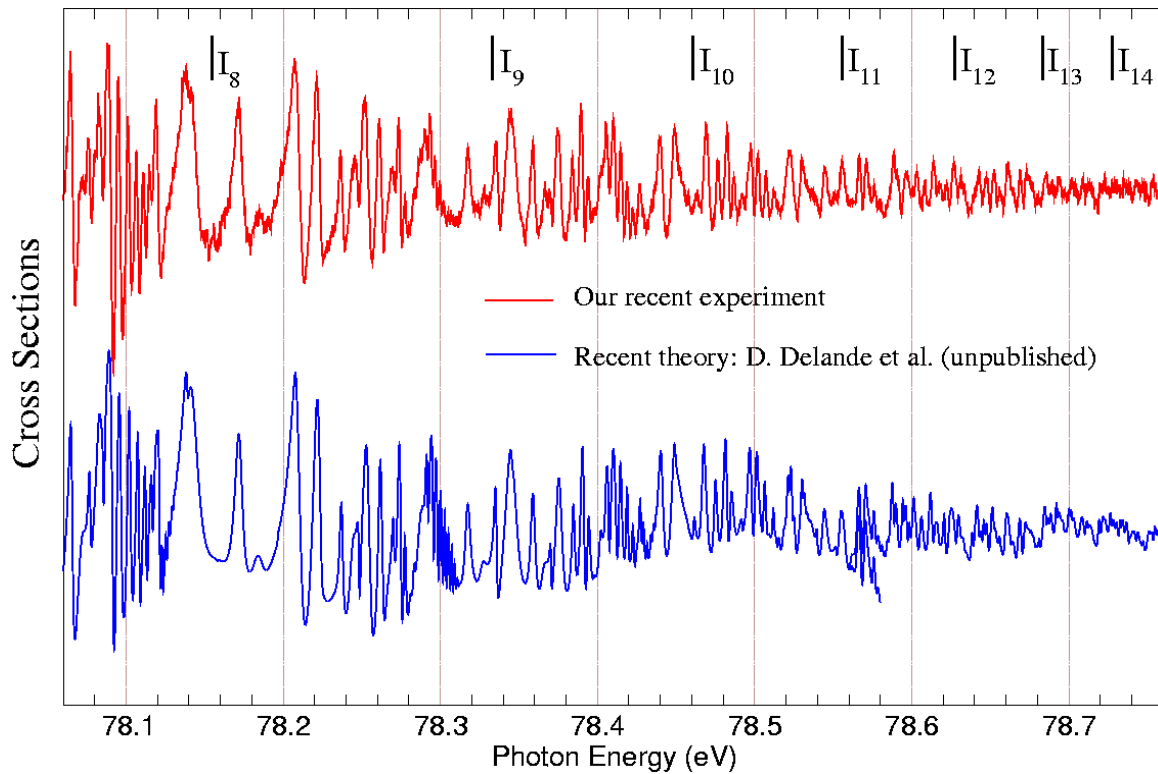


**Fig. 4:** The experimental (red) and theoretical (blue) TCS of helium in the region of the states with  $N = 9$  to 14.

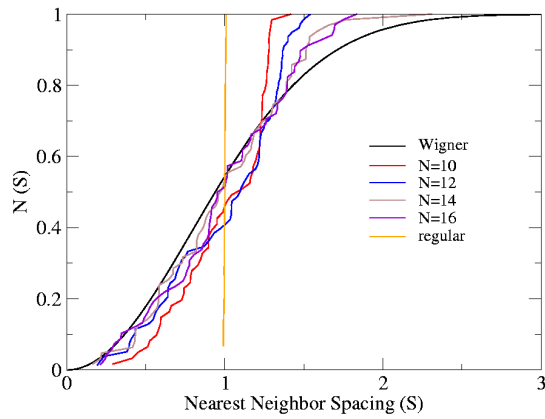


**Fig. 5:** The expectations of  $N(s)$  for a regular (orange) and chaotic (black) system together with the results of a statistical analysis for states with  $N = 10, 12, 14,$  and  $16$ .

function and a Wigner distribution for the cumulative distribution  $N(s) = \int_0^s P(s') ds'$  are expected for a regular and a chaotic system, respectively. As can be seen in Fig.

5, with increasing quantum number  $N$  of the inner electron, the statistical distribution based on the theoretical data matches more and more a Wigner distribution. This observation of the onset of chaotic dynamics in a simple three-body system shows for the first time how the underlying classical chaos manifests itself in a simple and well-studied quantum system [4].

## References

- [1] R. P. Madden and K. Codling, *Phys. Rev. Lett.* **10**, 516 (1963).
- [2] J. M. Feagin and J. S. Briggs, *Phys. Rev. Lett.* **57**, 984 (1986).
- [3] T. Schneider *et al.*, *Phys. Rev. A* **65**, 042715 (2002).
- [4] R. Püttner *et al.*, *Phys. Rev. Lett.* **86**, 3747 (2001).

## Probing molecular di-cations and highly excited cations with Auger spectroscopy

R. Püttner,<sup>1</sup> M. Poiguine,<sup>1</sup> Y. F. Hu,<sup>2</sup> M. Bancroft,<sup>3</sup> A. Kivimäki,<sup>4</sup>  
Y. H. Jiang,<sup>1</sup> G. Kaindl,<sup>1</sup> H. Aksela,<sup>4</sup> and S. Aksela<sup>4</sup>

<sup>1</sup>*Institut für Experimentalphysik, Freie Universität Berlin, Berlin, Germany*

<sup>2</sup>*Canadian Light Source, University of Saskatoon, Saskatoon, SK, Canada*

<sup>3</sup>*Department of Chemistry, The University of Western Ontario, London, ON, Canada*

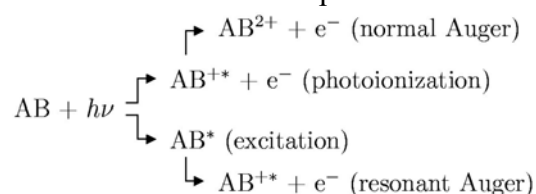
<sup>4</sup>*University of Oulu, Department of Physical Sciences, Oulu, Finland*

Removing two electrons from the valence shell of a molecule leads normally to a considerable weakening of the chemical bonds so that the Coulomb repulsion of the nuclei can no longer be compensated resulting in a dissociation of the molecule. In special case, however, namely when both electrons are removed from non-bonding orbitals, the resulting molecular di-cations  $AB^{++}$  are still stable or quasi-stable with respect to dissociation. These molecular di-cations play an important role in plasma physics and chemistry. The plasma state is abundant in nature (more than 99% of the observable universe is in the state of plasma) and is often occurring in commercial manufacturing processes. In addition, molecular di-cations occur in the ionosphere and in interstellar clouds, and they are also proposed as candidates for excimer lasers. Despite their importance, little is known about their electronic and geometrical structure. What are the reasons for this lack of knowledge?

One possibility to obtain information on the electronic and geometrical structure is to perform experiments directly with these molecular di-cations. Such experiments, however, are limited by the very low target densities that can be achieved under laboratory conditions. A second approach that has been widely used in recent years is provided by double ionization with one photon if both electrons are detected with a

coincidence technique [1]; this requires a sophisticated experimental setup. In addition, double ionization with one photon can only be explained on the basis of electron correlation. Due to this, the electronic matrix element of the transition is not constant requiring a complicated data analysis.

In our approach, we utilize the fact that these molecular di-cations as well as highly excited molecular cations can be created by photoionization or photoexcitation, respectively, of a shallow core level, with subsequent Auger decay. These processes can be described in two steps:



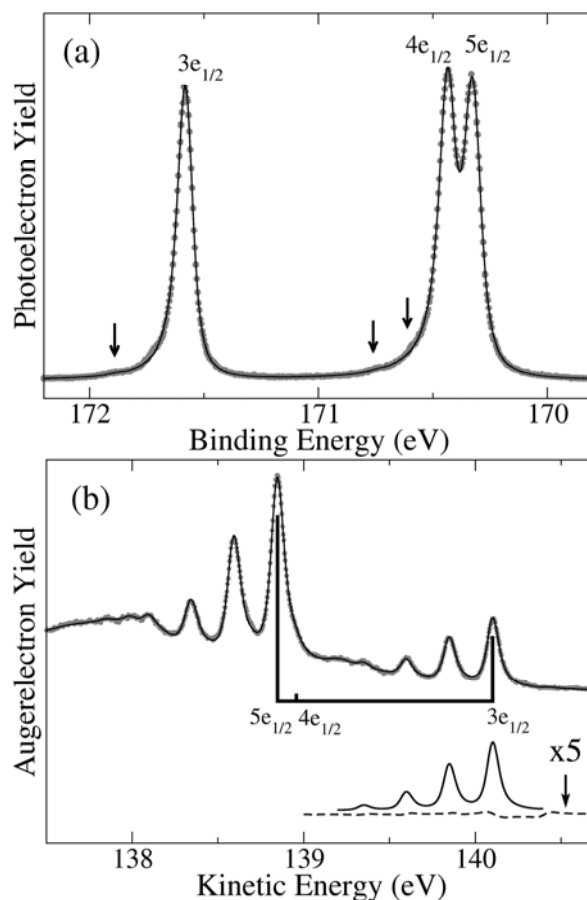
In this way, high count rates can be obtained with standard techniques, and the electronic matrix element can be considered constant. This allows one to perform a Franck-Condon analysis that provides detailed information on the equilibrium geometry of the states involved in this process. While this type of data analysis is quite simple, the photoionization and the Auger process lead, however, to further complications, which will be explained using the molecule  $H_2S$  as an example.

Fig. 1(a) displays the S  $2p$  photoelectron spectrum of  $H_2S$ . The threefold splitting of the main line is due to spin-orbit and ligand-field splitting. In addition, weak

contributions due to vibrational excitations of the symmetric stretching mode are marked by vertical arrows. Fig. 1(b) shows the spectrum resulting from normal Auger decay to the  $2b_1^{-2}$  final state. The vertical bar diagram indicates that spin-orbit and ligand-field splitting are also present in the Auger spectrum. In the  $2b_1^{-2}$  final state, both electrons are removed from a non-bonding valence orbital that is oriented perpendicular to the molecular plane. As a result, the molecular di-cation  $\text{H}_2\text{S}^{2+}$  is stable with respect to dissociation, and the Auger spectrum exhibits a vibrational progression as indicated by the solid subspectrum of Fig. 1(b).

Fig. 1(a) reveals that the linewidths of the various S  $2p$  levels are comparable to the splitting between the levels so that the lines overlap. This holds in particular for the main lines  $4e_{1/2}$  and  $5e_{1/2}$ , but also for all main lines and their vibrational satellites marked by the vertical arrows. Due to the energy overlap of the various states in the S  $2p$  spectrum, it is not exactly known in which way, i.e. through which core-hole state, the final state  $2b_1^{-2}$  is reached in the process. This situation is comparable to a double-slit experiment with an electron or a photon resulting in similar consequences: The lack of knowledge about the way leads to contributions from interference. Such contributions from interference between the level  $3e_{1/2}$  and its vibrational satellites at 171.9 eV, marked by a vertical arrow can be described analytically, and are given by the dashed subspectrum close to the solid subspectrum. The spin-orbit and ligand-field splitting of the S  $2p$  levels in combination with the excitation of vibrational substates and interference contributions render the data analysis more tedious, but all the above mentioned contributions can be handled on the basis of simple approaches within the Born-Oppenheimer approximation. By

subjecting the vibrational progressions to a Franck-Condon analysis, we derived for the first time the equilibrium geometry of the state  $2b_1^{-2}$  in the molecular di-cation  $\text{H}_2\text{S}^{2+}$ ; this state has an H-S bond distance of 1.424 Å and an H-S-H bond angle of 91.9°. Similar analyses have been performed for di-cationic HBr [2] and HCl [3] resulting in a remarkable agreement with advanced theoretical results.



**Fig. 1:** (a) Photoelectron spectrum of  $\text{H}_2\text{S}$  at the S  $2p$  ionization threshold. (b) S  $2p^{-1} \rightarrow 2b_1^{-2}$  Auger spectrum including vibrational fine structure.

In the case of HBr, the results from normal Auger decay were used to understand the resonant Auger spectra. These spectra allow to probe highly excited ionic states. Fig. 2 displays - as an example - the resonant Auger spectrum of the excitation of an electron from a Br  $3d$  core level into an  $8p\pi$  Rydberg orbital. As can be seen in Fig. 3, this orbital is mainly oriented perpendicular to the molecular axis. The spectrum shows

transitions with comparable intensity to approximately 60 different final states, as can be seen by the vertical-bar diagrams in the lower part of Fig. 2. This large number of transitions is in contradiction to previous expectations based on observations made with atoms and other molecules, where a much smaller number of transitions was found. This small number of transitions is due to so-called monopole transitions, i.e. symmetry-conserving shake processes. These shake processes describe transitions caused by reorganization of the electron density and the orbitals subsequent to the emission of the second electron, namely the Auger electron. Since the ejection of the Auger electron leads mainly to an increase of the charge at the center of the atom or molecule, this reorganization influences mainly the radial direction, which explains the symmetry-conserving character of the process. As a consequence, for the given example of a  $3d \rightarrow \delta p\pi$  excitation, the Auger process should lead to  $np\pi$  orbitals for the excited electron. The present experimental finding, with a larger number of final states, strongly violates this concept of monopole transitions; it can only be explained with final states other than  $np\pi$ , which requires an orientation of the orbital other than perpendicular to the molecular axis (see Fig. 3(b)).

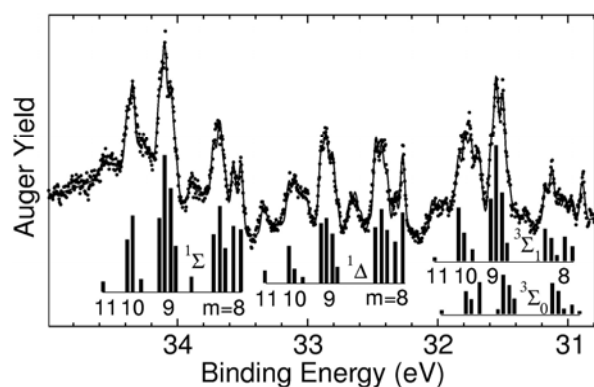


**Fig. 2:** The resonant Auger spectrum of the  $3d \rightarrow \delta p\pi$  excitation in HBr.

The existence of such additional final states can be explained in a semiclassical way by an interaction between the Auger electron and the Rydberg electron. As can be seen in Fig. 3(a), the average angle  $\langle \alpha \rangle$  between the direction of the outgoing Auger electron and the molecular axis amounts to  $57.3^\circ$ , i.e. the trajectory of the Auger electron comes close to the excited Rydberg electron in Fig. 3(a). For HBr, the kinetic energy of the Auger electron is much smaller than those of all other molecules studied up to now, so that the interaction time is larger. This results in a strong Coulomb repulsion between the two electrons so that the Rydberg electron is transferred to an orbital different from  $np\pi$  as can be seen in Fig. 3(b).

This process is expected to have considerable influence on the resonant Auger transitions if the Auger electron has low kinetic energy.

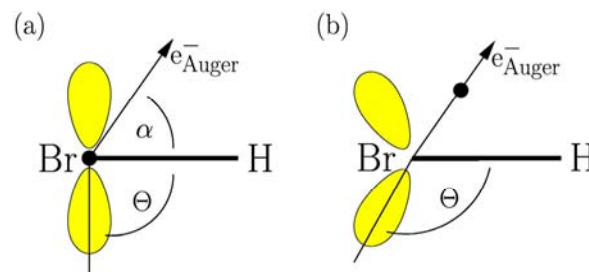


**Fig. 3:** Schematic picture of (a) the  $\delta p\pi$  orbital and (b) the Rydberg orbital upon Coulomb interaction with the Auger electron. The averaged direction of the Auger electron is also indicated.

## References

- [1] J. H. D. Eland, Chem. Phys. **204**, 171 (2004).
- [2] R. Püttner, Y. F. Hu, G. M. Bancroft, H. Aksela, E. Nömmiste, J. Karvonen, A. Kivimäki, and S. Aksela, Phys. Rev. A **59**, 4438 (1999).
- [3] R. Püttner, V. Pennanen, T. Matila, A. Kivimäki, M. Jurvansuu, H. Aksela, and S. Aksela, Phys. Rev. A **65**, 042505 (2002).

## Chemical mimics for small-molecule catalysis by proteins investigated by X-ray absorption spectroscopy

M. Haumann<sup>1</sup>, P. Liebisch<sup>1</sup>, M. Barra<sup>1</sup>, P. Loja<sup>1</sup>, S. Löscher<sup>1</sup>, O. Kirilenko<sup>1</sup>, M. Mertin<sup>2</sup>,  
F. Schäfers<sup>2</sup>, A. Magnusson<sup>3</sup>, M. Anderlund<sup>3</sup>, S. Ott<sup>3</sup>, and H. Dau<sup>1</sup>

<sup>1</sup>Freie Universität Berlin, Institut für Experimentalphysik

<sup>2</sup>BESSY GmbH, Berlin

<sup>3</sup>Uppsala University, Molecular Biomimetics, Uppsala, Sweden  
and Swedish Consortium of Artificial Photosynthesis

To understand the mechanism of small molecule catalysis (e.g. the conversion of O<sub>2</sub>, H<sub>2</sub>, H<sub>2</sub>O) by biological proteins, is one of the major challenges in life sciences. Particularly promising for biotechnological applications is the design of artificial molecules that mimic catalytic features of the biological templates (Fig. 1). Advanced approaches towards the characterization of such compounds are pursued in collaborative studies of our workgroup with investigators from Sweden.

In the center of interest are investigations on molecules containing transition metal atoms, generated by synthetic chemistry, that have been designed as mimics of photosynthetic water oxidation / oxygen production, i.e. mimics of the manganese-calcium complex of photosystem II, and of hydrogen conversion, i.e. mimics of the bimetallic sites of hydrogenases. The goal is to understand the restraints that govern the kinetics and energetics (that is the rates and routes) of the natural chemistry.

### Two biological systems connected by one vision

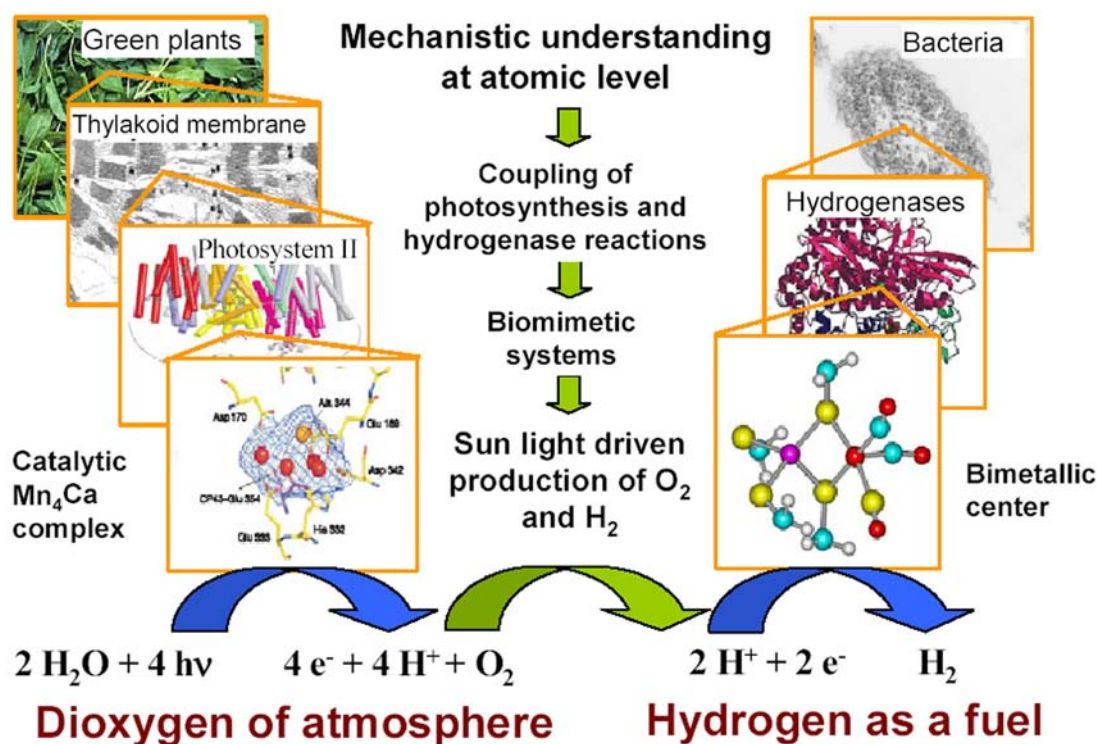


Fig. 1: Vision of the future coupling of two natural reactions to generate energy.

X-ray absorption spectroscopy (XAS) to analyze structural and oxidation state changes at the metal sites has evolved to a particularly powerful tool to unravel the catalytic mechanism.

XAS on various sets of synthetic molecules was performed at the beamline KMC-1 of the BESSY in Berlin. During several measuring periods the equipment and experimental setup of our group (e.g. energy-resolving large-area single-element germanium detector for X-ray fluorescence analysis, multichannel-analyzer, liquid-helium cryostat for XAS measurements at 10 K) was optimized to allow for high-quality EXAFS experiments on biological proteins and synthetic model compounds at beamline KMC-1.

### (1) Binuclear manganese compounds

A set of binuclear Mn-compounds, which mimic certain aspects of the  $Mn_4Ca$  complex of photosystem II, with variations in the O/N ratio of the Mn ligands (Fig. 2) was investigated by XAS in several oxidation states [1]. The goal was to gain information on the role of the metal ligation and of changes in the metal coordination, e.g. loss or formation of carboxylato and  $\mu$ -oxo

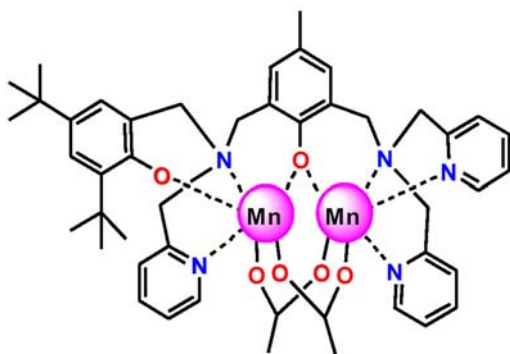


**Fig. 2:** Synthetic model compound that mimics certain aspects of the manganese complex of photosynthesis. Note the asymmetric coordination environment of the two Mn atoms.

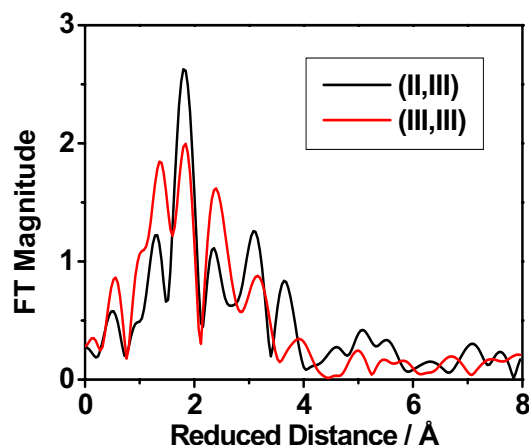


**Fig. 3:** Fourier-transforms of EXAFS spectra of the model in Fig. 2 in two oxidation states. Changes in the magnitude and position of the Fourier-peaks reveal changes in the coordination environment of the Mn atoms upon oxidation.

bridges, in compensation of charges as created during metal oxidation.

Analysis of XAS spectra (Fig. 3) suggested that changes in the bridging type between the two Mn atoms are crucial for maintaining a moderate and about constant redox potential for the next oxidation step. Similar bridging type changes may facilitate the stepwise oxidation of the manganese complex of photosynthesis during its catalytic cycle of water oxidation [1-3].

### (2) Fe-Fe models of hydrogenases

Hydrogenases containing an active site with two iron atoms are highly effective in hydrogen conversion. The design of model compounds for these enzymes may open the road towards biomimetic  $H_2$  production. One difficulty is the high sensitivity of hydrogenases to inhibition by dioxygen.

A synthetic compound was created [4] which closely resembles the active site of Fe-Fe hydrogenases and which can be prepared in four different states. In some states hydrogen may be bound between the iron atoms (Fig. 4). All states were investigated by EXAFS analysis.

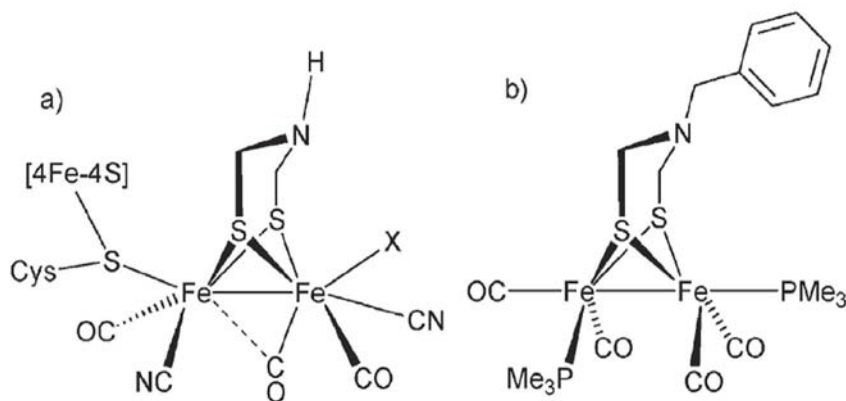


**Fig. 4:** Comparison of the active site of a Fe-Fe hydrogenase (a) with a synthetic model compound [4] (b). Note the close similarity between the key structural features of the bimetallic centers.

The results reveal changes in the distances between the iron atoms upon protonation of the nitrogen and, more pronounced, upon binding of hydrogen to the Fe atoms.

One hypothesis is that protonation and concomitant structural changes allow for efficient hydrogen binding to the metal atoms of the model. A similar mechanism may apply for the native enzymes.

*Outlook:* The “evolutionary” design of artificial compounds is inspired by the wealth of information from analysis of the natural enzymes by modern spectroscopic techniques, such as X-ray absorption spectroscopy, and also by attempts for their functional coupling *in vivo* (see Fig. 5) [5]. These investigations may pave the road towards the employment of photosynthetic water oxidation and hydrogen generation for fuel production in biomimetic and biotechnological applications.

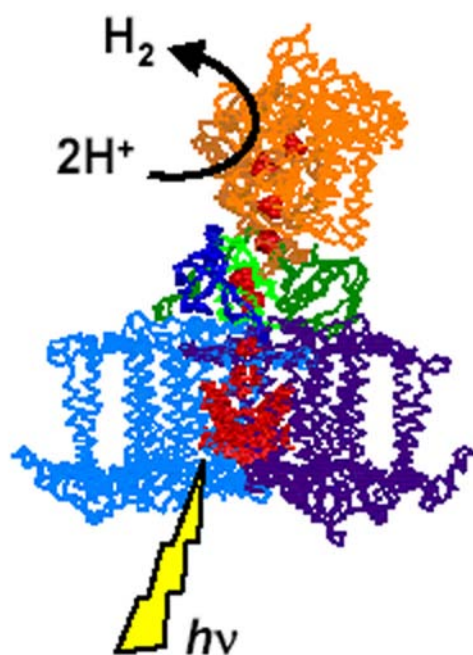


**Fig. 5:** A “hybrid” enzyme obtained by coupling of photosystem I from a cyano-bacterium and a hydrogenase from the bacterium *Ralstonia eutropha* [5]. Upon excitation of the photosystem by visible light, this hybrid is able to generate electron flow from artificial donors to the hydrogenase part where protons are reduced to molecular hydrogen.

## References

- [1] A. Magnuson, P. Liebisch, J. Höglblom, M. Anderlund, R. Lomoth, W. Meyer-Klaucke, M. Haumann, and H. Dau, *J. Bioinorg. Chem.*, in press (2006).
- [2] M. Haumann, C. Müller, P. Liebisch, L. Iuzzolino, J. Dittmer, M. Grabolle, T. Neisius, W. Meyer-Klaucke, and H. Dau, *Biochemistry* **44**, 1894-1908 (2005).
- [3] H. Dau and M. Haumann, *Photosynth. Res.* **84**, 325-331 (2005).
- [4] L. Schwartz, G. Eilers, L. Eriksson, A. Gogoll, R. Lomoth, and S. Ott, *Chem. Comm.* 520-522 (2006).
- [5] M. Ihara, I. Okura, H. Nishihara, K. Yoon, O. Lenz, B. Friedrich, H. Nakamoto, K. Kojima, D. Honma, and T. Kamachi, *Photochem. Photobiol.*, Epub ahead of print (2006).

## Reactions of halogens with surfaces stimulated by VUV light

V. Ney and N. Schwentner

*Institut für Experimentalphysik, Freie Universität Berlin, Berlin, Germany*

Reactions on surfaces remain a fascinating field of research now since decades and new facets of this subject develop at a fast pace. It is still a real challenge to reveal the basic chemical and photochemical elementary processes involved in surface reactions. In addition there is a strong request for structuring surfaces with increased spatial resolution. Localized desorption is a natural route to convert a light pattern on a surface into a permanent structural pattern. To improve the resolution it is necessary to resort to shorter wavelengths as displayed for example in the International Road Map for Semiconductors [1]. It shifts the emphasis from 193 nm wavelength further into the VUV spectral region to 157 nm and even to 13.5 nm in the EUV project.

In this contribution investigations on light induced surface reactions in the spectral range from 200 to 50 nm are summarized which have been carried out in our group [2-5]. An appropriate light source is Synchrotron radiation concerning tunability and stability. To achieve a sufficient photon flux remains however a challenge ever since the first patterning experiments carried out on beamlines in Japan [6, 7]. We have increased the photon flux from bending magnets [2] by introducing mirrors collecting a large angular range at the 3m-NIM-2 beamline at BESSY I as well as in the continuation at the 3m-NIM-1 beamline at BESSY II. Halogen molecules like  $\text{Cl}_2$ ,  $\text{F}_2$  and  $\text{XeF}_2$  are used as reagents. They are rather reactive already in the ground state. In addition they have strong electronic transitions in the spectral range from 150 to 50 nm and it is expected that the reactivity

can be enhanced furthermore by stimulating these excited states with light.

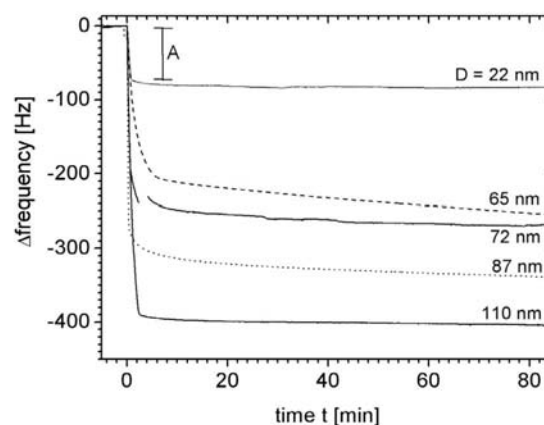


**Fig. 1:** Dark reaction of Cu with  $\text{Cl}_2$  for different film thicknesses  $D$ . Notice the extreme quick frequency change  $A$  at the beginning of the reaction.

An exemplary study has been carried out for Cu and  $\text{Cl}_2$  since it has the strongest dark reaction among the considered systems. In addition the reaction products are the stable  $\text{CuCl}$  and  $\text{CuCl}_2$  compounds. Therefore the accumulation of these products and their composition can be followed and analysed with exposure time. We adopted a quartz microbalance, to follow the development of light induced reactions [2]. It turns out that the stability and the sensitivity requirements are very demanding. However, now a continuous recording of the mass deposition in the reaction is possible as shown in Fig. 1.

These new results correct previous conclusions concerning the dark reaction. As a consequence modifications are derived which are necessary to slow down this dark reaction in order to favour the light induced one for the available photon flux.

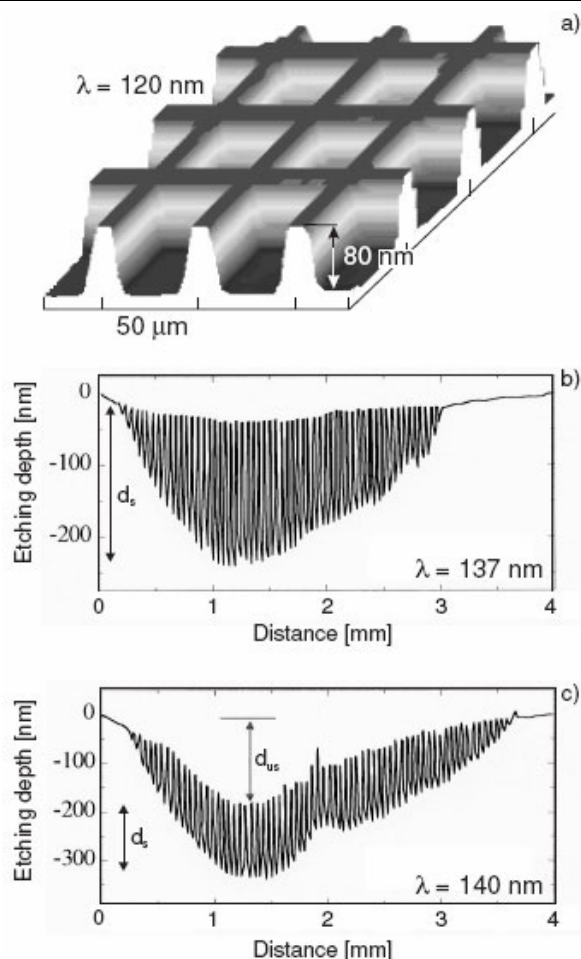


**Fig. 2:** Figure 2. Etching of Si with  $\text{XeF}_2$  produces good structures. a) AMF picture of a sample irradiated with 120 nm. The distance of the grids, which were covered by a mask is  $50 \mu\text{m}$ . b) Cross section measured with a stylus of an irradiated area, which was covered by a mask. Only a selective reaction is observed ( $d_s$ ) for  $\lambda = 137 \text{ nm}$ . c) Irradiating with 140 nm induces selective ( $d_s$ ) and non-selective reactions ( $d_{us}$ ).

A reaction cell consists of the substrate (metal, semiconductor) which is irradiated through the halogen gas in front of it. A photon can be absorbed in a reactive surface layer (or in the bulk). In this case the reaction is started in the laterally well defined spot of absorption and this reaction is called selective. If a photon is absorbed in the halogen gas, then diffusion of the excited species, until it reaches the surface and starts a reaction, will lead to a lateral displacement and the reaction is called non-selective. A lateral modulation of the light intensity for

example from the structure of a mask will be reproduced in the lateral distribution of reaction products on the surface in the selective case b) of Fig. 2 and it will be washed out in the non-selective case c) of Fig. 2.

Obviously selective processes have to be targeted for direct structuring with photochemical surface processes. Combinations have been chosen, for which several compounds from the reaction are volatile. Thus a direct reproduction of mask structures on a semiconductor surface becomes feasible by this so called light induced dry etching [2]. Inspection of the dependence on halogen pressure and wavelength reveals that a rich variety of passivation, dissociation and migration processes is involved.

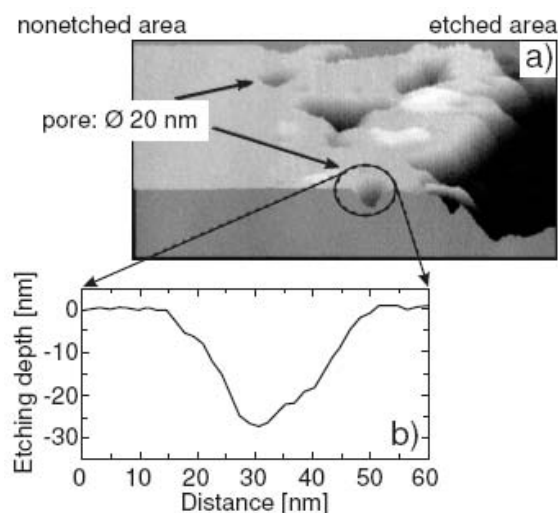


**Fig. 3:** Si pore at the border between etched and nonetched area resulting from a single photon event. AFM cross section shows that the pore has a diameter of 20 nm and corresponds to about  $3 \times 10^5$  Si atoms.

Concerning an efficient use of photons it turns out that the efficiencies are indeed very high and even exceed unity. This provides an immediate proof that the reaction extends beyond a single molecule and the underlying amplification processes still await for an explanation. The local expansion of the pit from a single photon event due to this amplification is directly displayed in Fig. 3. The pit

volume corresponds to  $3 \times 10^5$  atoms which have been removed due to one triggering photon and an optimum with respect to degradation and efficiency has to be chosen.

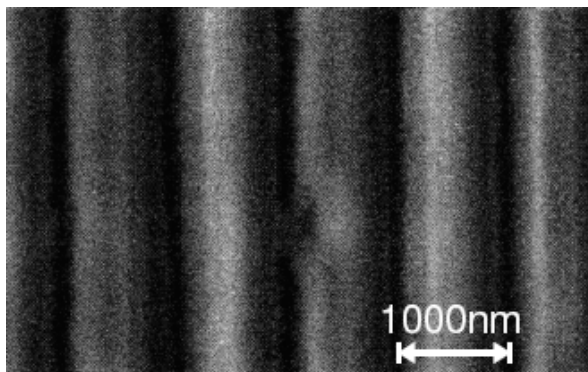


**Fig. 4:** GaAs etched with  $\text{Cl}_2$ . The stripes are 1000 nm apart.

In particular SEM pictures of etched GaAs wafers revealed very smooth surfaces and the structures are indeed only limited by diffraction. Thus the combination of GaAs and  $\text{Cl}_2$  seems to be very promising to proceed further in this direction. As an illustration we show in Figure 4 an SEM picture of a structure etched into GaAs as described above however with a much finer mask structure and a periodicity of 1000 nm. The lateral width of the etched wall is 100 nm or even less in agreement with the diffraction limit.

## Acknowledgments

Thanks to Dr. G. Reichard and the BESSY staff in general for support. The SAM and XPS measurements were carried out in the laboratory of Prof. Grabke, MPI Hannover. The SEM pictures were taken in the laboratory of Prof. Weinberger, FHI. Mrs. I. Dencks, HMI Berlin, assisted at the mechanical stylus.

## References

- [1] The International Roadmap for Semiconductors 2004 update Lithography, Figure 53.
- [2] V. Ney and N. Schwentner, *J. Phys. Condens. Matter* **18**, 1-25 (2006).
- [3] V. Dietz and N. Schwentner, *Surf. Sci.* **528**, 215 (2003)
- [4] H. Raaf and N. Schwentner, *Appl. Surf. Sci.* **174**, 13 (2001)
- [5] H. Raaf, M. Groen and N. Schwentner, *Appl. Surf. Sci.* **154-155**, 536 (2000)
- [6] N. Hayalaka, A. Hiraya and K. Shobatake, *Jpn. J. Appl. Phys.*, **26 L** 1110 (1987)
- [7] Y. Nonogaki, M. Katoh, K. Matsushita, M. Suzui and T. Urisu, *J. Electron Spectrosc. Relat. Phenom.* **144-147**, 1113 (2005)

## Electronic structure of two-dimensional adsorbate layers on transition metal surfaces using VUV and soft X-ray synchrotron radiation

Klaus Christmann

*Institut für Chemie und Biochemie, Freie Universität Berlin, Berlin, Germany*

In our synchrotron-related research three routes of interest were followed: i) the determination of the electronic band structure of clean and adsorbate-covered transition metal (TM) surfaces; ii) the orientation and local geometric structure of adsorbed (organic) molecules (bond length, bond angles) on Ag surfaces, and iii) the electronic and geometric structure and the growth mode(s) of thin metal films on refractory metal surfaces (Ru, Re). Accordingly, different synchrotron radiation ranges were used, viz., VUV light ( $\rightarrow$  angle-resolved photoemission ARUPS:  $10 < \hbar\omega < 50$  eV) and (soft) X-ray radiation:  $\hbar\omega > 100$  eV ( $\rightarrow$  X-ray absorption spectroscopy {NEXAFS and EXAFS} as well as X-ray photoelectron spectroscopy {XPS}). The samples investigated were low-index single crystal TM surfaces (Co, Ni, Ru, Rh, Pd, Ag, Re, Pt, Au) covered either with chemically reactive (oxygen, hydrogen and nitrogen) or inert gases (xenon and krypton), with larger organic molecules (cyclic ethers: 1,4-dioxane, 1,3,5-trioxane), or with thin films of Cu, Ag, and Au in monolayer (ML) and multilayer concentrations. In all our studies we supplemented the synchrotron data by results obtained from other surface analytical techniques such as LEED, Auger electron spectroscopy (AES), vibrational loss spectroscopy (HREELS), thermal desorption spectroscopy (TDS) and work function change ( $\Delta\phi$ ) measurements. This helped a lot to better understand our adsorption systems.

A crucial parameter in all adsorption experiments is the *sample temperature*: Exposing TM surfaces to  $H_2$ ,  $O_2$  and  $N_2$  at  $T \cong 30$  K often stabilises a molecular (phy-

sorbed) species ( $O_2$  and  $N_2$ , in particular) as the dissociation reaction is slowed down [1]. The molecular interaction resembles very much the one observed with noble gases and is characterised by the dispersing MOs of the molecular entities on an electronically unperturbed substrate. This is illustrated for Xe adsorbed at  $\sim 30$  K on a Ru(10-10) surface [2]. The sharp 5p (spin-orbit split) Xe levels can conveniently be followed through k space without perturbing substrate effects. Parallel LEED and TDS experiments reflect the long-range order and the concentration of the Xe phases. As an example, the band dispersion curves for a relaxed Xe monolayer on Ru(10-10) is shown in Fig. 1.

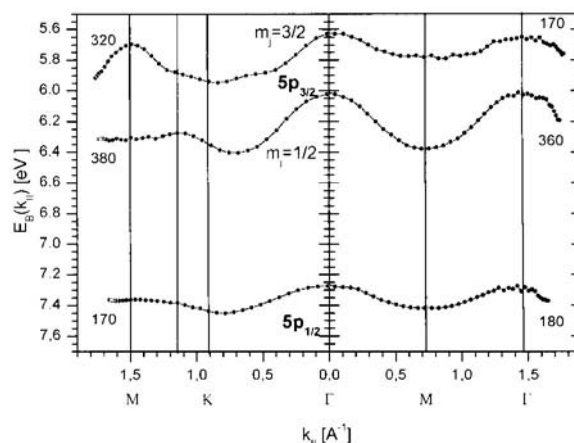


**Fig. 1.** Band dispersion of the Xe 5p levels for the quasi hexagonal full monolayer phase [2].

The interaction of hydrogen, oxygen, and nitrogen with TM surfaces (Fe, Ni, Co, Ru, Rh, Pd, Pt etc.) is of particular interest in view of chemical-catalytical applications. An additional effect is that the crystallographically more ‘open’ fcc(110) and hcp(10-10) surface orientations are susceptible to adsorbate-induced surface re-

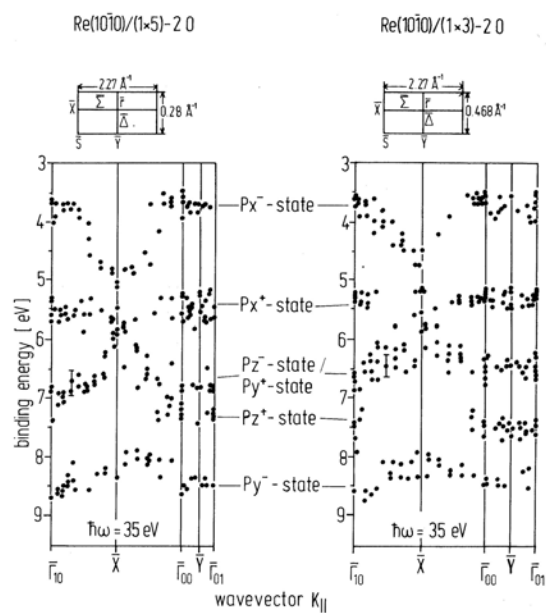


**Fig. 2.** Dispersion of the O-induced bands of the (1x5)-2O (left) and the (1x3)-2O phases (right) on a Re(10-10) surface [3].

constructions (changes in the lateral periodicities), one of the first stages of chemical attack towards hydridic, oxidic, or nitridic compounds. The respective surface Brillouin zones (SBZ) of the clean and adsorbate-covered surfaces can be mapped by means of ARUPS, although a clear-cut distinction between the *adsorbate*-related (likewise periodically arranged) molecular orbitals (MO) and the altered electronic bands of the *substrate* is difficult, because of the strong mutual interaction. Nevertheless, the O-induced electronic bands can sometimes be distinguished with respect to their symmetry properties (by performing polarisation-dependent ARUPS measurements) and followed through k-space. An example is taken from our work on the O + Re(10-10) system [3]. Five different ordered oxygen phases appear as a function of oxygen exposure at 300 K. The first phase, a c(2x4)-O structure, is best developed at a coverage of  $\Theta = 0,25$  and exhibits three O-2*p* derived states with practically no dispersion, neither along  $\bar{\Sigma}$  ( $=[12-10]$ ) direction, parallel to the densely packed rows, nor in  $\bar{\Delta}$  ( $=[0001]$ )

direction, perpendicular to the respective troughs. This behaviour is not unexpected, since the mean distances between the adsorbed O atoms are still relatively large at  $\Theta = 0,25$ . For two (higher coverage) O superstructures with non-primitive unit meshes, viz., the (1x5)-2O and the (1x3)-2O phase, the three 2*p*-derived oxygen bands could be detected and monitored over a fairly large range of the SBZ using angle-resolved and polarisation-dependent UPS. This is shown in Fig. 2 and helps to develop a real-space model of the O 2*p* orbital interactions [3].

Near-edge X-ray absorption fine structure is a powerful tool to determine the chemical state and the geometric orientation of adsorbed molecules. This is why we have constructed and built a NEXAFS chamber for use at BESSY II [4] and performed test measurements with 1,4-dioxane adsorbed on a Ag(110) surface, for various azimuthal and incidence angles. Only at coverages  $\Theta < 0,1$  the ether molecules are oriented parallel to the surface as apparent from the loss in intensity of the C 1*s*  $\rightarrow$   $\sigma^*$  transitions when changing the light incidence from normal to grazing conditions. Higher coverages apparently lead to the formation of disordered layers.

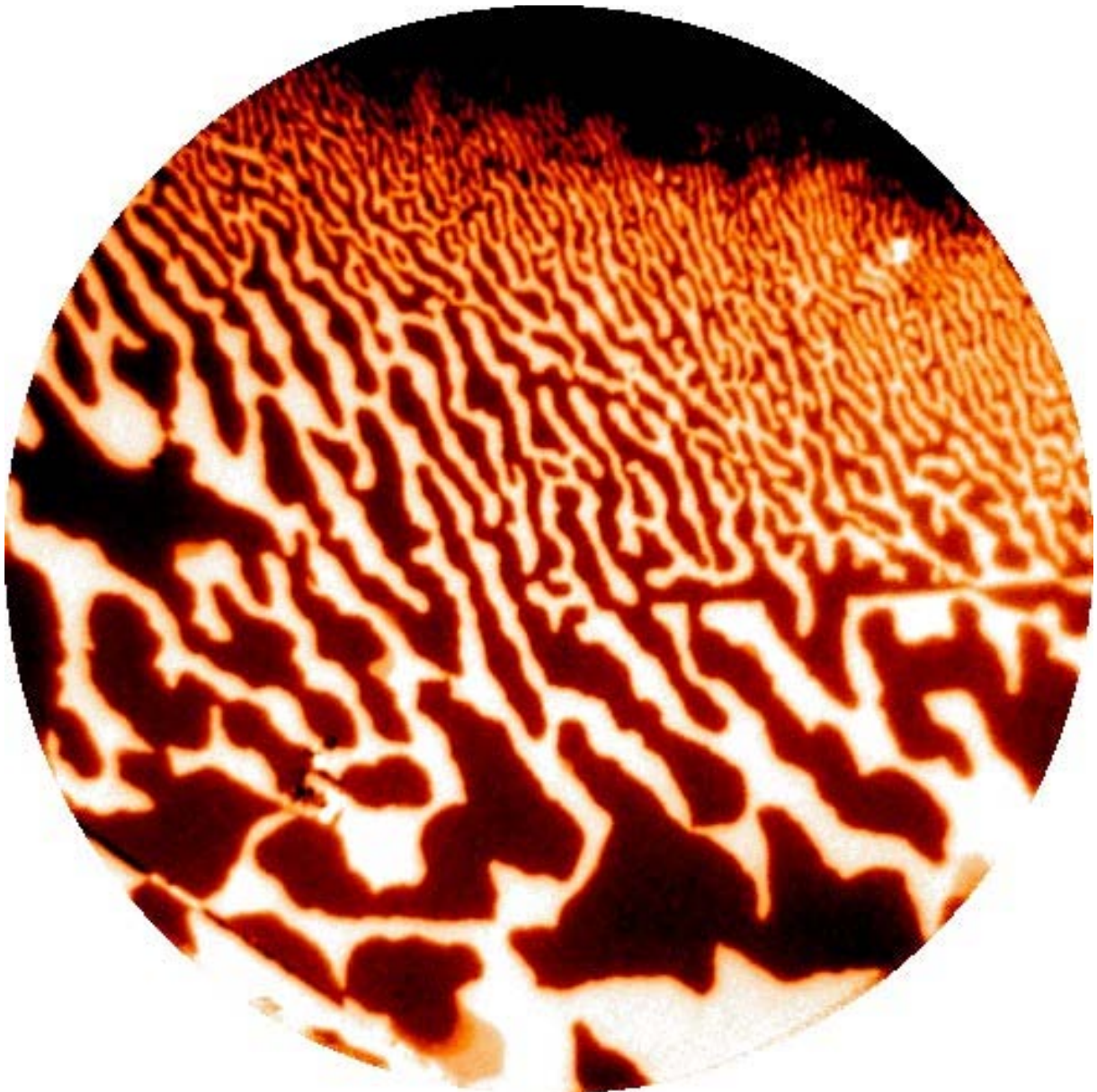
Finally, we followed the growth of thin Ag and Au films during their deposition onto Ru and Re(10-10) surfaces by ARUPS. Silver forms, in the submonolayer range, a c(2x2) and a (1x4) phase, depending on the deposition conditions. STM measurements showed that two occupied rows and two empty rows alternate in [0001] direction (perpendicular to the troughs) [5]. The resulting  $E(k)$  dispersion curves revealed, in both orthogonal directions, flat bands indicating the d character of the observed electron states of the Ag (Au) films.

## References

- [1] a) P. K. Schmidt et al., Phys. Rev. Lett. **87**, 096103 (2001).  
b) M. Gottfried, Ph.D. thesis, FU Berlin 2003.
- [2] K. J. Schmidt and K. Christmann, Surf. Sci. **525**, 159 (2003).
- [3] J. Lenz et al., Surf. Sci. **269/270**, 410 (2003).
- [4] a) A. Heiland and K. Christmann, Surf. Sci. **355**, 31 (1996).  
b) A. Heiland, Ph.D. thesis, FU Berlin 2003.
- [5] a) A. Volmer, Ph.D. thesis, FU Berlin 1999.  
b) A. Volmer, S.L.M. Schröder, K. Christmann, to be published.

---

# Material Science



Previous page: Like stripes of a nanoscale zebra, magnetic domains appear in thin film materials with perpendicular magnetization direction when made visible by synchrotron radiation. The example shows a photoelectron emission microscopy image (100  $\mu\text{m}$  diameter) of magnetic domains in a 2 nm thick nickel film on a Cu(001) single crystal substrate. Dark and bright areas correspond to magnetization out of the film plane and into the film plane alternate in a labyrinth-like pattern. Magnetic properties in the upper part of the image have been modified by deposition of less than 0.2 nm of cobalt.

## Material Science

Material science investigations with synchrotron radiation at the Freie Universität mainly focused on exploring the electronic and magnetic properties of solids by spectroscopic methods in the soft x-ray regime. The studies span the range from fundamental investigations of material properties to technology-oriented questions of magnetization reversal dynamics.

Synchrotron radiation has the great advantage of easily variable polarization, which allows access to the angle-dependence of electronic states. Starke *et al.* used x-ray absorption spectroscopy and photoelectron emission spectroscopy to study the electronic properties of rare earth materials. In particular, their data support the existence of a strong Rashba effect also in magnetic rare earth materials, which may have important consequences for devices based on these materials. Weschke *et al.* studied the electronic and magnetic properties of oxides by photoelectron emission spectroscopy. Oxides are an important class of materials for future magneto-electronic devices, since they unite magnetic behavior with high electric resistance.

X-ray magnetic circular dichroism (XMCD) is at the basis of many of these investigations. It is a very versatile technique, since it allows direct access to element-resolved magnetic properties. XMCD is based on transition selection rules from quantum mechanics, which tell us that if circularly polarized light is used, the excitation probability for spin-up and spin-down electrons will be different. Such transitions can thus directly probe the imbalance in the occupation of electrons with different spin direction, i.e., the ferromagnetism. Since the effect occurs only at elemental absorption edges, the technique is intrinsically element-selective, but requires x-rays of tunable wavelength, hence synchrotron radiation.

It is possible to extract from a quantitative analysis of such XMCD spectra the element-resolved magnetic moments, separated into their spin and orbital contributions. Scherz *et al.* have explored fundamentals of this quantification, and suggest a new basic concept to extend quantitative XMCD data analysis also to the light  $3d$  elements, for which some of the previously used approximations do not hold. Wilhelm *et al.* have used quantitative XMCD analysis in their study of the spin and orbital moments that appear in some of the normally non-magnetic  $5d$  elements by the contact to a ferromagnetic layer. They observed that, in contrast to what would be expected for free atoms from Hund's third rule, the spin and orbital moments in elements with less than half filled  $5d$  shell are oriented parallel to each other. Closely related is the question about the properties of magnetic impurities. Brewer *et al.* have used XMCD to study the magnetic properties of  $3d$  ferromagnetic atoms dispersed in gold. They could show that particularly Co atoms retain a significant degree of atomic behavior, while other  $3d$  elements do not.

The depth profile of magnetization was the subject of interest in the second contribution by Wilhelm *et al.* Here they compared the XMCD signal of magnetic multilayers with different layer thicknesses, and could deduce from these data the depth profile of the induced magnetic moments in the nominally non-magnetic spacer layers.

In combination with a microscopic technique, XMCD can be employed as a contrast mechanism to obtain element-resolved microscopic images of the magnetic domain pattern in thin films. Kuch *et al.* used their photoelectron emission microscope (PEEM) and XMCD to study the magnetic domains in layered systems consisting of ferromagnetic and antiferro-

magnetic layers. From the resulting domain patterns they could draw conclusions about the spin structure of the antiferromagnetic layer, important information that is not readily accessible by other techniques. The combination of XMCD, PEEM, and time-resolved measurements taking advantage of the pulsed nature of synchrotron radiation allowed exploring the magnetization dynamics in coupled trilayers, in which a non-magnetic spacer layer separates two ferromagnetic layers. Such trilayered systems are of high technological relevance for magnetic read heads, as sensors, or for future data storage technologies, for example magnetic random access memories.

The combination of resonant absorption of polarized synchrotron x-rays and x-ray diffraction opens the door to the simultaneous study of geometric and magnetic properties. This was done by Weschke *et al.* In their contribution they present a look at the magnetic order in thin magnetic layers and nanostructured materials.

# X-ray magneto-optics and electron structure of lanthanide materials

*K. Starke, J. E. Prieto, K. Döbrich, O. Krupin, G. Kaindl*

*Institut für Experimentalphysik, Freie Universität Berlin*

In recent years, our research on lanthanide materials with synchrotron radiation has focussed on two directions: analysis of magneto-optical (MO) effects in the soft x-ray regime of lanthanide metals including their application to the study of exchange coupled layered structures, and on the valence electronic structure of three- and two-dimensional magnetic lanthanide systems.

For a quantitative analysis of MO con-

starts in the spectral region of lanthanide  $4d$  and  $3d$  excitation thresholds, we measured absorption spectra at grazing incidence from in-plane magnetized lanthanide metal films using circularly polarized x-ray beams from BESSY undulator beamlines [1]. As an example, Fig. 1 (a) shows absorption spectra at the Tb  $N_{4,5}$  edge. Owing to their wide photon energy range, the spectra could be calibrated by matching them to off-resonance

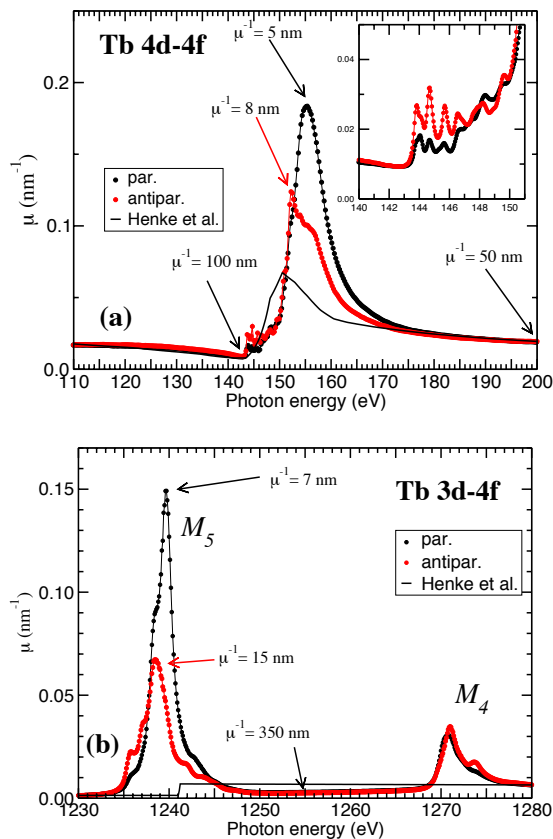


**Fig. 1:** (a) Tb  $N_{4,5}$  absorption spectra measured with circularly polarized x-rays parallel and antiparallel to the in-plane magnetization of a 13-nm thick Tb film at 25 K. (b) Analogous spectra at the Tb  $M_{4,5}$  edge. After saturation correction, the experimental spectra are normalized to tabulated off-resonance data [5]; Fig. from Ref. [4].

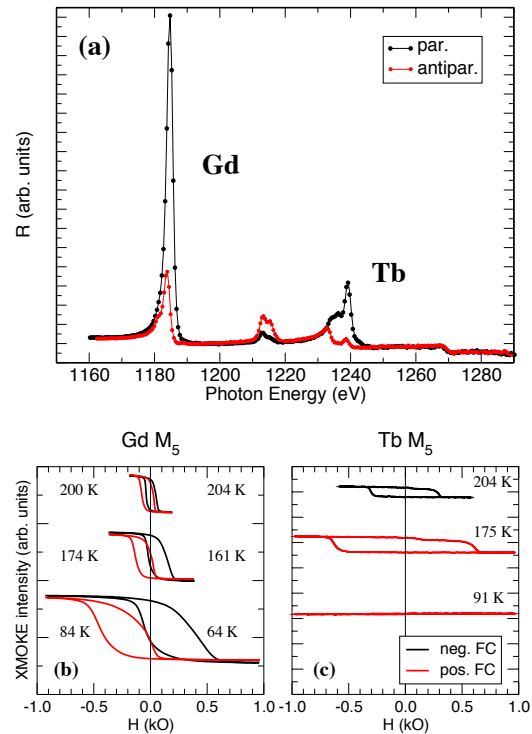


**Fig. 2:** (a) Specular-reflection spectra from a Gd/Y/Tb trilayer film in the region of the Gd  $M_{4,5}$  and Tb  $M_{4,5}$  edges, recorded at  $8^\circ$  with respect to the film plane. Element-specific hysteresis loops of (b) the Gd layer and (c) the Tb layer. The trilayers were epitaxially grown on a W(110) single crystal by metal vapor deposition in ultra-high vacuum ( $5 \cdot 10^{-11}$  mbar). Gd, Y, and Tb layer thicknesses were 2.0, 1.2, and 10 nm, respectively; Fig. from Ref. [4].

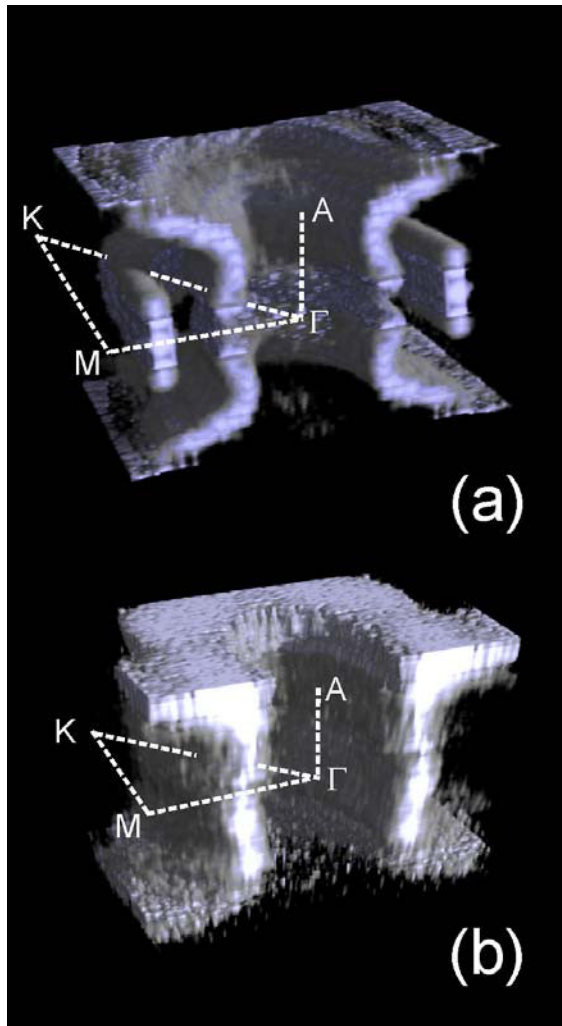


**Fig. 3:** Change of the Tb Fermi surface with temperature from (a) the ferromagnetic phase at 20 K to (b) the paramagnetic phase at 240 K. The 3D images show regions of high photoemission intensity that correspond to regions of high density of states at the Fermi level (0.2 eV energy window). High-symmetry points of the hcp Brillouin zone are indicated by the symbols  $\Gamma$ , M, K and A (the  $\Gamma$ -point is accessed at 102 eV photon energy); Fig. from Ref. [6].

tabulated data of Henke *et al.* [5], yielding the imaginary part of the refractive index. The real part was calculated via Kramers-Kronig transformation [2–4].

Knowledge of the soft x-ray magneto-optical constants enabled us to study magnetic systems that contain different (lanthanide) elements, simply by measuring the specularly reflected intensity of circularly polarized x-ray beams with the photon energy tuned to an

excitation threshold of the element in question. As an example, Fig. 2 (a) shows grazing-incidence reflectivity spectra of a magnetically saturated Gd/Y/Tb(0001) trilayer film with in-plane magnetization.

Figures 2 (b) and (c) show hysteresis loops at various temperatures of (b) the magnetically soft Gd layer and (c) the ‘hard’ Tb layer, with the x-ray energy tuned to the respective  $M_5$  reflectivity maxima [see Fig. 2 (a)]. The Tb hysteresis loops indicate the external field range in which the Tb layer magnetization is constant. The Gd loops reveal a pronounced shift due to coupling to the Tb layer, mediated via valence electrons of the Y interlayer. The interlayer exchange coupling becomes stronger at low temperatures. While this behavior has been observed earlier in transition-metal systems, we find that in rare-earth trilayers the direction of interlayer coupling changes with temperature.

This new phenomenon of temperature-induced change between ferro- and antiferromagnetic interlayer coupling motivated detailed studies of the temperature-dependent Fermi surfaces and valence band structure of lanthanide metals using angular resolved vacuum ultraviolet (VUV) photoemission.

Figure 3 shows how the Tb Fermi surface

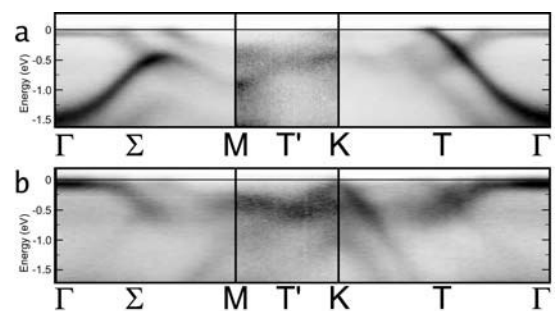


**Fig. 4:** Valence band structure of ferromagnetic Tb metal along high-symmetry lines of the hcp crystal (indicated by the symbols  $\Gamma$ -M-K- $\Gamma$ ). Bands of different crystal symmetry can be ‘switched on and off’ by choosing the appropriate photon energy: (a)  $h\nu=102$  eV and (b)  $h\nu=150$  eV; Fig. from Ref. [7].

changes with the phase transition between (a) the ferromagnetic and (b) the paramagnetic phase. Owing to the valence band exchange splitting in the ferromagnetic phase, there is a double ring structure around the center; it collapses at the phase transition. The corresponding band structure at energies below the Fermi level is presented in Fig. 4.

Furthermore, we have started a joint experimental and theoretical project to investigate the Rashba effect at surfaces and interfaces of magnetic systems [8]. The effect is based on the fact that an electric field acts as a magnetic field in the rest frame of a moving electron, and electric fields of appropriate shape and strength exist at surfaces and interfaces of solid crystals (broken structural inversion symmetry). Up to now, studies of the Rashba effect had focused on semiconductors [9] and nonmagnetic metals [10,11], yet there are interfaces between ferromagnetic and nonmagnetic materials in practically all spintronic device schemes currently suggested [9].

Fig. 5(a) shows the dispersion of the majority spin surface state of ferromagnetic Gd(0001), recorded by angle-resolved photoemission ( $h\nu = 36$  eV). The dispersion changes from red to black when reversing the sample magnetization, i.e., the surface-state energy changes upon flipping the electron spin (with respect to the crystal electric field and the propagation direction) in the 2-D system. The energy shift ('Rashba shift') is given in Fig. 5 (c) by blue data points. A much larger Rashba shift is found upon modification of the system by adsorbing a small amount of oxygen on the surface in such a way that the O atoms form a two-dimensional lattice of GdO on top of the metal surface. As is shown in Fig. 5 (b), the electronegative O atoms strongly affect the entire surface electronic structure: now both the majority-spin state and the (exchange split) minority-spin state are occupied, both

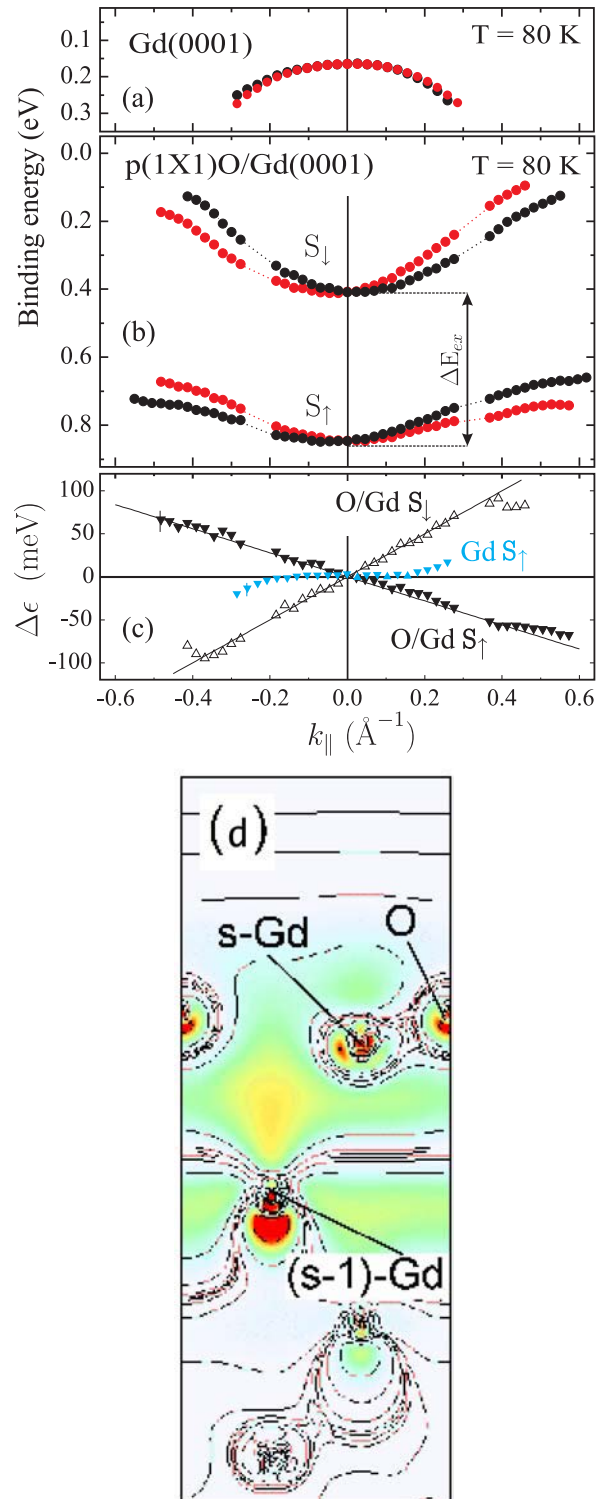


**Fig. 5:** At ferromagnetic surfaces, the dispersion of two-dimensional states changes upon magnetization reversal due to the Rashba effect. The effect is small (a) at the Gd(0001) metal surface; it becomes considerably larger upon formation of (b) the metal-oxide/metal interface. (c) Rashba shift of the states; (d) calculated charge density distribution at a GdO surface layer on top of Gd; Fig. from Ref. [8].

dispersing upwards towards the Fermi energy with increasing momentum. Again, their positions change between red and black upon magnetization reversal; the associated shift is plotted in Fig. 5 (c).

This is the first experimental investigation of two-dimensional electronic states in which magnetic exchange interaction and the Rashba effect coexist. To understand the present observations for Gd(0001) and p(1x1)O/Gd(0001) with their strikingly different Rashba shifts in a quantitative way, G. Bihlmayer *et al.* (FZ Jülich) have performed ab-initio calculations using density functional theory (DFT) in the so-called LDA+U approximation [8]. The charge density distribution in Fig. 5 (d) shows that the two-dimensional state is distributed over the whole region between the GdO layer and the sub-surface Gd layer revealing that the state is actually an interface state. Obviously, the enhanced Rashba effect originates from the steep charge density gradients in the interface region, driven by the electronegative O atoms.

We suggest to utilize the spin sensitivity of the Rashba effect in magnetic systems to study two-dimensional spin structures at surfaces and interfaces. Moreover, the present findings can be of interest for future spintronic devices, especially at interfaces where Rashba and exchange interaction both control the electron spin. The Rashba effect at a metal/metal-oxide interface could in principle be used in a device that would become as thin as a few atomic layers.

## References

- [1] K. Starke, F. Heigl, A. Vollmer, M. Weiss, G. Reichardt, and G. Kaindl, *Phys. Rev. Lett.* **86**, 3415 (2001).
- [2] J. E. Prieto, F. Heigl, O. Krupin, G. Kaindl and K. Starke, *Phys. Rev. B* **68**, 134453 (2003).
- [3] J. E. Prieto, F. Heigl, O. Krupin, G. Kaindl, and K. Starke, *Phys. Rev. B* **66**, 172408 (2002).
- [4] J. E. Prieto, O. Krupin, K. Döbrich, F. Heigl, G. Kaindl, and K. Starke., *Appl. Phys. A* **80**, 1021 (2005).
- [5] B. L. Henke, E. M. Gullikson, J. C. Davis, *At. Data Nucl. Data Tables* **54**, 181 (1993).
- [6] K. M. Döbrich, G. Bihlmayer, K. Starke, J. E. Prieto, K. Rossnagel, E. Rotenberg, S. Blügel, and G. Kaindl, (unpublished).
- [7] K. M. Döbrich, G. Bihlmayer, K. Starke, J. E. Prieto, K. Rossnagel, H. Koh, E. Rotenberg, S. Blügel, G. Kaindl., (preprint 2006).
- [8] O. Krupin, G. Bihlmayer, K. Starke, S. Gorovikov, J. E. Prieto, K. Döbrich, S. Blügel, and G. Kaindl, *Phys. Rev. B* **71**, 201403(R) (2005).
- [9] I. Žutić, J. Fabian, and S. Das Sarma., *Rev. Mod. Phys.* **76**, 323 (2004).
- [10] E. Rotenberg and S. D. Kevan, *Phys. Rev. Lett.* **80**, 2905 (1998).
- [11] F. Reinert, G. Nicolay, S. Schmidt, D. Ehm, and S. Hüfner, *Phys. Rev. B* **63**, 115415 (2001).

## Electronic structure of thin films

*E. Weschke, A. Gottberg, E. Schierle, H. Ott, C. Schüßler-Langeheine, G. Kaindl*

*Institut für Experimentalphysik, Freie Universität Berlin*

The electronic structure of solids, i.e., the allowed energy levels of electrons, determines their macroscopic properties, whether the material is metallic or a semiconductor, or if it is magnetic. Detailed knowledge of the electronic structure is therefore a key to the microscopic understanding of the properties of any material. Arguably the most direct method to study the energy levels of electrons in solids, i.e., the band structure, is angle-resolved photoelectron spectroscopy. The method is based on the photoelectric effect, explained by Einstein in the beginning of the 20<sup>th</sup> century, where light of sufficiently high energy ejects electrons from the target. Due to the energy and momentum conservation of the process, a direct image of the energy distribution inside the material is obtained. Photoelectron spectroscopy using synchrotron radiation is a particularly versatile tool, as it can make use of the tunable photon energy. The method is applied to study thin films and nanostructures, where interesting finite-size effects are observed.

As an example of mapping band structures by photoelectron spectroscopy, Fig. 1 shows the electron band dispersion of a thin film of nickel oxide. NiO has played an important role in basic research, being a prototype insulating antiferromagnet with a band structure dominated by strong electron correlations. Recently, NiO has regained interest due to its application in magnetic multilayer systems with exchange bias. Fig. 1 shows a two-dimensional photoemission intensity plot as a function of the binding energy and the electron emission angle, which was obtained with a high-resolution photoelectron spectrometer at the beamline of the Berlin universities at BESSY. The mapping of the band structure revealed an interesting result, namely the crossing of the topmost band with the Fermi energy. This indicates metallic properties of the thin film in contrast to bulk NiO, which is an insulator.

With the reduction of the dimensions, also the properties of metals may deviate substantially from those of the corresponding bulk materials. This is illustrated in Fig. 2, which

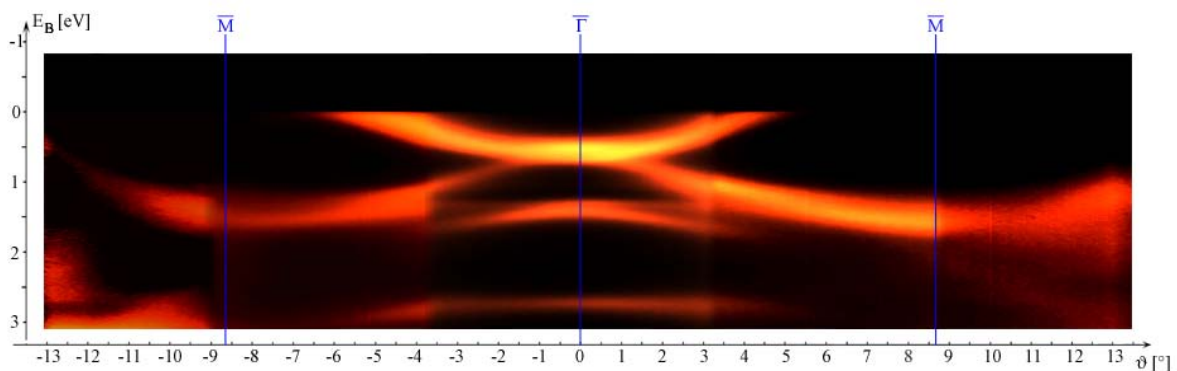


**Fig. 1:** Valence-band structure of a thin nickel oxide film. Modern photoelectron spectrometers such as the experimental station of the Freie Universität Berlin at BESSY allow to record spectra as a function of energy and electron emission angle with a two-dimensional detector, yielding directly the electronic band dispersion.

displays photoelectron spectra recorded from silver films in the thickness range from 7 to 20 atomic layers. The spectra on the top panel exhibit a number of regular peaks labeled 1 to 6, which change their position with increasing film thickness in a systematic way. This is typical for so-called quantum-well states, which are induced by the spatial confinement of the electrons in the material on a length scale of atomic distances. The electrons are forced to occupy discrete energy levels in contrast to the continuous band structure of bulk silver [1]. Nevertheless, the discrete electronic states closely resemble the bulk band structure, as evidenced by the red data points in the bottom panel of Fig. 1 representing the energy positions of the quantum-well states. They fit the behavior of the bulk band (solid blue line) very well.

The magnetic properties of a material are determined by the coupling of the magnetic

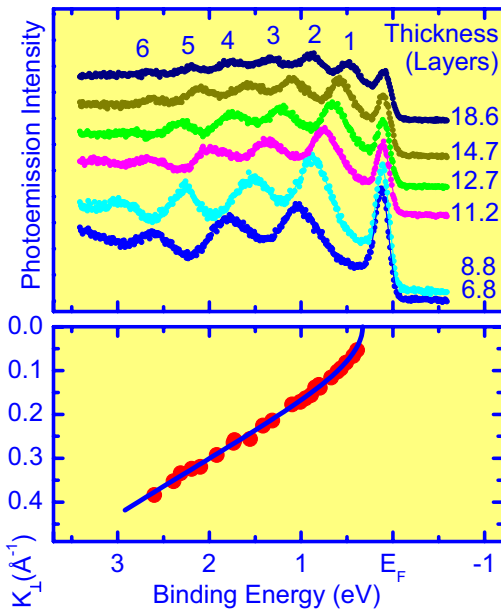


**Fig. 2:** Top: Quantized electronic states in Ag films with thicknesses of only a few atomic layers. Due to the confinement in atomic dimensions, quantum effects on the electronic structure are visible as discrete energy levels (top). Bottom: The discrete energies (red data points) nicely fit the bulk band structure (blue solid line) of Ag metal.

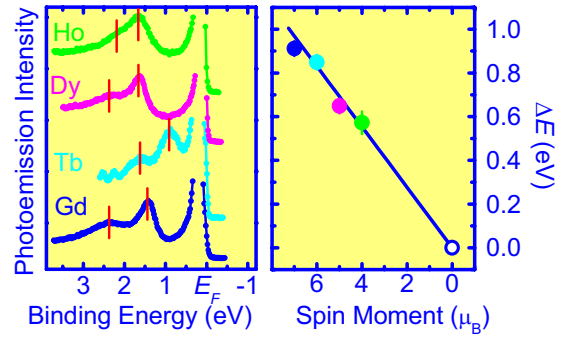


**Fig. 3:** Systematic behavior of magnetic exchange splitting in the lanthanide metals Gd, Tb, Dy, and Ho. The left panel shows valence-band photoelectron spectra recorded in the magnetic phase, revealing a decreasing splitting from Gd to Ho (red bars). The right panel shows the linear scaling with the  $4f$  spin moment.

moments associated with the electrons and hence are also directly connected to the electronic structure. In metallic systems, the spin polarization of conduction electrons provides a mechanism to couple magnetic moments. This polarization is also reflected in the fact that the degeneracy of electron energies is lifted, leading to a so-called exchange splitting of energy levels. This splitting has been studied systematically for a particular class of magnetic materials, the lanthanide elements. These metals are characterized by an open  $4f$  electronic shell, which carries a large magnetic moment interesting for applications as permanent magnets. Fig. 3 shows angle-resolved photoelectron spectra of selected lanthanide metals from Gd with seven  $4f$  electrons to Ho with ten  $4f$  electrons. Evidently, the magnetic splitting decreases systematically, establishing a linear scaling with the  $4f$  spin moment. This interesting result indicates that the magnetic exchange splitting is independent of the type of magnetic order [2], since Gd is a ferromagnet, while Ho is characterized by a helical antiferromagnetic structure.

**References**

- [1] A. M. Shikin, D. V. Vyalikh, Yu. S. Dedkov, G. V. Prudnikova, V. K. Adamchuk, E. Weschke, and G. Kaindl, *Phys. Rev. B* **62**, R2303 (2000).
- [2] C. Schüßler-Langeheine, E. Weschke, Chandan Mazumdar, R. Meier, A. Yu. Grigoriev, G. Kaindl, C. Sutter, D. Abernathy, G. Grübel, and M. Richter, *Phys. Rev. Lett.* **84**, 5624 (2000).

## New concept to study magnetic behavior of early 3d elements

A. Scherz<sup>1</sup>, H. Wende<sup>1</sup>, C. Sorg<sup>1</sup>, K. Baberschke<sup>1</sup>, J. Minar<sup>2</sup>, D. Bened<sup>2</sup>, H. Ebert<sup>2</sup>

<sup>1</sup> *Institut für Experimentalphysik, Freie Universität Berlin*

<sup>2</sup> *Institut für Physikalische Chemie, Ludwig-Maximilians-Universität München*

Nearly everyone uses magnetic nanostructures similar to those which will be presented here, for example as read head sensor of the hard disk drive in a computer. These nanostructures consist of a sandwich of magnetic layers with a non-magnetic layer in between (see Fig. 1). Such structures exhibit new magnetic properties as compared to bulk magnets, e.g. the giant magneto resistance – the effect used nowadays to read data stored on hard disks. Even though magnetic nanostructures are widely used and function reasonably well, fundamental questions about them remain unsolved, e. g. the behavior of the non-magnetic material placed between the stack of magnetic layers is unclear. In the ongoing process of miniaturization only a few atomic layers of each material are used and therefore the importance of the interfacial properties increases dramatically. To study the magnetic properties of those nanostructures and especially their interfaces one needs an element-specific method to distinguish contributions of the various layers. X-ray magnetic circular dichroism (XMCD) is a method of choice since the energy positions of the x-ray absorption edges are characteristic for each element. If a magnetic sample is illuminated with circularly polarized synchrotron radiation, the absorption, especially close to certain absorption edges, will be significantly different whether left or right circular x-rays are used. The circular dichroism is defined as the difference of the corresponding absorption coefficients. Since the XMCD signal can be related to the difference of the spin-split densities of states close to Fermi level, the direc-

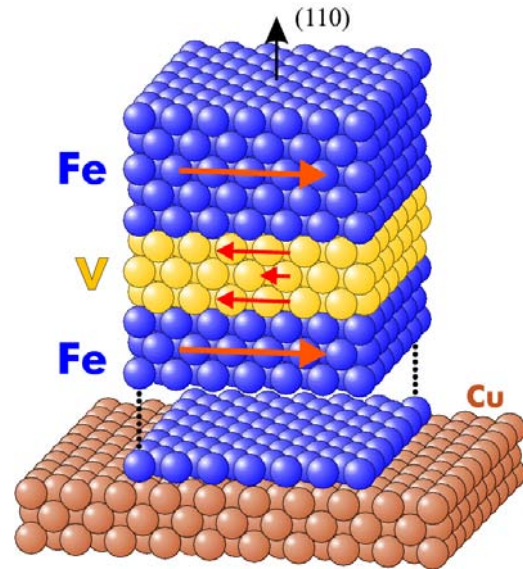


**Fig. 1:** Schematic view of the Fe/V/Fe(110) trilayers grown on Cu(100). The arrows indicate the layer-dependent magnetic moments of Fe and V.

tion and the size of the spin and orbital magnetic moments can be determined.

Up to now, the classical ferromagnets Fe, Co, and Ni have been investigated. A systematic study of XMCD throughout the 3d transition-metals (TMs) series is lacking. There are several reasons for this: (i) In insulators the 3d ions may carry a magnetic moment, however, e.g. ferromagnetic oxides are difficult to investigate because the energy ranges of the *L* edges (about 400–600 eV) and the O-*K* edge (532 eV and fine structures) coincide. (ii) The XMCD signals of the early 3d TMs Ti, V, and Cr are expected to be much smaller than those of Fe, Co, and Ni. (iii) The spin-orbit splitting of the core hole reduces towards the early 3d TMs leading to considerable overlap of the *L*<sub>3</sub> with the *L*<sub>2</sub> edge. The latter is also related to the

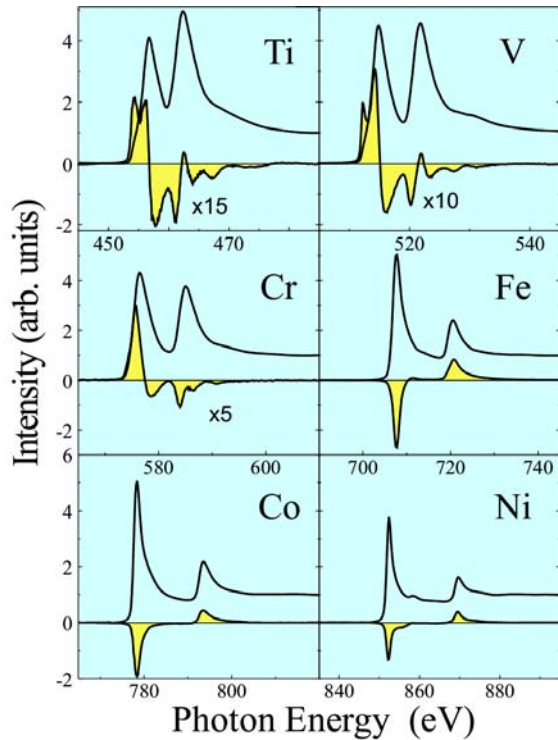


**Fig. 2:** The isotropic x-ray absorption spectroscopy and XMCD spectra at the  $L_{2,3}$  edges for part of the  $3d$  TMs. The spectra for the early  $3d$  TMs are determined from Fe/TM/Fe trilayers [3].

appearance of core-hole correlation effects [1,2] which strongly modify the relative intensities of the  $L_{2,3}$  edges (see Fig. 2).

We have investigated Ti, V, and Cr layers sandwiched between two Fe layers (Fig. 1) [3]. The spectra are shown in Fig. 2 with Fe for comparison. For the first time, we obtained nearly noise-free data with clear fine structure, bridging the gap from classical ferromagnets to the early  $3d$  elements. This was made possible by two technical developments [4]: (i) optimized *in-situ* preparation guaranteed for flat interfaces without oxygen contamination, (ii) high photon fluxes together with a constant high polarization degree in the required energy-range provided by the BESSY undulator beamline UE56/1-PGM using the gap-scan mode. The presence of an XMCD signal itself demonstrates that the so-called non-magnetic layer of V indeed exhibits an induced moment at

the interface [5]. The relative orientation of the magnetic moments of Ti, V, and Cr at the interface to Fe can be determined: As indicated in Fig. 1, the V spin moments are anti-parallel to the Fe moments as it is revealed from the *positive* sign of the V XMCD onset at the  $L_3$  edge in Fig. 2 (compared to the *negative* sign for Fe).

Even though the spectra reveal a large variety of different spectral features, the so-called integral sum rules are commonly applied to extract magnetic moments. In fact the validity of sum rules is rather limited [6] in particular for the early  $3d$  TMs because of the considerable overlap of the  $L_{2,3}$  edges. Hence, we used a new analysis concept, which compares the experimental fine structure to *ab initio* calculated x-ray absorption spectroscopy (XAS) and XMCD spectra (for details see Ref. [7]). The calculations are based on a fully relativistic spin-polarized Korringa-Kohn-Rostoker (SPR-KKR) Greens-function method, which is appropriate for itinerant magnetic systems as investigated here. In Fig. 3 the new concept is demonstrated for vanadium in a Fe/V trilayer and a Fe/V alloy serving as an experimental standard. Core-hole correlation effects were not included accounting for the deviation of the experimental branching ratio (close to 1:1) of the V XAS (see top panels). Looking at the XMCD (bottom panels), we find that nearly all fine structures in the experimental data are reproduced by theory. The feature (S) in the experimental XAS spectra located at the high-energy side ( $\sim 530$  eV) could be falsely assigned to contamination with oxygen whereas the theory correlates the satellite to the vanadium band structure (Fig. 3, inset). The asymmetric contributions of the V XMCD in Fig. 3 at the  $L_3$  edge (B) and, less distinct, at the  $L_2$  edge (C) are perfectly obtained by theory. In particular, the oscillatory fine structure (D) is elucidated as a contribution coming from the  $L_2$  edge (shaded

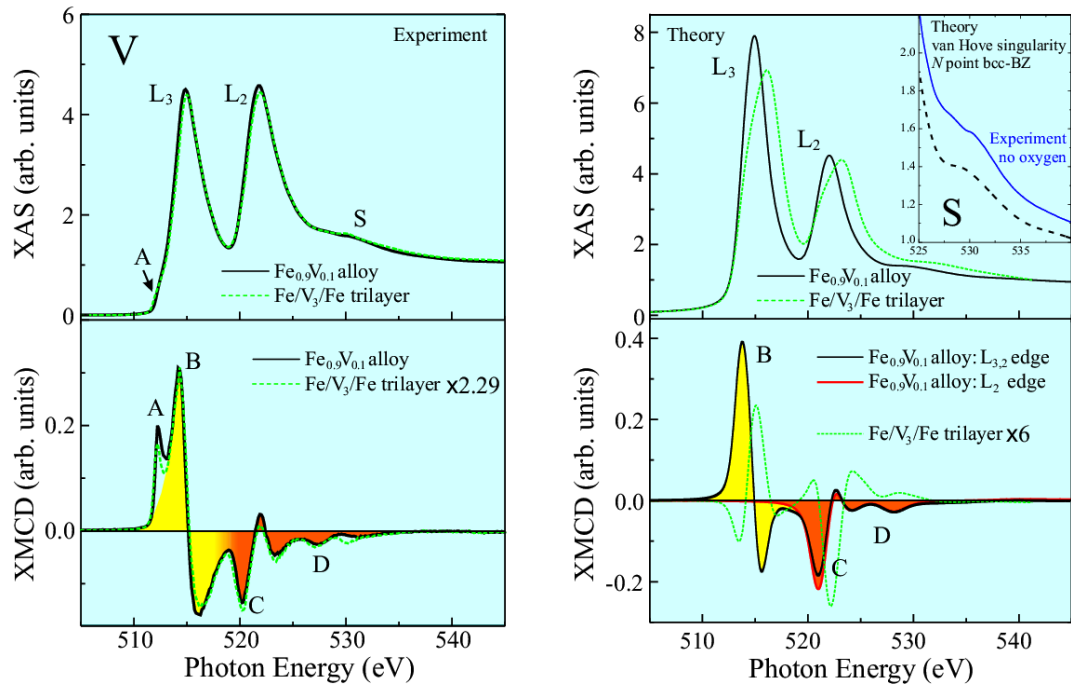


**Fig. 3:** Comparison of the experimental XAS and corresponding XMCD at the V  $L_{2,3}$  edges (left panel) to the SPR-KKR calculations (right panel) for an Fe/V alloy and an Fe/V layered structure [7].

red in Fig. 3). Only the pre-edge feature (A) cannot be reproduced. It most likely stems from a multiplet feature. This is supported by comparable atomic-multiplet calculations of  $3d$  ions in a crystal field [8]. Therefore, similar to Ni, the inspection of the XAS and XMCD with the help of theory indicates some localized character of the  $3d$  electrons.

For the experimental standard the band structure calculations provide the induced spin and orbital moments being  $\mu_s = -1.01 \mu_B$  and  $\mu_l = 0.02 \mu_B$  for V. The results are in agreement with an independent polarized neutron study [9]. For the Fe/V trilayers the deviations of the calculated XAS and XMCD is mostly related to differences in the band structure, see [7]. However, this allowed us to determine the vanadium moments in an absolute manner by using an experimental standard, avoiding the application of the “traditional” approaches like the sum rules, which lead to erroneous results for the early  $3d$  TMs as demonstrated in [7].

## References

- [1] A. Scherz, E. K. U. Gross, H. Appel, C. Sorg, K. Baberschke, H. Wende, and K. Burke, *Phys. Rev. Lett.* **95**, 253006 (2005).
- [2] J. Schwitalla and H. Ebert, *Phys. Rev. Lett.* **80**, 4586 (1998).
- [3] A. Scherz, H. Wende, and K. Baberschke, *Appl. Phys. A* **78**, 843 (2004).
- [4] H. Wende, *Rep. Prog. Phys.* **67**, 2105 (2004).
- [5] A. Scherz, P. Pouloupoulos, H. Wende, G. Ceballos, K. Baberschke, and F. Wilhelm, *J. Appl. Phys.* **91**, 8760 (2002).
- [6] H. Ebert, *Rep. Prog. Phys.* **59**, 1665 (1996).
- [7] A. Scherz, H. Wende, K. Baberschke, J. Minar, D. Benea, and H. Ebert, *Phys. Rev. B* **66**, 184401 (2002).
- [8] G. van der Laan and B. T. Thole, *Phys. Rev. B* **43**, 13401 (1991).
- [9] I. Mirebeau, G. Parette, and J. W. Cable, *J. Phys. F: Met. Phys.* **17**, 191 (1987).

## Systematics of the induced magnetic moments in 5d layers and the violation of Hund's third rule

F. Wilhelm<sup>1</sup>, P. Poulopoulos<sup>1</sup>, H. Wende<sup>1</sup>, A. Scherz<sup>1</sup>, K. Baberschke<sup>1</sup>, M. Angelakeris<sup>2</sup>, N. K. Flevaris<sup>2</sup>, A. Rogalev<sup>3</sup>.

<sup>1</sup> Institut für Experimentalphysik, Freie Universität Berlin

<sup>2</sup> Aristotle University of Thessaloniki (Greece)

<sup>3</sup> European Synchrotron Radiation Facility (ESRF), Grenoble (France)

Magnetic multilayers are formed by periodic alternation of ferromagnetic and non-magnetic layers. Nowadays, these structures are used in magnetic storage devices, e.g. in read heads of hard disks, or as possible candidates for magnetic random access memories. For these systems a large fraction of the atoms are located at the interfaces, and two-dimensional directly-coupled non-magnetic layers are formed facing a ferromagnetic layer. This special configuration allows the tailoring of magnetic moments, magnetic anisotropy, magneto-optics and magneto-transport properties for each application. Here we focus on the induced magnetic moments of the 5d elements in magnetic multilayers. While induced magnetic moments in alloys have been studied previously, it was difficult to separate the small induced

moments from the total magnetization in ultrathin magnetic structures due to the lack of element-specific techniques with monolayer sensitivity. The experimental technique that allows one to study the induced magnetism is X-ray magnetic circular dichroism (XMCD), which provides quantitative information on spin and orbital magnetic moments of the absorbing atom in both amplitude and direction. It is demonstrated that the induced magnetism in magnetic multilayers may be radically different from that in alloys due to the different geometry and electronic structure, and so unexpected phenomena may be observed.

In Fig. 1 we plot the normalized X-ray absorption (XAS) and X-ray magnetic circular dichroism (XMCD) spectra at the  $L_{3,2}$  edges of W in a Fe/W magnetic multilayer with three monolayers of W in each period. The spectra were recorded at the ID12 beamline of the ESRF using the total fluorescence detection mode. The XMCD signals are very small compared to XAS, as the large scaling factor of 50 reveals. However, the signal-to-noise ratios are still large due to the high photon flux and degree of polarization offered at the ESRF. By knowing the direction of the magnetic field and the helicity of the beam we conclude that W is polarized antiparallel to Fe, in agreement with previous reports for alloys. This behavior is consistent with the general trend for the transition metals with a less-than-half-filled  $d$  shell. However, contrary to the third Hund's rule, the W spin  $\mu_s$  and orbital  $\mu_L$  magnetic moments are

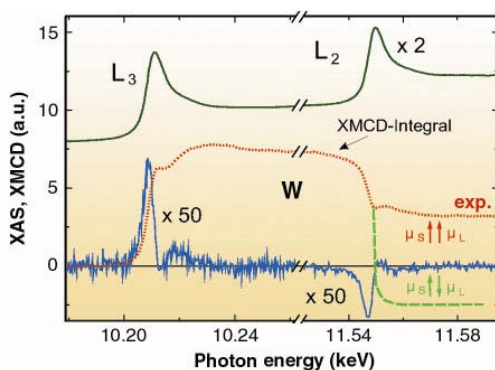
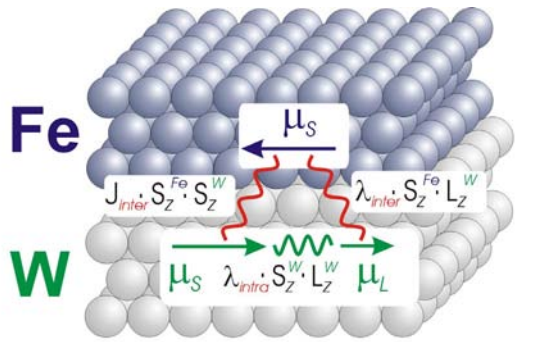


**Fig. 1:** Normalized XAS (top) and XMCD (bottom) spectra at the  $L_{3,2}$  edges of W. For better illustration, the XMCD spectra have been multiplied by 50, while the XAS spectra have been shifted vertically. The XMCD integrals (dotted line: measured, dashed line: hypothetical) serve to visualise the relative orientation of  $\mu_L$  and  $\mu_s$ .



$$J_{\text{inter}} \cdot S_z^{\text{Fe}} \cdot S_z^{\text{W}} > \lambda_{\text{inter}} \cdot S_z^{\text{Fe}} \cdot L_z^{\text{W}} > \lambda_{\text{intra}} \cdot S_z^{\text{W}} \cdot L_z^{\text{W}}$$

**Fig. 2:** Schematic representation of the Fe/W layers and the various type of interactions that one needs in order to describe the violation of the third Hund's rule in a simple atomic model.

coupled in parallel. This is visualized via the XMCD integrals in Fig. 1. The measured integral (dotted line) does not change sign, showing that  $\mu_L/\mu_S > 0$ . For a negative sign (antiparallel coupling) the XMCD integral should change sign as the hypothetical dashed line of Fig. 1 reveals. This can not be understood in a single atomic picture. One has rather to consider interatomic spin-orbit coupling. We consider three types of possible interactions: (i) the largest is the spin-spin coupling between Fe and W,  $J_{\text{inter}} \cdot S_z^{\text{Fe}} \cdot S_z^{\text{W}}$ ; (ii) in addition, we have the classical intra-atomic spin-orbit coupling for W,  $\lambda_{\text{intra}} \cdot S_z^{\text{W}} \cdot L_z^{\text{W}}$ . If this was all,  $\mu_L$  should be antiparallel to  $\mu_S$ . To understand the opposite observation (parallel coupling) one may propose (iii) an interatomic Fe-W spin-orbit interaction  $\lambda_{\text{inter}} \cdot S_z^{\text{Fe}} \cdot L_z^{\text{W}}$ . As shown in Fig. 2, we conclude the inequality that the interatomic spin-orbit coupling is smaller than the exchange coupling but larger than the intra-atomic spin-orbit coupling of W. Such an effect is attributed to hybridisation effects at the Fe/W interface [1].

Results for the ratio  $\mu_L/\mu_S$  and the total moment  $\mu_{\text{tot}}$  derived by application of the sum rules for the beginning (W) and the end (Ir, Pt) of the  $5d$  series in magnetic multilayers are listed in Table 1 [2].  $\mu_L/\mu_S$  is significant

	<i>Pt</i>	<i>Ir</i>	<i>W</i>
$\mu_L/\mu_S$	0.2-0.3	0.10	0.09
$\mu_{\text{tot}}$	0.17-0.29	0.2	-0.2

**Table 1:** Data for the ratio  $\mu_L/\mu_S$  and the total magnetic moment  $\mu_{\text{tot}}$  (in  $\mu_B/\text{atom}$ ) for three  $5d$  elements (Pt, Ir, W).

only for Pt ( $\sim 0.2-0.3$ ), revealing a large orbital magnetism contribution. Moreover, we find  $\mu_{\text{tot}} \sim 0.2 \mu_B/\text{atom}$  for both Ir and W, which is in fair agreement with recent *ab initio* calculations.

In conclusion, systematic trends for the induced magnetism of elements of the  $5d$  series in multilayers are shown. These multilayers may serve as a demonstration of a prototype experimental case of a 'violation' of the pure intra-atomic Hund's rule picture, which can be understood via the existence of strong interatomic interactions at the  $3d/5d$  interfaces.

## References

- [1] F. Wilhelm, P. Pouloupoulos, H. Wende, A. Scherz, K. Baberschke, M. Angelakeris, N. K. Flevaris, and A. Rogalev, *Phys. Rev. Lett.* **87**, 207202 (2001).
- [2] P. Pouloupoulos, A. Scherz, F. Wilhelm, H. Wende, and K. Baberschke, *phys. stat. sol. (a)* **189**, 293 (2002).

## Direct observation of orbital magnetism in cubic solids

W. D. Brewer<sup>1</sup>, A. Scherz<sup>1</sup>, C. Sorg<sup>1</sup>, H. Wende<sup>1</sup>, K. Baberschke<sup>1</sup>, P. Bencok<sup>2</sup>, S. Frota-Pessôa<sup>3</sup>

<sup>1</sup> Institut für Experimentalphysik, Freie Universität Berlin

<sup>2</sup> European Synchrotron Radiation Facility (ESRF), Grenoble (France)

<sup>3</sup> Universidade de São Paulo (Brazil)

The magnetic moment of the 3d transition metals consists of two contributions: the spin moment  $\mu_s$  and the orbital moment  $\mu_\ell$ . However, an enormous amount of literature discusses the magnetic phenomena in terms of spin magnetism only. From a different point of view the orbital magnetism may be even more important: a finite orbital momentum  $\ell$  is an indication of a non-spherical charge distribution, be it for an atom or in solids. Such a non-spherical charge distribution is the primary source for magnetic anisotropy energy (MAE), which is important e.g. for the fabrication of hard or soft magnets and new magnetic storage devices. Often it may be sufficient to treat in theory the spin-orbit-coupling (SOC) as a weak perturbation. However, strictly speaking magnetism is a relativistic effect and may require a fully relativistic treatment.

Nowadays the investigation of 3d transition metal clusters on surfaces has become very important in view of magnetic

nanotechnology. “Giant magnetic anisotropy” has been recently reported [1]. Several groups have shown that on surfaces or in nanoclusters one observes giant orbital magnetic moments and MAE, respectively, confirming an old theory by L. Néel that the symmetry breaking at surfaces keeps the orbital momentum “alive”. For 3d elements in three-dimensional bulk materials the opposite limit seems to hold: the research in the 1970’s and 1980’s on dilute alloys [2] focused mostly on the spin magnetism, e.g. the Kondo Hamiltonian ( $JS \cdot \sigma$ ). This is in agreement with a standard exercise in solid state physics showing that the expectation value of  $L_z$  vanishes in cubic symmetry ( $\langle L_z \rangle = 0$ ). Prototype cases in experiment and theory were e.g. Mn, Fe, and Co impurities in cubic Cu, Ag, and Au host materials.

The present work shows that under certain conditions orbital magnetism survives even in cubic symmetry [3]. X-ray magnetic circular dichroism (XMCD) at the  $L_{2,3}$  edges is

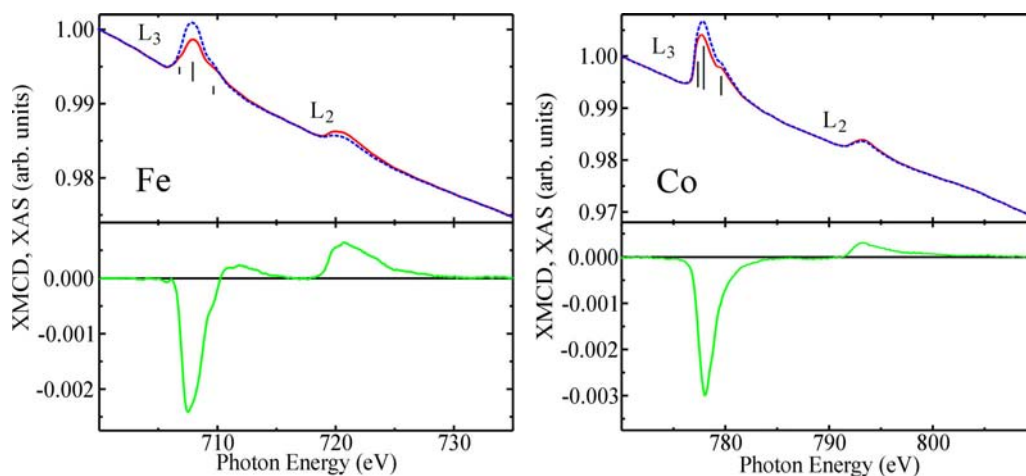


**Fig. 1:** XAS (upper plots) for left and right circular polarization and XMCD spectra (lower plots) of  $\sim 1$  at.% Fe and Co in Au at the  $L_{2,3}$  edges. Note the strongly reduced relative intensity at the  $L_2$  edge of Co, indicating its enhanced orbital moment [3].

an excellent handle to study the ratio  $\mu_\ell / \mu_s$ . Plenty of evidence exists from hyperfine interaction measurements that the orbital magnetism may survive in cubic structures. However, only the 3<sup>rd</sup> generation synchrotron facilities made it possible to measure  $\mu_s$  and  $\mu_\ell$  in a direct way. A very high sensitivity is needed because dilute alloys with  $\sim 1\%$  impurities correspond to 1/10 of an atomic monolayer of 3d ions. Moreover, to measure dilute paramagnets, a large magnetic field and low temperatures are required. All this is available at beamline ID8 of the ESRF. Fig. 1 shows the normalized XAS of Fe and Co impurities and the corresponding XMCD. The spectra were measured in an external field  $B = 7$  T at temperatures down to  $T = 4$  K at normal incidence of the X-rays. A complete analysis via the sum rules [4] was applied to determine the ratio  $\mu_\ell / \mu_s$ . Here we use a simplified reasoning: For spin magnetism only, theory predicts a ratio 1:1 of the integrated XMCD areas at the  $L_3$  and the  $L_2$  edge. If the experimental ratio differs from this (obviously for Co), a finite orbital moment survives. The experimental numbers are given in Fig. 2 (circles). The experiments find that  $\mu_\ell / \mu_s$  is almost zero for Cr, Mn, and Fe in Au, but 33% for Co/Au. Can this be understood? Is this in conflict with the quenching of orbital momentum in cubic symmetry? Some insight is given by *ab initio* calculations (Fig. 2, triangles and squares). The calculations also yield a vanishing ratio for all 3d elements except Co. Two values for  $\mu_\ell / \mu_s$  are given: 15 % and 70 %. The lower number was calculated scalar relativistically including SOC only as a weak perturbation (3<sup>rd</sup> Hund's rule). The larger number takes also into account orbital polarization (OP, 2<sup>nd</sup> Hund's rule).

These XMCD experiments on paramagnetic dilute alloys of Co/Au are the first direct measurements of the 3d magnetic moment which show that in cubic symmetry

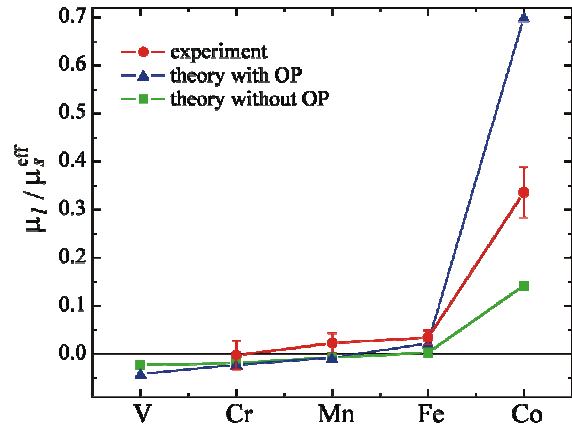


**Fig. 2:** Systematics of the ratio  $\mu_\ell / \mu_s$  of the 3d series as impurities in Au [3].

an appreciable amount of orbital magnetism may survive. The text book arguments about the quenching of orbital moments are derived on the basis of weak SOC, distinct separation of  $t_{2g}$  and  $e_g$  states as well as no intermixing. A strong hybridization of the 3d impurity levels with the 5d host band structure and the delicate balance of the spin-up and spin-down filling of the 3d impurity bands can indeed explain this experimental finding. Nowadays, Co atoms or clusters on Cu(001) surfaces may be used to study the Kondo-effect on surfaces, e.g. by means of STM. For future work of this kind it will be relevant not only to apply the classic theoretical models of spin magnetism [2], but to consider also a surviving orbital magnetic moment in these multi-particle effects.

## References

- [1] P. Gambardella et al., ESRF Highlights 2003, p. 85.
- [2] G. Rado and H. Suhl (Eds.), "Magnetism", Vol. 5, Academic Press, New York/London (1973).
- [3] W. D. Brewer et al., Phys. Rev. Lett. **93**, 077205 (2004).
- [4] B. T. Thole, P. Carra, F. Sette, and G. van der Laan, Phys. Rev. Lett. **68**, 1943 (1992); P. Carra, B. T. Thole, M. Altarelli, and X. Wang, Phys. Rev. Lett. **70**, 694 (1993).

## Monolayer-resolved magnetic moment profile in Ni/Pt multilayers

F. Wilhelm<sup>1</sup>, P. Pouloupoulos<sup>1</sup>, G. Ceballos<sup>1</sup>, H. Wende<sup>1</sup>, K. Baberschke<sup>1</sup>, P. Srivastava<sup>2</sup>,  
D. Bena<sup>3</sup>, H. Ebert<sup>3</sup>, M. Angelakeris<sup>4</sup>, N. K. Flevaris<sup>4</sup>, D. Niarchos<sup>5</sup>, A. Rogalev<sup>6</sup>,  
N. B. Brookes<sup>6</sup>

<sup>1</sup> *Institut für Experimentalphysik, Freie Universität Berlin*

<sup>2</sup> *Indian Institute of Technology, New Delhi (India)*

<sup>3</sup> *Institut für Physikalische Chemie, Ludwig-Maximilians-Universität München*

<sup>4</sup> *Aristotle University of Thessaloniki (Greece)*

<sup>5</sup> *National Centre for Scientific Research, Athena (Greece)*

<sup>6</sup> *European Synchrotron Radiation Facility (ESRF), Grenoble (France)*

Magnetic multilayers constitute a new class of materials exhibiting novel phenomena for basic and applied science. Usually, they are produced by a periodic repetition in one dimension of a unit cell consisting of a small number of monolayers (ML) of a ferromagnetic and a non-ferromagnetic element (Fig. 1). Hybridization effects, strain, and reduced coordination numbers at the interfaces of multilayers modify the magnetic behavior with respect to the bulk. In addition, remarkably, the non-ferromagnetic element acquires an induced magnetic moment. The magnetic properties of multilayers depend essentially on the layer-dependent distribution of the magnetic moments of both elements. Only recently, progress in experimental techniques with element specificity and theory allows us to study interface magnetism at the ML limit.

Here, we have selected Ni/Pt multilayers because (i) they have sharp interfaces at the ML limit, and (ii) are of technological importance as candidates for magneto-optic recording. X-ray magnetic circular dichroism (XMCD) experiments on a set of Ni<sub>n</sub>/Pt<sub>m</sub> multilayers with *n* and *m* between 2 and 13 ML were performed at 10 K under an applied field of 2–5 T. The Pt *L*<sub>2,3</sub>-edges were recorded at the hard x-ray regime at the ID12A beamline of the ESRF by using the fluorescence detection scheme. The Ni *L*<sub>2,3</sub>-edges were recorded at the soft x-rays at the

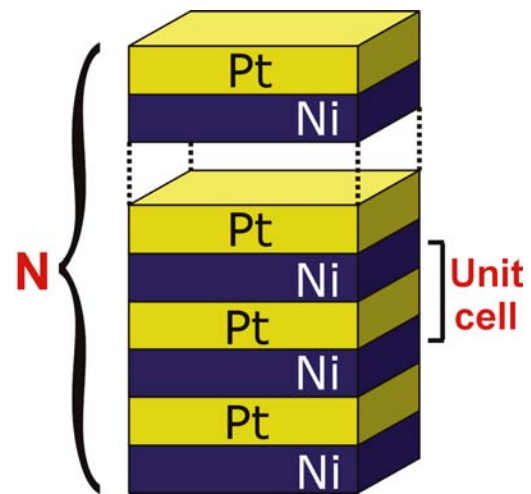


**Fig. 1:** Schematic representation of a Ni/Pt multilayer consisting of *N* repetitions of a unit cell. The unit cell is also indicated.

ID12B beamline by using the total electron yield detection mode. Intense dichroic signals were recorded for all multilayers. In Fig. 2 (a) and (b) we show XMCD signals at the Pt and Ni edges for a Ni<sub>2</sub>/Pt<sub>2</sub> multilayer, respectively. The determination of Ni and Pt magnetic moments was done by application of the sum-rules. In addition to the determination of magnetic moments, XMCD allows for the separation into spin and orbital contributions [1]. We probed a strong anisotropy in the orbital moment of Ni of about 25% for the Ni<sub>2</sub>/Pt<sub>2</sub> multilayer to be the source of perpendicular anisotropy, which is a demand for applications [2].

The XMCD data allowed us to construct a monolayer-resolved magnetic moment pro-

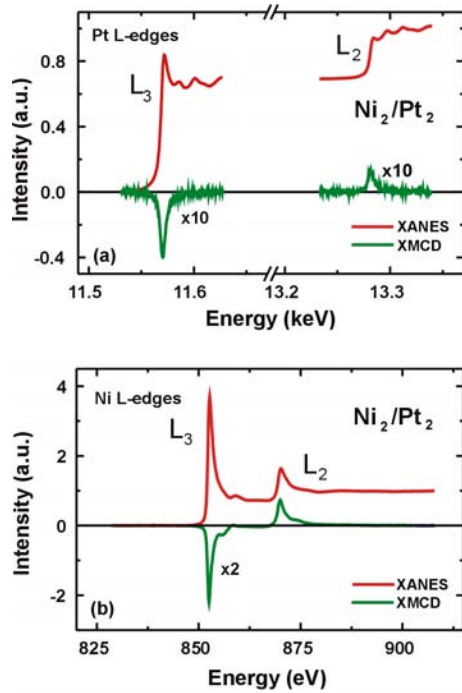


**Fig. 2:** XMCD and XANES spectra recorded at the  $L_{2,3}$  edges of (a) Pt and (b) Ni in a  $\text{Ni}_2/\text{Pt}_2$  multilayer. The measurements have been performed at normal incidence,  $T = 10$  K and  $H = 2$  T. Spectra were corrected for the degree of circular polarization.

file for both Pt and Ni. Such a profile for a  $\text{Ni}_6/\text{Pt}_5$  multilayer is shown in Figure 3 (a). At the Ni/Pt interface, Pt acquires a large induced magnetic moment of about  $0.29 \mu_B/\text{atom}$ . The moment profile on the Pt-side decays sharply from the interface. The Ni interface magnetic moment of about  $0.32 \mu_B/\text{atom}$  is strongly reduced compared to bulk Ni. The second Ni layer from the interface possesses practically the bulk moment. Figure 3 (b) shows *ab initio* theoretical calculations using the tight binding linearized muffin-tin orbital (TB-LMTO) method. Qualitatively, for both elements, theory shows the same trends as the experiment: Hybridization effects are mostly localized at the interface [3].

In conclusion, a complete monolayer-resolved magnetic moment profile is presented for the first time for both constituents of a magnetic multilayer in one experiment

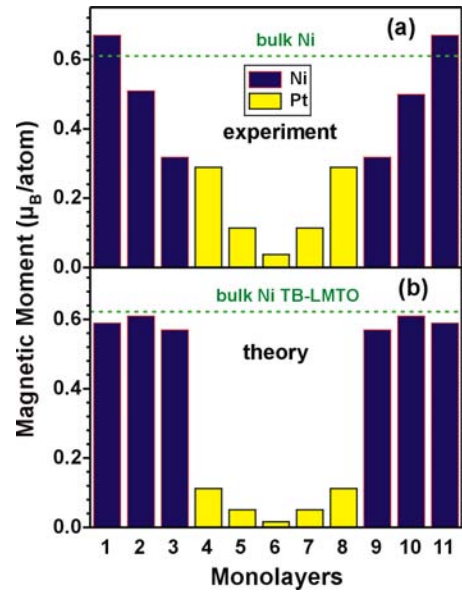


**Fig. 3:** (a) Experimental and (b) theoretical magnetic moment profile for the unit cell in a  $\text{Ni}_6/\text{Pt}_5$  multilayer [3].

and in theory. It gives new insight into the fundamental understanding of interface magnetism.

## References

- [1] P. Pouloupoulos, F. Wilhelm, H. Wende, G. Ceballos, K. Baberschke, D. Benea, H. Ebert, M. Angelakeris, N. K. Flevaris, A. Rogalev, and N. B. Brookes, *J. Appl. Phys.* **89**, 3874 (2001).
- [2] F. Wilhelm, P. Pouloupoulos, P. Srivastava, H. Wende, M. Farle, K. Baberschke, M. Angelakeris, N. K. Flevaris, W. Grange, J.-P. Kappler, G. Ghiringhelli, and N. B. Brookes, *Phys. Rev. B* **61**, 8647 (2000).
- [3] F. Wilhelm, P. Pouloupoulos, G. Ceballos, P. Srivastava, H. Wende, K. Baberschke, D. Benea, H. Ebert, M. Angelakeris, N. K. Flevaris, D. Niarchos, A. Rogalev, and N. B. Brookes, *Phys. Rev. Lett.* **85**, 413 (2000).

## Probing the antiferromagnetic spin structure of ultrathin FeMn films by photoelectron emission microscopy

W. Kuch<sup>1</sup>, L. I. Chelaru<sup>2</sup>, F. Offt<sup>2</sup>, J. Wang<sup>2</sup>, M. Kotsugi<sup>2</sup>, J. Kirschner<sup>2</sup>

<sup>1</sup> *Institut für Experimentalphysik, Freie Universität Berlin*

<sup>2</sup> *Max-Planck-Institut für Mikrostrukturphysik, Halle*

Antiferromagnets are an important class of materials for several applications. Ultrathin antiferromagnetic films are frequently employed in magnetic thin film devices like magnetoresistive sensors in magnetic hard disk read heads to manipulate the magnetic properties of adjacent ferromagnetic layers. The knowledge of the spin structure of the antiferromagnetic layer is crucial for both the design and operation of these devices as well as the fundamental understanding of the magnetic interaction between ferromagnetic and antiferromagnetic layers, often referred to as exchange bias effect.

In ferromagnetic materials the spins of the individual atoms are subject to long range parallel order, giving rise to a macroscopically observable magnetization. In antiferromagnetic materials, in contrast, the atomic moments—although also long range ordered—average to zero within a few atomic distances, and are thus much more difficult to detect. The spin structure of many antiferromagnetic materials has been investigated in bulk samples already decades ago by methods like neutron scattering or Mössbauer spectroscopy. The spin structure of ultrathin antiferromagnetic films with thicknesses of only a few nanometers, however, has mainly remained concealed, because these methods require thick samples to obtain sufficient signal. In atomically thin films the spin structure may be altered significantly compared to bulk materials by the enhanced influence of the interfaces and the reduced dimensionality.

Photoelectron emission microscopy

(PEEM) with X-ray magnetic circular dichroism (XMCD) as magnetic contrast mechanism was used to study the magnetic interface coupling in single-crystalline stacks containing ultrathin antiferromagnetic FeMn layers that are sandwiched between two ferromagnetic layers. XMCD-PEEM detects the difference in absorption of circularly polarized x-rays that are resonantly tuned to elemental absorption edges between parallel and antiparallel alignment of sample magnetization and helicity of the exciting x-rays. By assembling trilayer stacks that have non-collinear axes of magnetization of the ferromagnetic layers the collinearity of the antiferromagnetic spin structure can be probed.

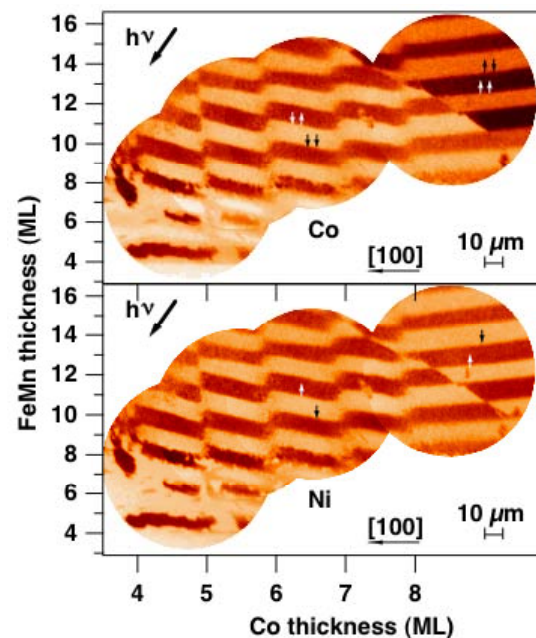


**Fig. 1:** Element-resolved magnetic domain images of 3 ML Co/15 ML Ni/FeMn (wedge)/Co (wedge)/Cu(001). Top: domain image at the Co  $L_3$  edge, bottom: domain image at the Ni  $L_3$  edge.

Single-crystalline, virtually unstrained fcc FeMn films with no indications for chemical order were obtained by deposition on a Cu(001) single crystal substrate [1]. Scanning tunneling microscopy measurements had revealed that the FeMn films grow on Cu(001) in a near-perfect layer by layer-mode in which the surface roughness is confined to monatomic islands or vacancy islands [2] due to the low lattice mismatch between FeMn and Cu ( $\approx 0.4\%$ ). Some of the layers were prepared as wedges suitable for microscopic imaging in order to explore the thickness dependence of the magnetic domain patterns. The XMCD-PEEM measurements were performed using synchrotron radiation at the UE56/2-PGM2 beamline at BESSY.

Fig. 1 shows element-resolved magnetic domain images of a sample in which an FeMn wedge (thickness increasing from bottom to top, left axis) was sandwiched between a Co wedge as the bottom ferromagnetic layer (thickness increasing from left to right, bottom axis), and a top ferromagnetic layer consisting of 15 atomic monolayers (ML) of Ni and 3 ML Co. The top panel shows the magnetic domain image obtained at the Co  $L_3$  absorption edge; its signal is therefore composed by contributions of both the bottom and top ferromagnetic layers, since both of them contain Co. The bottom panel shows the magnetic domain pattern obtained at the Ni  $L_3$  edge, which represents the domain pattern of the top ferromagnetic layer only. Regular stripes with alternating parallel and antiparallel coupling between the two ferromagnetic layers across the antiferromagnetic FeMn spacer layer are recognized as the FeMn thickness is increased. The period of 2 ML in FeMn thickness indicates direct exchange coupling through the antiferromagnetic spacer layer. In addition to these stripes, a sawtooth-like wiggling of the phase of this periodic

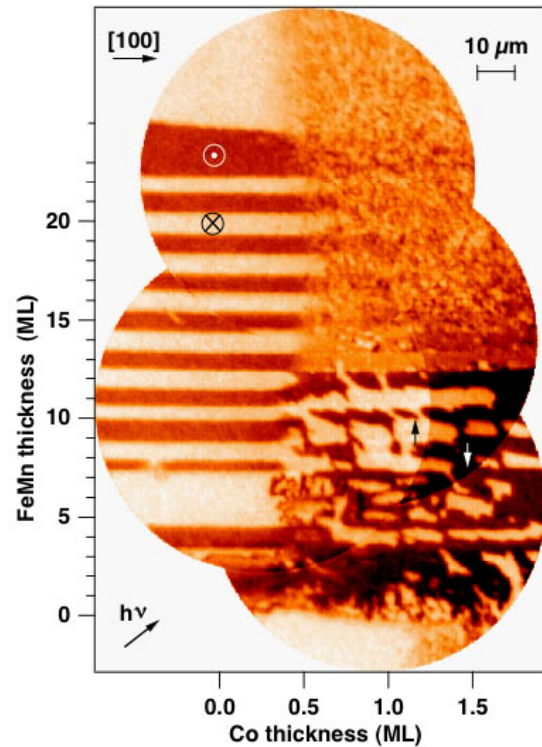


**Fig. 2:** Magnetic domain image at the Ni  $L_3$  edge of Co (wedge)/15 ML Ni/FeMn (wedge)/15 ML Ni/Cu(001). In the left part of the image the magnetization of the top layer is perpendicular to the film plane, while it is in-plane for Co thicknesses above 0.5 ML.

interlayer coupling is observed as the Co bottom layer thickness is increased. It is attributed to the periodic modulation of the bottom interface roughness due to the layer-by-layer growth of the films.

Fig. 2 shows the magnetic domain pattern at the Ni  $L_3$  edge of a trilayer in which an FeMn wedge (left axis) is sandwiched between 15 ML Ni on the bottom and Co (wedge, bottom axis)/15 ML Ni on the top. The bottom layer had been magnetized into a single domain state by an external magnetic field after deposition. The image thus represents the domain pattern of the top Co/Ni layer. In the left part of the image, for zero or low Co thickness, a stripe-like domain pattern with a stripe period of 2 ML FeMn thickness as before is observed at FeMn thicknesses above 9 ML. Here the magnetization directions of the bottom and top fer-

romagnetic layers are perpendicular to the film plane, with alternating parallel and anti-parallel alignment between the two ferromagnetic layers. At Co thicknesses above 0.5 ML the magnetization of the top ferromagnetic layer turns into the film plane. The small domains observed in this region for FeMn thicknesses above 12 ML show that in addition to an oscillatory coupling of the spin component perpendicular to the film plane, the spin component in the plane experiences a laterally fluctuating pinning [3]. This provides direct experimental evidence that a three-dimensional non-collinear antiferromagnetic spin structure, reminiscent of that of bulk FeMn, must be also present in its near-two dimensional realization. Such a spin structure, the so-called  $3Q$  structure, is schematically depicted in Fig. 3. It is characterized by four different sublattices in which the spins point along four different  $\langle 111 \rangle$  directions.

This interesting result has also major implications on theoretical models of the interaction between antiferromagnets and ferromagnets that try to describe the exchange bias effect.

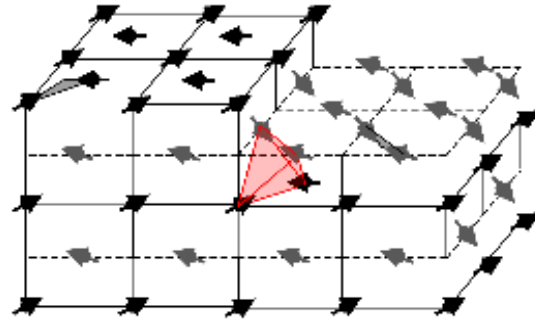


**Fig. 3:** Sketch of the  $3Q$  non-collinear antiferromagnetic spin structure. Monatomic steps at the (001) surface exhibit  $90^\circ$  different axes of the spin component in the film plane, and opposite sign of the spin component perpendicular to the film plane.

## References

- [1] F. Offi, W. Kuch, and J. Kirschner, Phys. Rev. B **66**, 064419 (2002).
- [2] W. Kuch, L. I. Chelaru, and J. Kirschner, Surf. Sci. **566–568**, 221 (2004).
- [3] W. Kuch, L. I. Chelaru, F. Offi, J. Wang, M. Kotsugi, and J. Kirschner, Phys. Rev. Lett. **92**, 017201 (2004).

## Exploring magnetization reversal dynamics in magnetic multilayers with temporal, spatial and layer resolution

W. Kuch<sup>1</sup>, K. Fukumoto<sup>1</sup>, J. Vogel<sup>2</sup>, Y. Pennec<sup>2</sup>, S. Pizzini<sup>2</sup>, M. Bonfim<sup>2</sup>,  
J. Camarero<sup>3</sup>, J. Kirschner<sup>4</sup>

<sup>1</sup> *Institut für Experimentalphysik, Freie Universität Berlin*

<sup>2</sup> *Laboratoire Louis Néel, CNRS Grenoble (France)*

<sup>3</sup> *Universidad Autónoma de Madrid (Spain)*

<sup>4</sup> *Max-Planck-Institut für Mikrostrukturphysik, Halle*

How long does it take to load this text from the hard disk of your computer? With the current technology this depends on the time needed to turn the magnetization of a soft magnetic layer in the read head of the hard disk drive. A magnetoresistive spin valve read head sensor, as it is nowadays commonly used in magnetic hard disk read heads, consists of a trilayer system in which two ultrathin ferromagnetic layers are separated by a non-magnetic spacer layer. The magnetization direction of one of the magnetic layers is switched by the magnetic bits on the disk over which the head passes, leading to a change in electrical resistance. Presently, read and write times approach one nanosecond, corresponding to 1 GHz frequency. Controlling and understanding the magnetization reversal dynamics in magnetic thin films is thus a major issue for accelerating the speed at which data can be stored and read back.

Only very few experimental techniques can address the microscopic magnetization reversal behavior of the different magnetic layers in a spin valve separately. One of them is photoelectron emission microscopy (PEEM) with synchrotron radiation, which employs x-ray magnetic circular dichroism (XMCD) as magnetic contrast mechanism [1]. Because of the element selectivity of XMCD, different magnetic layers in a multilayered stack can be imaged separately. Time resolution is obtained using a pump-probe approach (Fig. 1). Magnetic field pulses provided by a microcoil and a fast power supply

(the pump) are synchronized with the X-ray photon pulses from BESSY (the probe) [2]. Images are acquired for different constant delays between pump and probe, i.e., at different times before, during, or after the application of the magnetic field pulses. In this way the magnetization dynamics of each magnetic layer can be visualized separately with a time resolution limited by the X-ray pulse width (about 60 ps).

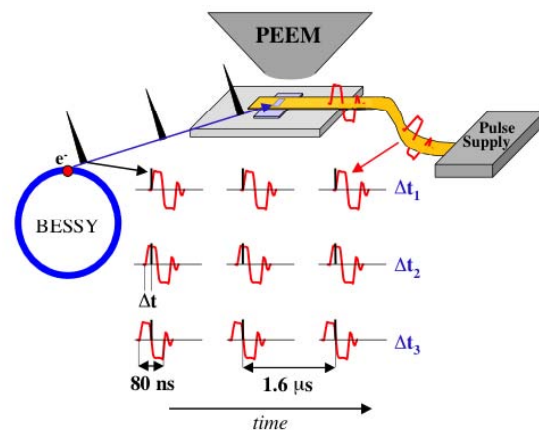


**Fig. 1:** Sketch of the stroboscopic time-resolved magnetic imaging technique. Current pulses with a period of  $1.6 \mu\text{s}$  from a fast pulse power supply induce magnetic field pulses of several nanoseconds (red curves) in a microcoil close to the sample position. Synchronized X-ray pulses of about 60 ps length hit the sample at a variable time delay  $\Delta t$  relative to the magnetic pulses [2]. Electrons excited by these x-ray pulses are used to obtain dynamic stroboscopic and layer-resolved domain images in a photoelectron emission microscope (PEEM).

We have used the combined temporal, spatial, and layer resolution of time-resolved XMCD-PEEM to study the magnetization reversal dynamics of a 5 nm  $\text{Fe}_{20}\text{Ni}_{80}$ /4 nm Cu/5 nm Co spin valve on the nanosecond time scale. Fig. 2 shows stroboscopic domain images of the  $\text{Fe}_{20}\text{Ni}_{80}$  layer (domain contrast green/blue) and of the Co layer (domain contrast yellow/red). A 4 nm non-magnetic metallic Cu spacer layer separates the two magnetic layers. The images were acquired at different times during the application of short field pulses as indicated in the upper left

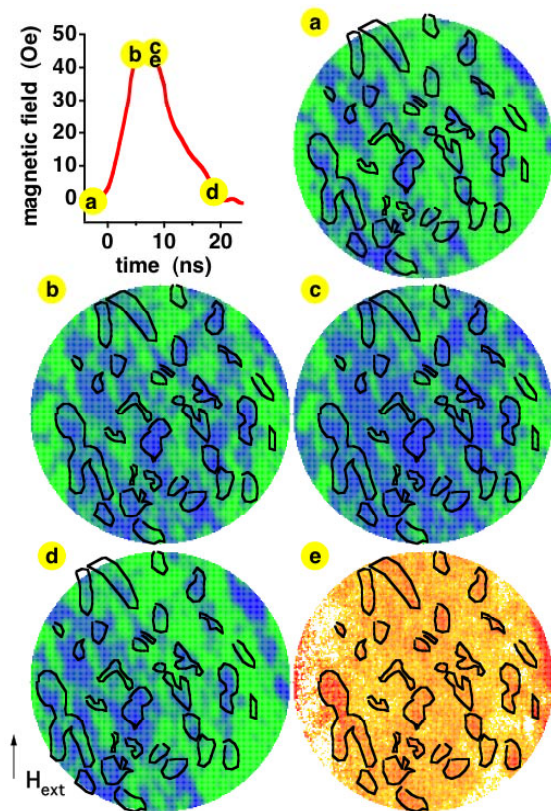


**Fig. 2:** Layer-resolved stroboscopic magnetic domain images of an  $\text{Fe}_{20}\text{Ni}_{80}$ /Cu/Co spin valve at different times during the periodic application of 18 ns-long magnetic field pulses (red curve). Panels a–d represent the magnetic domain pattern of the magnetically softer  $\text{Fe}_{20}\text{Ni}_{80}$  layer at the time delays indicated in the graph, panel e represents the magnetic domain pattern of the magnetically harder Co layer. Black lines in the images indicate the position of domain boundaries domains in the Co layer.

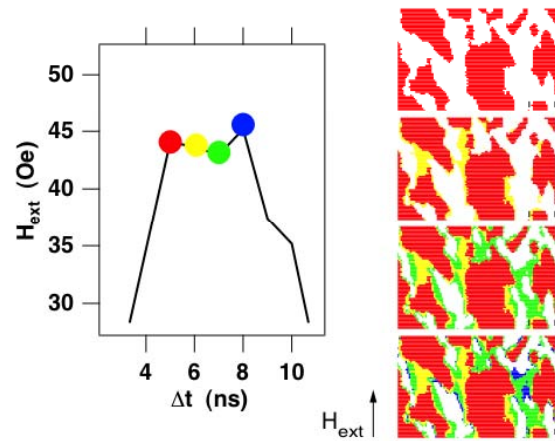


**Fig. 3:** Analysis of magnetic switching of the  $\text{Fe}_{20}\text{Ni}_{80}$  layer by expansion of domains during the plateau of the field pulse, shown in a magnified view on the left. The images at the right represent the expansion of the switched areas in one nanosecond time steps. Differently colored areas indicate the increase of switched domains at the times indicated by symbols of the corresponding color in the graph on the left.

panel. The magnetic pulse amplitude is adjusted so that the magnetization of the magnetically harder Co layer is not affected by these pulses, i.e., the Co layer shows the same pattern as in panel e for all times. In the  $\text{Fe}_{20}\text{Ni}_{80}$  layer, the magnetic field pulses favor the growth of the blue domains through propagation of domain walls (panels a–c). Upon reduction of the field, magnetic coupling to the Co layer leads to a shrinking of the blue domains (panel d), until after 1.6  $\mu\text{s}$  eventually the starting configuration is restored (panel a), and the same cycle starts over again.

Closer analysis of the domain wall motion of the  $\text{Fe}_{20}\text{Ni}_{80}$  layer during the plateau of the field pulse (between panels b and c of Fig. 2) is shown in Fig. 3. The right hand side shows the evolution of the  $\text{Fe}_{20}\text{Ni}_{80}$  domain pattern in time steps of 1 ns. Different colors represent the incremental expansion of regions of switched magnetization at the times indicated in the graph at the left hand side, which

shows a blow-up of the peak of the field pulses. Due to the domain wall energy, which opposes the expansion of small domains, the domain wall velocity is greatest in areas where two existing domains merge together [3]. Measurements on similar samples have shown that the magnetization reversal dynamics depends also on the competition between local magnetic interlayer coupling and intrinsic properties of the sample [4]. The combination of temporal, spatial and layer resolution makes this technique so extremely powerful for studying magnetization dynamics in layered magnetic systems.

## References

- [1] W. Kuch, *Appl. Phys. A* **76**, 665 (2003).
- [2] J. Vogel, W. Kuch, M. Bonfim, J. Camarero, Y. Pennec, F. Offi, K. Fukumoto, J. Kirschner, A. Fontaine, and S. Pizzini, *Appl. Phys. Lett.* **82**, 2299 (2003).
- [3] W. Kuch, J. Vogel, J. Camarero, K. Fukumoto, Y. Pennec, S. Pizzini, M. Bonfim, and J. Kirschner, *Appl. Phys. Lett.* **85**, 440 (2004).
- [4] J. Vogel, W. Kuch, J. Camarero, K. Fukumoto, Y. Pennec, M. Bonfim, S. Pizzini, F. Petroff, A. Fontaine, and J. Kirschner, *J. Appl. Phys.* **95**, 6533 (2004).

## Magnetic structures and phase transitions in nanostructured materials

*E. Weschke, E. Schierle, H. Ott, C. Schüßler-Langeheine, G. Kaindl*

*Institut für Experimentalphysik, Freie Universität Berlin*

Nanostructured magnetic materials play an important role for applications in sensors and magnetic storage media. The interesting properties of these materials arise from complex magnetic structures induced by interaction across non-magnetic layers or coupling at magnetic interfaces. Like other material properties, also magnetism on the nanoscale can deviate substantially from the behavior of the corresponding bulk materials.

The characterization of the magnetic structures and the understanding of these phenomena is a challenging task of fundamental research, the classical method for these studies is magnetic neutron diffraction. With the tunable, high-intensity photon beams at synchrotron radiation sources, however, a new method has emerged, which provides unprecedented sensitivity. Tuning the photon energy to the energy of a resonance excitation in a magnetic material can enhance the magnetic photon scattering cross section by several orders of magnitude, which allows

to study thin films and nanostructures [1].

The power of resonant x-ray scattering is illustrated in Fig. 1, showing a comparison of the two methods. The experiments were carried out on a thin film of the lanthanide metal holmium with a thickness of only 13 atomic layers. Holmium is characterized by a complex magnetic structure consisting of a helical arrangement of magnetic moments. This magnetic modulation gives rise to a diffraction peak as shown in Fig. 1. In case of neutron diffraction, a count rate of approximately 10 counts/sec is obtained (blue data), while x-rays at resonance yield an orders of magnitude higher count rate from the same sample (red data). This enormous intensity opens new fields of research in magnetic nanostructures hitherto not accessible.

However, the important resonance energies lie in the soft x-ray region, aggravating the application of the method. Due to the strong absorption of soft x-rays in air the entire experiment must be carried out in vacuum. This technical difficulty was overcome by the construction of a dedicated diffractometer financed by the BMBF. The instrument is based on a newly developed vacuum rotation feedthrough and operates even in ultrahigh vacuum. Another property of the soft x-rays associated with the resonance energies is the comparably large wavelength, of the order of 1–3 nm. This prevents to probe magnetic correlations on an atomic length scale, but is ideally suited for the study of ordering phenomena on the nanometer scale.

An important finite-size effect in magnetic materials is the observation of a reduced ordering temperature in thin films. This phe-

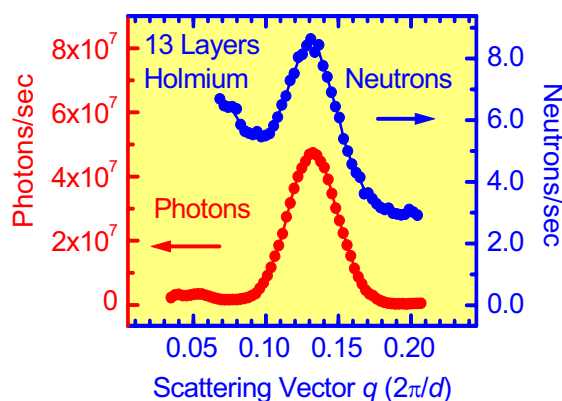


**Fig. 1:** Magnetic diffraction peaks recorded from a thin film of holmium metal with neutrons (blue) and with synchrotron radiation exploiting a holmium resonance. In the latter case, count rates are orders of magnitude higher than in case of neutrons.

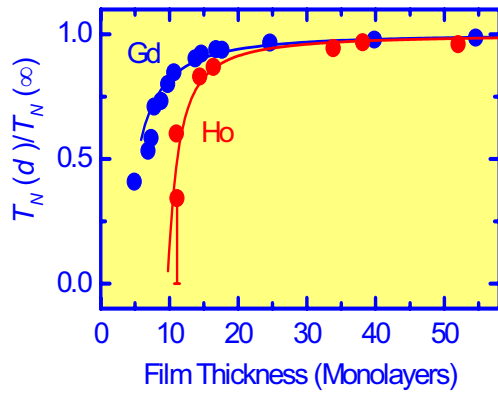


**Fig. 2:** Reduced magnetic ordering temperatures  $T_N(d)$  in magnetic films. For a complex antiferromagnet (holmium, red data)  $T_N(d)$  decreases faster with the film thickness than for a ferromagnet (gadolinium, blue data).

nomenon is due to the reduced number of magnetic neighbors at surfaces and interfaces, which becomes increasingly important with decreasing film thickness. This is well understood for ferromagnets, while little is known about systems with more complex magnetic structures.

For the helical antiferromagnet holmium, temperature-dependent studies of magnetic diffraction peaks as in Fig. 1 allow to probe the behavior across the magnetic phase transition and hence to determine the ordering temperature  $T_N$ . The thickness-dependent  $T_N$

of holmium is compared to that of the ferromagnetic lanthanide metal gadolinium in Fig. 2. In contrast to the latter,  $T_N$  in holmium already drops around 10 layers, establishing a close relationship to the bulk helix period [2].

The high sensitivity of the method provides high-quality diffraction patterns that allow to reconstruct real-space magnetic profiles in thin films with monolayer resolution. This is shown in Fig. 3 for a 20-layer-thick film of the antiferromagnetic semiconductor EuTe. Temperature-dependent profiles reveal that the magnetization does not decay in a homogeneous way, but that the outer layers of the film demagnetize faster than the inner layers, confirming a 30-years-old theoretical prediction [3]. Even details like chemical intermixing, which is important for the material properties of such layered systems, is readily obtained from the reconstruction of the diffraction patterns.

## References

- [1] E. Weschke, H. Ott, C. Schüßler-Langeheine, A. Yu. Grigoriev, R. Meier, and G. Kaindl, *Synchrotron Radiation News* **17**, No. 6, 11 (2004).

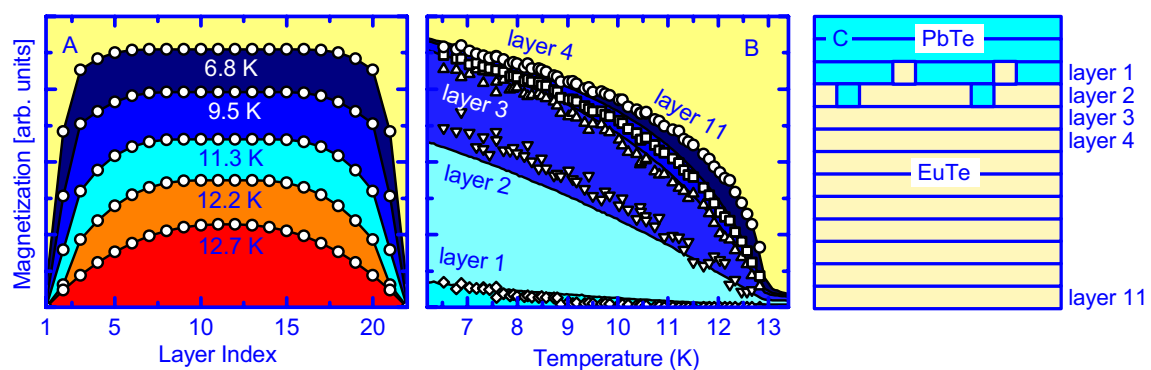
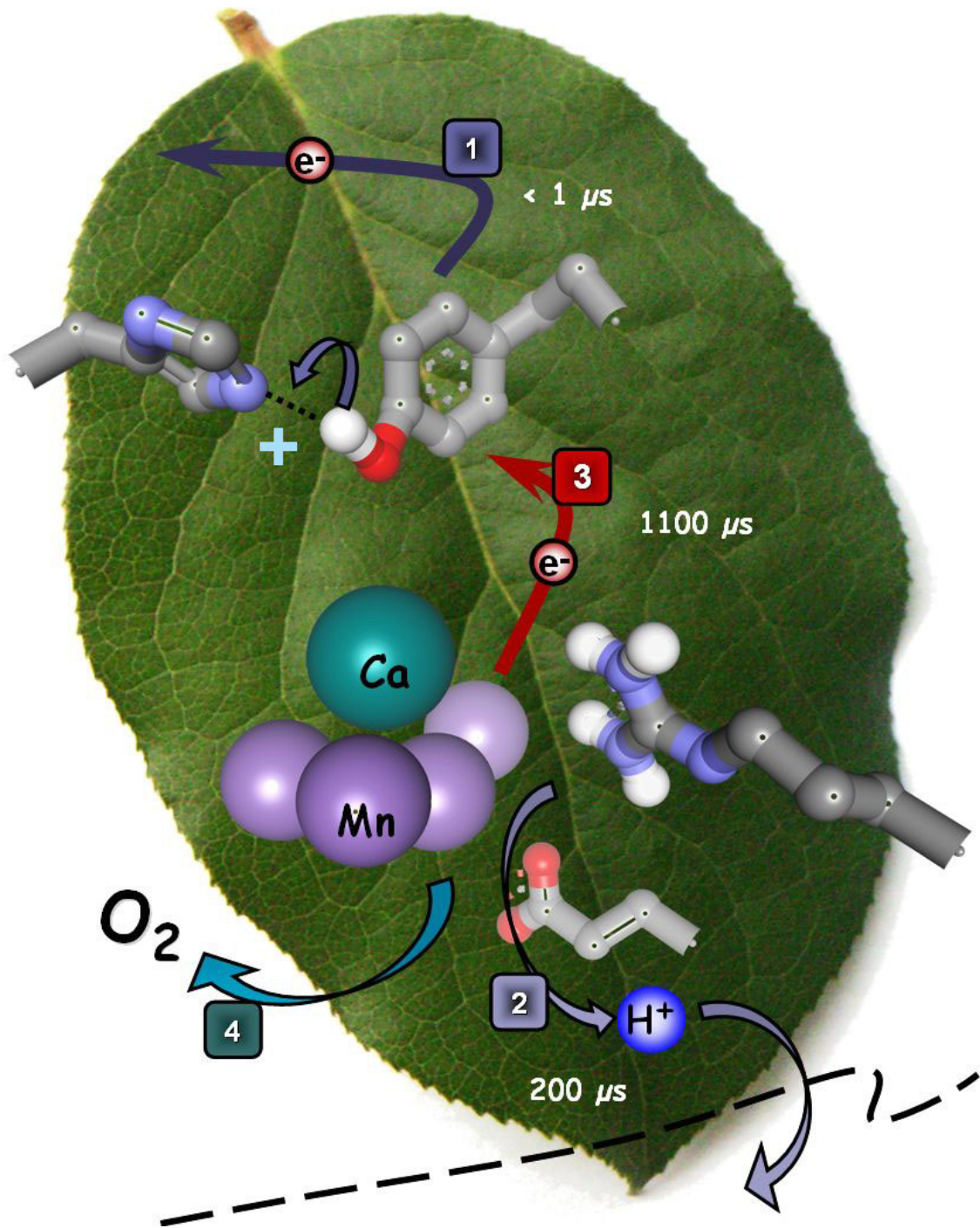


**Fig. 3:** A: Temperature-dependent magnetization profiles of a 20-layer-thick EuTe film, sandwiched between PbTe layers. One observes a reduced magnetization in the outer layers due to the lack of magnetic neighbors at the interface to PbTe. B: Temperature-dependent magnetizations of individual layers. The inner layer 11 behaves like bulk EuTe, while the magnetization in the outer layers (1-4) decays faster. C: Schematic view of the EuTe/PbTe interface with intermixed layers 1 and 2. These intermixed layers have the smallest magnetization.

- [2] E. Weschke, H. Ott, E. Schierle, C. Schüßler-Langeheine, D. V. Vyalikh, G. Kaindl, V. Leiner, M. Ay, T. Schmitte, H. Zabel, and P. J. Jensen, Phys. Rev. Lett. **93**, 157204 (2004).
- [3] K. Binder and P. C. Hohenberg, Phys. Rev. B **9**, 2194 (1974).



# Life Sciences



Previous page: Crucial steps in the reaction sequence leading to the photosynthetic formation of the atmospheric dioxygen (O<sub>2</sub>). In plants and cyanobacteria, the absorption of four quanta (or photons) of visible light drives the splitting of water molecules. Electrons and protons are removed from water, and O<sub>2</sub> is formed. The reaction sequence preceding dioxygen formation has been tracked by time-resolved X-ray absorption spectroscopy with microsecond resolution (steps 1 to 3 in the shown scheme). Selected atoms are depicted as colored balls, covalent bonds as tubes. The shown arrangement of amino acids and metal ions has been determined by protein crystallography with synchrotron radiation.

---

## Life Sciences

In 1953, Watson and Crick proposed their model of the DNA double helix, based on the X-ray diffraction data of Rosalind Franklin. This legendary model represents the starting point for two research directions that shaped the modern life sciences: *molecular biology* and *structural biology*. In 1953, X-ray tubes were used and synchrotrons were an instrument for a small circle of particle physicists. In the last decades, this situation has changed radically. Particle physicists moved on to other, even bigger instruments and synchrotron radiation became a prime tool to investigate at the atomic level the structure of matter, including the bewildering variety of biological macromolecules.

Today the superior properties of the X-ray beams of synchrotron radiation sources facilitate the collection of diffraction data on tiny crystals and the determination of the individual three-dimensional coordinates of ten thousands of atoms in huge macromolecular complexes. In addition, novel techniques have been developed that do not require the tedious and often futile attempts to create well-ordered crystals from solutions of macromolecules. A prominent example is X-ray absorption spectroscopy (XAS) for tracking the catalytic process of the numerous proteins that carry a metal ion at their active site.

*Protein crystallography* with synchrotron radiation is the powerful workhorse in structural biology. Soon after the crystallographic elucidation of the DNA structure, proteins moved into focus. Understanding the variety of their function on the basis of the three dimensional structure became the goal. The Protein Structure Factory of the Freie Universität at the BESSY II is a state-of-the-art facility, which makes possible highly efficient crystallographic data collection. In four of the following research papers progress is described that has been obtained by protein crystallography. Rossocha *et al* characterize an enzyme, which is crucial for the ‘bacterial flora’ of our digestive system; its malfunction may be related to gall stones and colorectal cancer. Not only storage of genetic information by DNA is vital, but also the controlled read-out prior to protein synthesis. This control frequently is facilitated by promotor and repressor proteins. Weihofen *et al* describe the structure of a Watson-Crick helix with a pair of attached repressor proteins.

The molecular world of cells consists not only of nucleic acids (DNA, RNA) and proteins, but also of membranes separating the cell from the extracellular world as well as intracellular compartments. However, matter has to move across these lipid bilayer membranes in a well-controlled way. Kümmel *et al.* investigated a protein complex involved in the vesicular transport of proteins across a membrane. Before the transport occurs, the transport vesicle is tethered to the target membrane; the tethering complex was crystallographically characterized.

Life on Earth is driven by solar energy; the atmospheric dioxygen is formed as a byproduct. The molecular power plant for solar energy conversion and O<sub>2</sub>-formation is called Photosystem II. The leading role of Berlin researchers in this field was reestablished by a really special breakthrough—an almost complete atomic-resolution model of the photosystem comprising 20 non-identical protein subunits as well as 77 (!) organic and inorganic cofactors as described in the contribution of Loll *et al.*

*X-ray absorption spectroscopy (XAS)* with synchrotron radiation complements protein crystallography. A major fraction of proteins exploits the specific properties of metal ions. Prominent examples are the iron of hemoglobin and the manganese complex that facilitates

dioxygen formation in Photosystem II. To unravel the function of metalloproteins at the atomic level, it is of prime importance to monitor the structural dynamics which is associated with advancement in the catalytic cycle. Frequently this can be achieved by X-ray absorption spectroscopy on protein suspensions. Only recently, XAS investigations on dilute protein suspensions became possible at the BESSY-II (*Dau et al.* in Instrumentation section).

Investigations on reaction intermediates in the process of photosynthetic oxygen formation by Photosystem II are described by Haumann *et al.* Among the highlights of this work are time-resolved XAS experiments resulting in the identification of a crucial reaction intermediate, which for more than 35 years had been searched for. Water-splitting by Photosystem II and hydrogen formation by metalloproteins called hydrogenases are connected by a vision—to develop biotechnological or biomimetic system for environmentally friendly, solar-energy-driven production of molecular hydrogen, the fuel of the future, as described by Löscher *et al.*

Using microcapillaries to focus X-rays, two-dimensional *X-ray microscopy*, on the one hand, and atomic-level structural studies, on the other hand, have been combined by Liebisch *et al.* Brown ‘volcanoes’ at the cell wall of a unicellular green alga are found to be a layered form of manganese oxide with calcium ions in the intercalating water layers. This still enigmatic biomineralization phenomenon is likely to become an exciting subject of future research.

Not only X-rays, but also the *brilliant ultraviolet and infrared light* provided by synchrotron radiation sources is employed in investigations on protein function. Borucki *et al.* track structural changes in biological photoreceptors by synchrotron-radiation circular dichroism (SRCD) spectroscopy. Photoreceptors comprise the rhodopsins facilitating human vision and the phytochromes, which in plants, *inter alia*, direct sprouts towards the light. The worldwide efforts to understand their function is one of the focal points of biophysical research in Berlin.

The two most prestigious journals in the world of science are the British magazine *Nature*, where also Watson and Crick presented their double-helix model, and the American journal *Science*. Publication of breakthrough results in *Nature* and *Science* proves the high level of science and international recognition of the life-science research with synchrotron radiation at the Freie Universität Berlin (*Zouni et al.* 2001, *Nature*; *Haumann et al.* 2005, *Science*; *Loll et al.* 2005, *Nature*).

## Digesting Conjugated Bile Acids with the Help of Bacterial Enzymes

M. Rossocha<sup>1</sup>, R. Schultz-Heienbrok<sup>1</sup>, H. von Moeller<sup>1</sup>, J. Coleman<sup>2</sup> and W. Saenger<sup>1</sup>

<sup>1</sup> Institut für Chemie und Biochemie/Kristallographie, Freie Universität Berlin

<sup>2</sup> Department of Microbiology and Immunology, East Carolina University, Greenville, North Carolina

In the digestive system of human beings and other mammals many bacteria are hosted that make up the so-called “bacterial flora”. Nutrition entering the intestine is emulsified by conjugated bile acids that are formed in the liver and consist of deoxycholic acid linked by a peptide bond to taurin or glycin (Fig. 1) formed in the liver. The conjugated bile acids allow uptake of essential fats and are necessary for digestion. Breakdown of unused conjugated bile acids is ensured by an enzyme called “Conjugated Bile Acid Hydrolase” or CBAH. This enzyme can be found in virtually any bacterial strain in the intestine. Malfunction of CBAH plays a role in human (patho)physiology as deconjugated bile salts are associated with gall stones and colorectal cancer.

We have purified CBAH from a bacterium called “*Clostridium perfringens*”. After purification, the protein was co-crystallised with the substrate taurocholic acid using two different solutions: One containing polyethylene glycol and the other containing ammonium sulfate (Fig. 2). Using synchro-

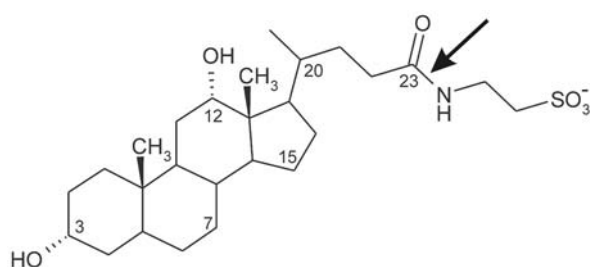


**Fig. 1:** Chemical structure of taurodeoxycholate, a common bile acid found in the intestine. The substrate is cleaved at the peptide bond (arrow).

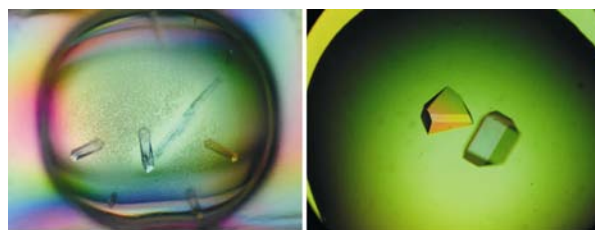


**Fig. 2:** Protein crystals of CBAH. (Left) crystals were grown from polyethylene glycol solution and (right) from ammonium sulfate solution.

tron radiation from BESSY II/Berlin, we were able to obtain X-ray diffraction data from these crystals suitable for structure determination [1]. The structure allowed us not only to visualize the tertiary structure of the protein, i.e. the folding pattern of the polypeptide chain, but also its higher structural (quaternary) organisation. Bio-chemical experiments had indicated that CBAH exists

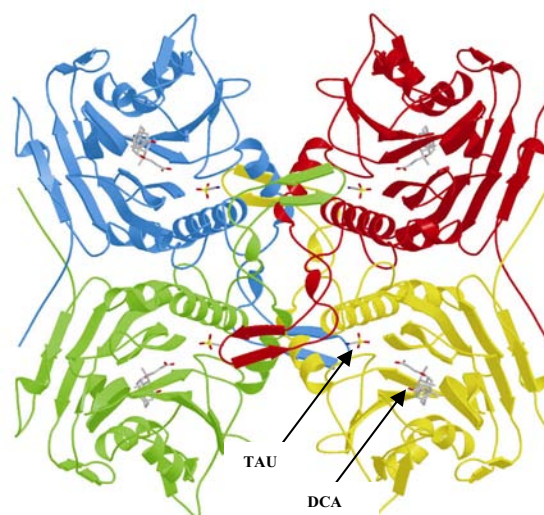


**Fig. 3:** CBAH forms a homo-tetramer with dihedral symmetry. The reaction products taurine (TAU) and deoxycholate (DCA) are shown in grey and indicated in one (yellow) subunit.

as a tetramer in solution. We confirmed these earlier experiments and could also show how the enzyme assembles into a tetramer (Fig. 3).

The crystals obtained from ammonium sulfate also contained the hydrolysis products taurine and deoxycholate besides tetrameric CBAH. By identifying these molecules in the crystal structure, we were able to map out the active centre as well as the binding pocket of the enzyme (Fig. 4). It could be shown that CBAH belongs to a class of enzymes that uses the N-terminus as a nucleophile in catalysis and, hence, is called the Ntn-hydrolase superfamily. The nucleophilic N-terminus is exposed after autocatalytic cleavage of a pre-protein of varying length. Since mutations in the active centre of the enzyme would prohibit autocatalytic cleavage of the pre-protein, it is very difficult if not impossible to reveal the reaction mechanism of this class of enzymes by studying structures of an

enzyme-substrate complex.

To overcome this problem, an Ntn-hydrolase is needed that has no pre-protein. In CBAH from *Clostridium perfringens* the pre-protein consists of a single amino acid (f-Met). When the protein is expressed in *Escherichia coli* this initial amino acid is, at least partially, cleaved off by the enzyme methionyl-aminopeptidase. It is, therefore, possible to obtain CBAH which is fully processed and active and can be mutated at positions involved in the catalytic cleavage of conjugated bile acids. We plan to analyse structures of complexes formed by substrates and various mutant forms of CBAH to establish the reaction mechanism of this enzyme. These studies would also be of importance for the whole class of Ntn-hydrolases. In order to study enzyme-substrate complexes, high resolution structures are necessary which can only be gained using a high brilliance synchrotron beamline such as BESSY II/Berlin.

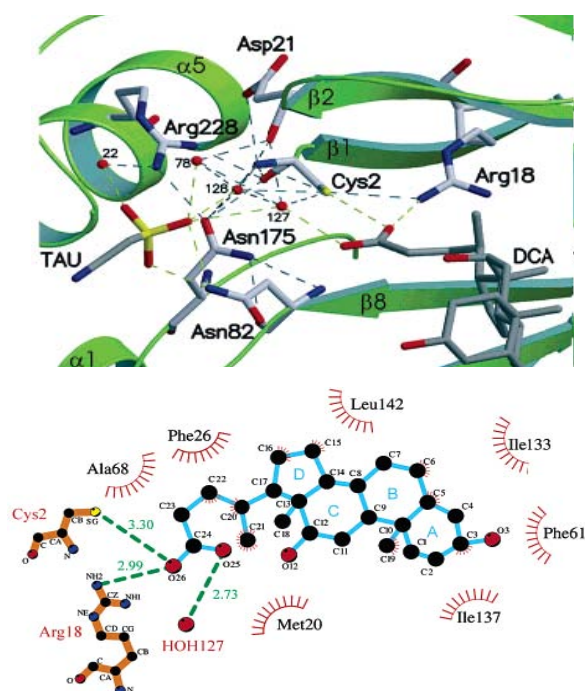


**Fig. 4:** (top) Active site and substrate binding pocket of CBAH. Residues of the active site and the binding pocket are labeled. TAU, taurine; DCA, deoxycholic acid,  $\beta$ -sheets as green arrows and  $\alpha$ -helices as spirals. (bottom) Contacts to deoxycholic acid, hydrogen bonds as dashed lines, van der Waals contacts as evelashes.

## References

- [1] M. Rossocha, R. Schultz-Heienbrok, H. v. Moeller, J. P. Coleman, W Saenger, *Biochemistry* **44**, 5739 (2005).

## Structures of $\omega$ repressors bound to direct and inverted cognate DNA repeats reveal a unique mechanism to modulate transcription

Wilhelm A. Weihofen<sup>1</sup>, Aslan Cicek<sup>1</sup>, Florencia Pratto<sup>2</sup>, Juan C. Alonso<sup>2</sup>, Wolfram Saenger<sup>1</sup>

<sup>1</sup>Institut für Chemie und Biochemie/Kristallographie, Freie Universität Berlin

<sup>2</sup>Departamento de Biotecnología Microbiana, Centro Nacional de Biotecnología, Madrid,

In all organisms the expression of genes (transcription) is regulated by repressor proteins that bind to DNA sequences (operators) located upstream of the respective gene. Repressor  $\omega$  is the common regulator of genes for copy number control, accurate segregation and stable maintenance of broad-host-range *inc18* plasmids hosted by Gram-positive bacteria.  $\omega$  belongs to the MetJ/Arc family of homodimeric ribbon-helix-helix (RHH<sub>2</sub>) proteins that feature a symmetric antiparallel  $\beta$ -sheet for DNA major groove binding. Generally two or more RHH<sub>2</sub> bind to severely bent, palindromic operators, and because adjacent RHH<sub>2</sub> contact each other, the interaction is cooperative and strong. The cognate repeat sequence for  $\omega_2$  is a DNA

heptad (5'-<sup>A</sup>/TATCAC<sup>A</sup>/T-3' symbolized by  $\rightarrow$ ) that is aligned in natural operators with 7 to 10 consecutive copies as palindromic, inverted ( $\rightarrow\leftarrow$ ) and divergent ( $\leftarrow\rightarrow$ ) repeats or as non-palindromic, direct repeats ( $\rightarrow\rightarrow$ ), Fig. 1.

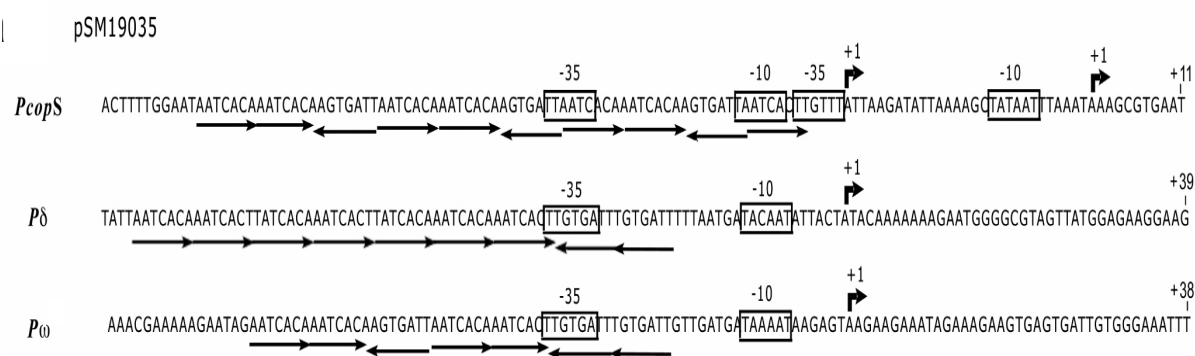
Since the binding affinity of  $\omega_2$  to each operator depends on the number and the arrangement of heptad repeats, different genes can be controlled by the common regulator  $\omega_2$  (Fig. 1).

To our knowledge only repressor  $\omega_2$  features the unique ability to bind to palindromic as well as to non-palindromic operators consisting of consecutive DNA cognate repeats. Therefore it was of interest to elucidate the structural determinants for cooperative binding of  $\omega_2$  repressor to natural operators with different heptad arrangements.

We crystallized  $\omega_2$  bound to two minimal operators comprising direct ( $\rightarrow\rightarrow$ ) and inverted ( $\rightarrow\leftarrow$ ) heptads (Fig. 2).

X-ray diffraction data were collected at the Protein Structure Factory beamline BL14.1 of Free University Berlin at BESSY

**Fig. 1:** Comparison of the nucleotide sequences of  $\omega_2$  target sites in *inc18* plasmids. The experimentally defined conserved -35 and -10 consensus regions of the *P<sub>copS</sub>*, *P $\delta$*  and *P $\omega$*  promoters are boxed, heptad position and orientation indicated by arrows [1].



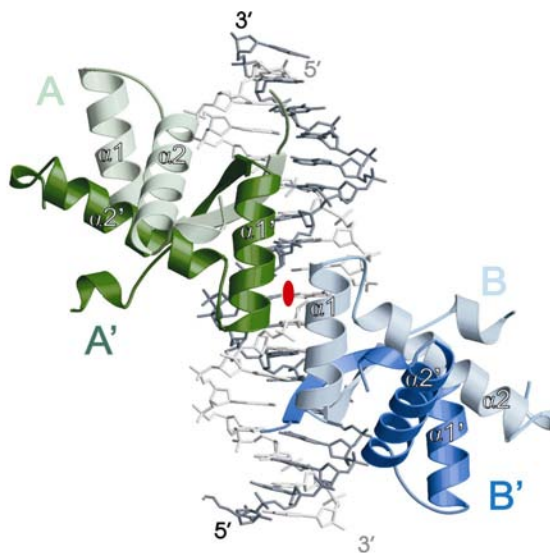


**Fig. 2:** Structure of  $[\omega_2]_2-(\rightarrow\rightarrow)$ . DNA backbone trace in light and dark grey.  $\omega$  monomers A/A' and B/B' in light and dark green and blue, respectively, helices  $\alpha_1$  and  $\alpha_2$  labelled with white letters. The A/A' dimer transforms to the B/B' dimer by 7/10 rotation and translation along the DNA axis. The  $\omega_2 \cdots \omega_2$  interface is formed between helices  $\alpha_1'$  of A' and  $\alpha_1$  of B that are related by a pseudo-twofold axis perpendicular to the paper plane (red ellipse).

and structures were determined by molecular replacement, see Fig. 2 for the structure of  $[\omega_2]_2-(\rightarrow\rightarrow)$  [2].

A comparison of  $[\omega_2]_2-(\rightarrow\rightarrow)$  and  $[\omega_2]_2-(\rightarrow\leftarrow)$  showed that the pseudo-twofold axis relating the monomers in  $\omega_2$  passes with  $\sim 0.3$  Å downstream offset through the central G-C base pair of each heptad see Fig. 3. Consequently, these symmetry axes are separated by 7 base pair in  $[\omega_2]_2-(\rightarrow\rightarrow)$  but they are 0.6 Å closer in  $[\omega_2]_2-(\rightarrow\leftarrow)$ . Helices  $\alpha_1$  and  $\alpha_1'$  forming the  $\omega_2 \cdots \omega_2$  interfaces superimpose well, consistent with similar dissociation constants for both complexes.

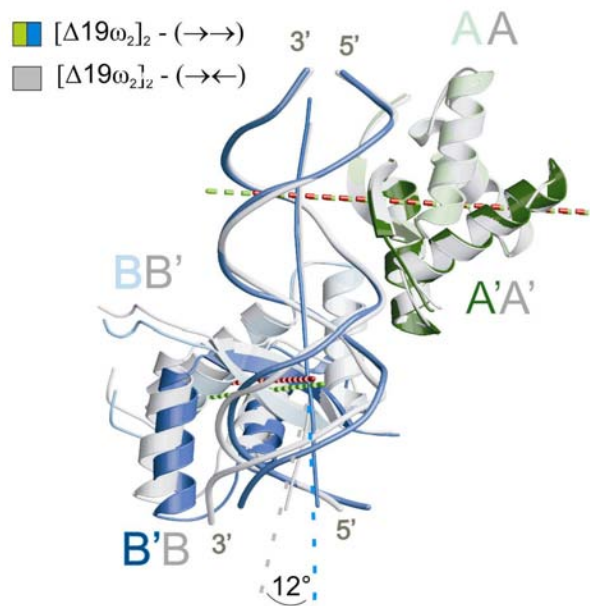


**Fig. 3:** Superimposition of A/A' of  $[\omega_2]_2-(\rightarrow\rightarrow)$  (green) and A/A' of  $[\omega_2]_2-(\rightarrow\leftarrow)$  (grey) to show slight positional differences of  $\omega$  B/B' associated with palindromic symmetry in  $(\rightarrow\leftarrow)$  but not in  $(\rightarrow\rightarrow)$ . Pseudo-twofold axes relating monomers in  $\omega_2$  indicated by dashed lines coloured green for  $[\omega_2]_2-(\rightarrow\rightarrow)$  and red for  $[\omega_2]_2-(\rightarrow\leftarrow)$ . Helices  $\alpha_1$ ,  $\alpha_1'$  involved in  $\omega_2 \cdots \omega_2$  interactions superimpose well allowing cooperative binding in both complexes. DNA in  $[\omega_2]_2-(\rightarrow\leftarrow)$  is locally kinked by  $12^\circ$  at the centre of the bottom heptad, and  $\omega_2$  are  $\sim 0.6$  Å closer (vertical distance between pseudo-twofold red axes) than in  $[\omega_2]_2-(\rightarrow\rightarrow)$ , see text.

By contrast, the separation between the two  $\omega_2$  will be  $\sim 0.6$  Å wider in  $[\omega_2]_2-(\leftarrow\rightarrow)$ . Assuming that the interaction pattern between  $\omega_2$  and heptads with  $(\leftarrow\rightarrow)$  orientation is similar as in  $(\rightarrow\rightarrow)$  and  $(\rightarrow\leftarrow)$  heptad orientations, the expected  $\sim 0.6$  Å longer  $\alpha_1 \cdots \alpha_1$  contacts are probably less favorable, in agreement with the six-fold weaker affinity of wt  $\omega_2$  to heptads in  $(\leftarrow\rightarrow)$  arrangement and the finding that  $[\omega_2]_2-(\leftarrow\rightarrow)$  dissociated during gel filtration.

Protein-DNA interactions in both complexes bury  $1610$  Å<sup>2</sup> of solvent accessible surface area. Another  $550$  Å<sup>2</sup> are buried by interaction of pseudo-twofold axis

related  $\alpha 1$  helices of adjacent monomers A' and B in  $[\omega_2]_2-(\rightarrow\rightarrow)$  and A' and B' in  $[\omega_2]_2-(\rightarrow\leftarrow)$ , respectively (Figs. 2 and 3). The  $\alpha 1$  helices of both subunits interact by hydrogen bonds, and hydrophobic contacts ensure cooperative binding when several  $\omega_2$  associate with multiple heptad repeats as found in natural operators, Fig. 4.

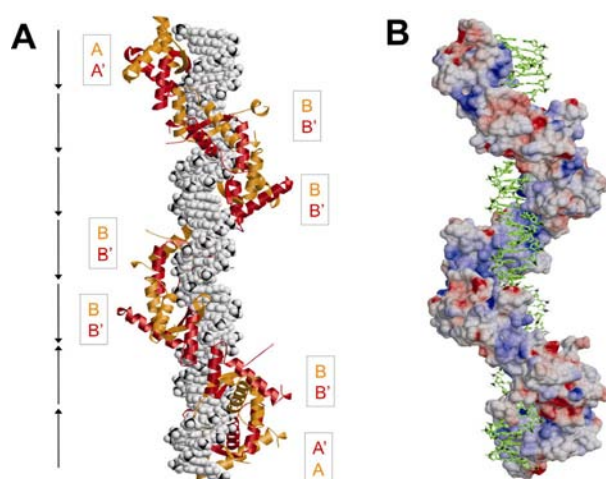


**Fig. 4:** Model of seven  $\omega_2$ -bound heptads ( $\rightarrow\rightarrow\rightarrow\rightarrow\rightarrow\leftarrow\leftarrow$ ) of the natural promoter  $P\delta$  (Fig. 1). (A) DNA in space filling (grey) and  $\omega_2$  as orange/red ribbons, (B) DNA in stick (green) and  $\omega_2$  in surface representation coloured according to electrostatic potential (negative and positive charges red and blue, respectively). The model is based on the structures of  $[\omega_2]_2-(\rightarrow\rightarrow)$  and  $[\omega_2]_2-(\rightarrow\leftarrow)$ . Repressors form a left-handed protein-matrix winding around the nearly straight right-handed operator.

Extrapolation of the structures of  $[\omega_2]_2-(\rightarrow\rightarrow)$  and  $[\omega_2]_2-(\rightarrow\leftarrow)$  allowed modeling of natural promoter  $P\delta$  comprising 9 heptad repeats and bound  $\omega_2$  (Fig. 4). The model implies that  $\omega_2$  binds as left-handed matrix to right-handed, straight B-type operator DNA, each  $\omega_2$  being displaced by its neighbor by  $\sim 7$  base pair and rotated by  $252^\circ$ . Fig. 4 shows that the negatively charged sugar-phosphate backbone of DNA faces

positively charged electrostatic potential of  $\omega_2$ .

The implications of the determined  $\omega_2$ -DNA structures for regulation of transcription can be summarized as follows: In gram-positive bacteria, *inc18* family plasmids harbour genes to control their copy-number, stable maintenance and accurate segregation during cell division. Since expression of these genes is regulated by the common  $\omega_2$  repressor, a unique mechanism has evolved to fine-tune repressor affinity for the different operators. How this is achieved is shown by the present study. It clearly indicates that the pseudo-symmetric  $\omega_2$  binds with  $0.3 \text{ \AA}$  downstream ( $5'$ - $3'$ ) offset relative to the center G-C base pair of the cognate DNA heptad. Since the operators are nearly straight B-DNA, different heptad numbers and orientations lead to different distances between  $\alpha 1$ -helices of adjacent  $\omega_2$ , thereby modulating cooperative interactions between  $\omega_2$  and different operators. The ability to bind to palindromic as well as to non-palindromic operators is a unique feature of  $\omega_2$  and is not shared by other members of the RHH<sub>2</sub> family.

#### Acknowledgements

These studies were supported by EU-project QLK3-CT-2001-00277

#### References

- [1] A. B. de la Hoz, F. Pratto, R. Misselwitz, C. Speck, W. A. Weihofen, K. Welfle, W. Saenger, H. Welfle, and J. C. Alonso, *Nucleic Acids Res.* 32, 3136-47 (2004)
- [2] W. A. Weihofen, A. Cicek, F. Pratto, J.C. Alonso, and W. Saenger, *Nucleic Acids Res.* 34, 1450-1458 (2006)
- [3] A. B. de la Hoz, F. Pratto, R. Misselwitz, C. Speck, W. A. Weihofen, K. Welfle, W. Saenger, H. Welfle, and J. C. Alonso, *Nucleic Acids Res.* 32, 3136-47 (2004)

## Structural Studies of the Human Tethering Complex TRAPP Involved in Vesicular Transport

Daniel Kümmel<sup>1,2</sup>, Andrew P. Turnbull<sup>1,3</sup>, Jürgen J. Müller<sup>1</sup>, Yvette Roske<sup>1</sup>  
and Udo Heinemann<sup>1,2</sup>

<sup>1</sup>Max-Delbrück-Centrum für Molekulare Medizin, Berlin

<sup>2</sup>Institut für Chemie und Biochemie, Freie Universität, Berlin

<sup>3</sup>Proteinstrukturfabrik, c/o BESSY GmbH, Berlin

Living cells are separated from their surrounding by lipid bilayer membranes which fence off the interior of the cell, the cytosol, from the outside world. In addition, the cells of all higher organisms contain specialized compartments which are separated from the cytosol also by lipid membranes. Because of their chemical properties, membranes constitute a barrier for exchange of substances. This allows the maintenance of distinct environments for different processes carried out in these areas. A controlled transport across biological membranes is mediated by membrane proteins that can act as specific transporters or regulated channels.

The exchange of proteins and other molecules between different compartments or the cell and the outside world is achieved by vesicular transport: Small membrane vesicles bud at a donor membrane and load cargo in their interior. The vesicles travel through the cell to their destination compartment where the vesicle is first tethered to the target membrane and then fuses, thus delivering its cargo (Fig. 1).

The tethering process is required for the specificity of vesicle transport, ensuring that

the right vesicle is bound to the corresponding target membrane. This recruitment of vesicles to their destination compartment is mediated through tethering factors, such as long coiled-coil proteins or tethering complexes. The tethering process is followed by membrane fusion, catalyzed through the class of SNARE (soluble NSF-attachment protein receptor) proteins.

We are interested in the TRAPP (Transport Protein Particle) tethering complex which is involved in the transport of vesicles from the endoplasmic reticulum (ER), where proteins are synthesized, to the Golgi network, where proteins are further processed. TRAPP was shown to interact with ER-derived vesicles and to promote nucleotide exchange of a regulatory protein, the Rab-GTPase Ypt1p. The human TRAPP complex contains at least seven subunits. Our goal is to structurally characterize the different TRAPP subunits and subcomplexes. This information will allow us to gain better understanding of the essential vesicle tethering process.

We have so far succeeded in the crystallization and structure determination of two

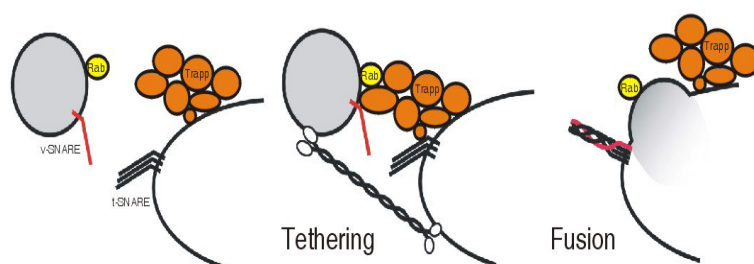


**Fig. 1:** The cargo delivery of a vesicle to the target compartment requires tethering and membrane fusion (after [1]).



to modulate protein–protein interactions. However, palmitoylation of BET3 was shown not to be essential for cell viability or membrane localization of BET3 in yeast. The membrane attachment of BET3 may be mediated by an additional modification or through interactions with an other component of the TRAPP complex. The hydrophobic cavity of BET3 might also represent a binding pocket for acylated interacting proteins. TPC6, another subunit of TRAPP, was also found to be dimeric and the overall structure resembles strikingly that of BET3 (Fig. 2B). In spite of only 17% sequence identity, the superposition of the  $\alpha$ -carbon backbones of the monomers of both proteins shows high similarity. Differences in struc-

ture are mainly confined to the loop regions, whereas the  $\alpha/\beta$ -plait cores of both proteins show little divergence. Considering the structural similarity between TPC6 and BET3 we suggest that the  $\alpha/\beta$ -plait fold might represent the common fold for all paralogous BET3 family members including an third TRAPP subunit, TPC5. A sequence alignment of the human proteins TPC6, TPC5, and BET3 (Fig. 2C) shows that conserved and similar residues between different family members are predominantly located in the  $\alpha$ -helical secondary structure elements. Major variations in length and conservation of the primary structure are only found in loop regions. In addition, the proteins differ in the length and sequence of their N- and C-termini. The

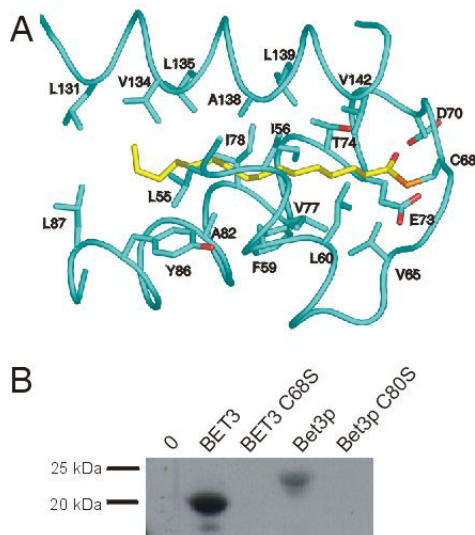


**Fig. 3:** **A** A palmitoyl group, linked to the conserved residue C68, is located in a cavity formed by hydrophobic amino acids. **B** BET3 is specifically palmitoylated at the conserved cysteine residue.

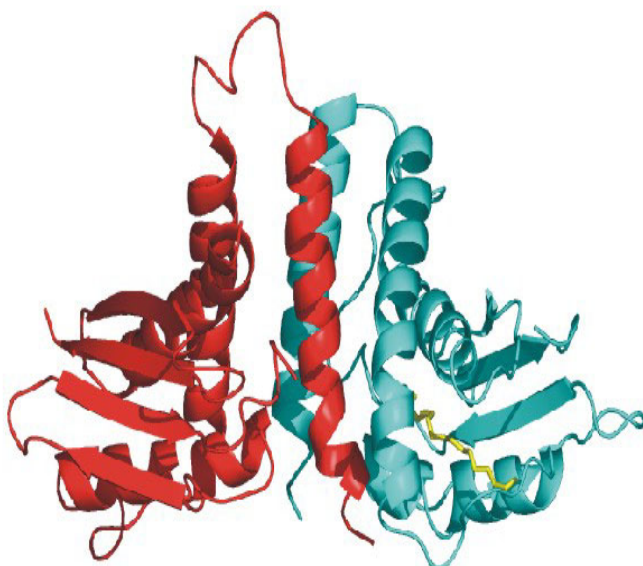


**Fig. 4:** Model of a TPC6-BET3 heterodimer. The structure of this TRAPP subcomplex is derived from a superposition of the TPC6 (red) and BET3 (cyan) dimers.

highest similarity is found for two motifs (LX<sub>2</sub>#GX<sub>2</sub>#GX<sub>2</sub>LXE and G#<sub>2</sub>XGXL) that have been previously described, and these motifs are located in the interior of the proteins. Taken together these data suggest that TPC5 may adopt a similar fold as TPC6 and BET3.

The similarity between BET3 and TPC6 is especially prominent at the dimerization interfaces of the proteins leading to the intriguing possibility of a heterodimerization between TPC6 and BET3. Heterodimerization could be demonstrated by *in vitro* and *in vivo* association studies. We therefore suggest a model of a BET3-TPC6 heterodimer, representing a putative TRAPP subcomplex (Fig. 4).

## References

- [1] Whyte JR, Munro S (2002) *J Cell Sci*, **115**: 2627-2637
- [2] Turnbull AP, Kümmel D, Prinz B, Holz C, Schultchen J, Lang C, Niesen FH, Hofmann KP, Delbrück H, Behlke J, Müller EC, Jarosch E, Sommer T, Heinemann U (2005) *EMBO J*, **24**: 875-884
- [3] Kümmel D, Müller JJ, Roske Y, Misselwitz R, Heinemann U (2005) *EMBO Rep*, **6**: 787-793
- [4] Heinemann U, Büssow K, Mueller U, Umbach P (2003) *Acc Chem Res*, **36**: 157-163
- [5] Jang SB, Kim YG, Cho YS, Suh PG, Kim KH, Oh BH (2002) *J Biol Chem*, **277**: 49863-49869
- [6] Kim YG, Sohn EJ, Seo J, Lee KJ, Lee HS, Hwang I, Whiteway M, Sacher M, Oh BH (2005) *Nat Struct Mol Biol*, **12**: 38-45

## Crystal Structure of Photosystem II at 3.0 Å Resolution

*B. Loll<sup>1</sup>, J. Kern<sup>2</sup>, W. Saenger<sup>1</sup>, A. Zouni<sup>2</sup>, J Biesiadka<sup>1</sup>*

<sup>1</sup> *Institut für Chemie und Biochemie/Kristallographie, Freie Universität Berlin*

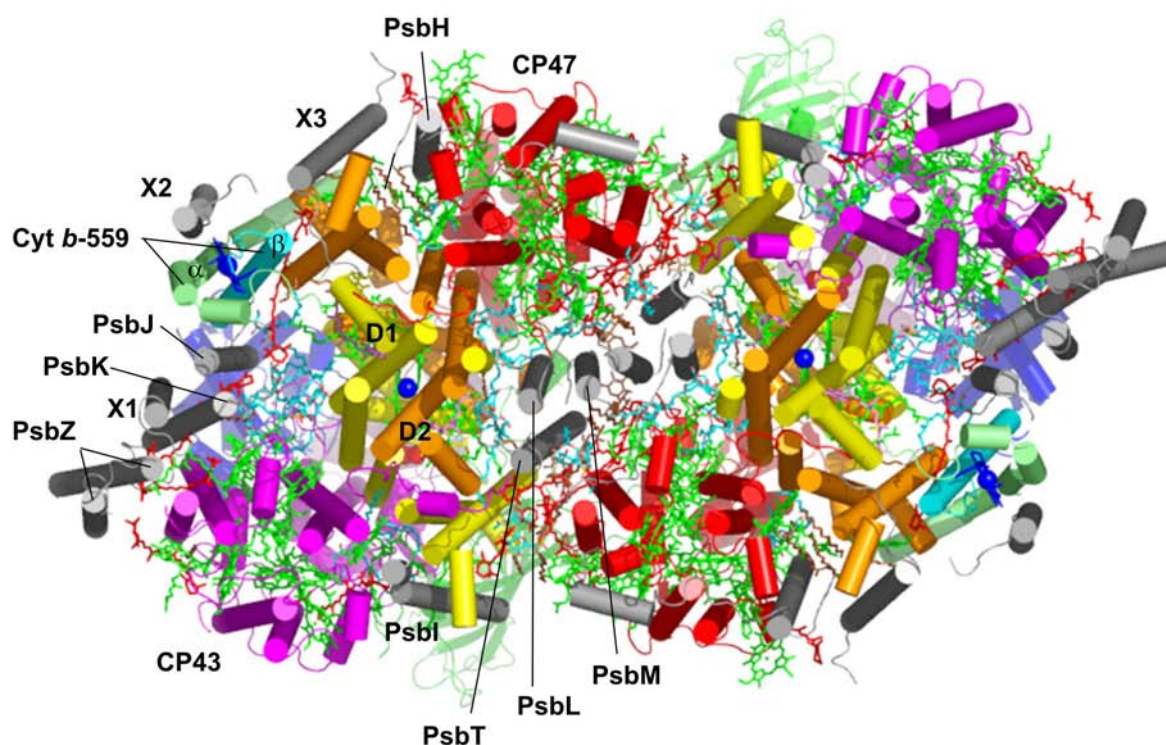
<sup>2</sup> *Institut für Chemie/Max Volmer Laboratorium für Biophysikalische Chemie, Technische Universität Berlin*

Oxygenic photosynthesis is the principal energy converter on earth. It is driven by photosystems I and II (PSI, PSII), two large protein-cofactor complexes located in the thylakoid membrane of plants, green algae and cyanobacteria and acting in series. In PSII, water is oxidized at a manganese-calcium cluster (Mn<sub>4</sub>-Ca). This event provides the overall process with the necessary electrons and protons, and the atmosphere with oxygen.

The X-ray crystal structure of cyanobacterial photosystem II at 3.0 Å resolution [1] shows the arrangement of the 20 protein subunits: the reaction centre proteins D1 and D2, the chlorophyll containing inner-antenna subunits CP43 and CP47, subunits  $\alpha$  and  $\beta$  of cytochrome b-559 and the smaller subunits PsbH, PsbI, PsbJ,

PsbK, PsbL, PsbM, PsbT and PsbZ (Fig. 1). In addition, 3 subunits are membrane-extrinsic: cytochrome c-550, PsbU and PsbO (Fig. 2). The locations and orientations of 77 organic and inorganic cofactors are defined, including 35 chlorophyll *a*, 2 pheophytins, 2 plastoquinones, 11  $\beta$ -carotenes, 14 lipids, bicarbonate, 1 non-haem iron, 2 haem-bound irons, putative calcium and the Mn<sub>4</sub>-Ca cluster which catalyzes water oxidation.

**Fig. 1:** Overall structure of PSII dimer seen from the cytoplasmic side of the thylakoid membrane (see Fig. 4). The monomers are related by a C<sub>2</sub>-rotation axis, located in the centre near PsbM; subunits X1, X2, X3 not yet assigned. Individual subunits are depicted in different colours, cofactors in stick representation (green, chlorophyll *a*; red, carotenes; blue, lipids).



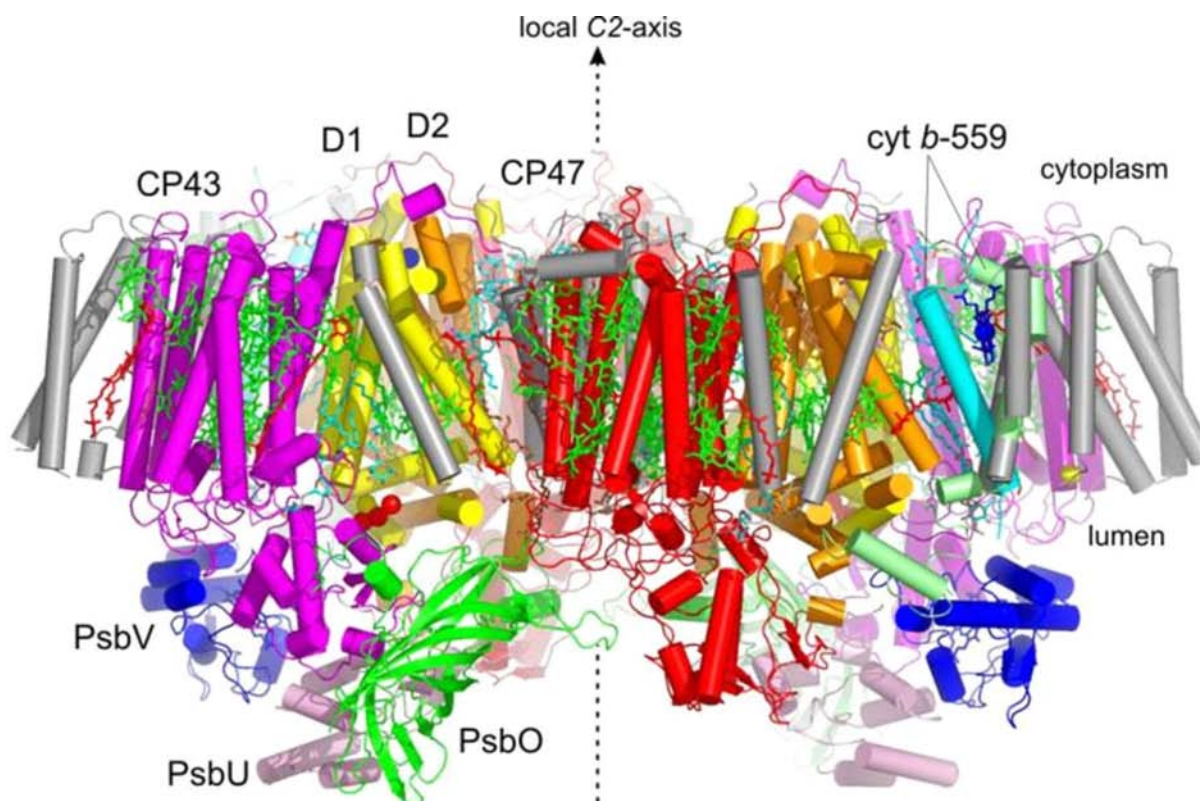


**Fig. 2:** View of PSII in direction along the membrane plane; the position of local- $C_2$  rotation axis, that relates the monomers in the PSII dimer, is shown.

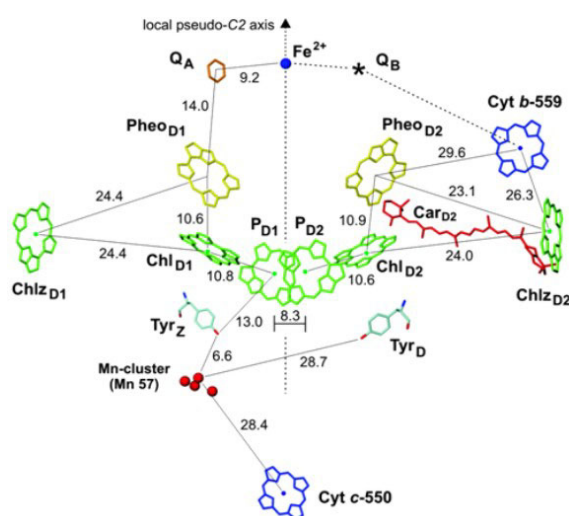


**Fig. 3:** Cofactors of the photosynthetic reaction centre, including the electron transfer chain where charge separation occurs, distances between centres of cofactor in Å. The asterisk indicates  $Q_B$  that is only half-occupied.

Photosynthesis is initiated at PSII by light energy, harvested by chlorophyll *a* in the antenna subunits CP43 and CP47. Excitation energy is guided to the primary electron

donor P680, a chlorophyll *a* in the heart of the PSII reaction centre, formed by cofactors embedded within subunits D1 and D2 (Fig. 3). P680 becomes excited and ejects an electron to form the cationic radical  $P680^{\bullet+}$ . The electron moves by means of electron transfer chain to the acceptor  $Q_A$ , a plastoquinone that is tightly bound at the stromal side of subunit D2.

After each of four light induced successive charge separating steps,  $P680^{\bullet+}$  abstracts one electron from the  $Mn_4$ -Ca cluster by means of the redox-active  $Tyr_Z$ . In turn, the four oxidation equivalents accumulated in the  $Mn_4$ -Ca cluster oxidize two water molecules, coupled with the release of one  $O_2$  and four  $H^+$ . In the first two charge separations,  $Q_A^{\bullet-}$  doubly reduces the mobile plastoquinone molecule  $Q_B$  docked to the binding site in subunit D1. After uptake of two protons,  $Q_BH_2$  ( $PQH_2$  in Fig. 4) is released into the plastoquinone pool in the thylakoid membrane and replaced by a new plastoquinone from the pool for another photosynthetic cycle.

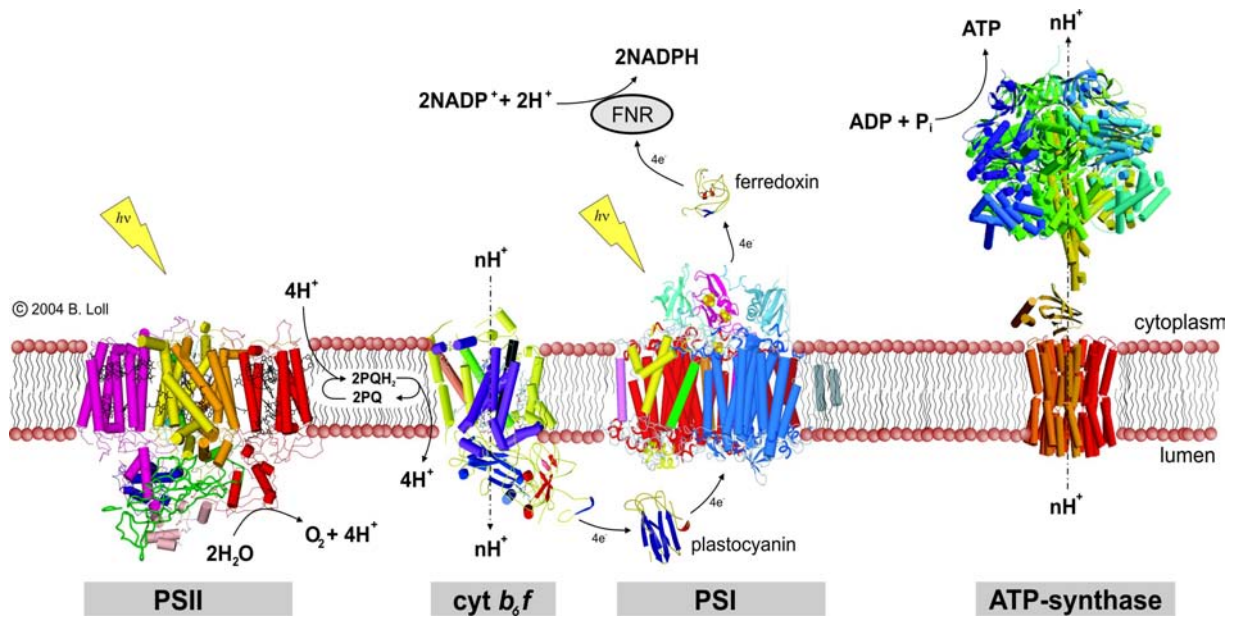


**Fig. 4** Light reactions of oxygenic photosynthesis occurring in the thylakoid membrane.

PQH<sub>2</sub> is oxidized at the membrane-embedded cytochrome b<sub>6</sub>/f complex, and the released electrons are transported by water-soluble plastocyanin to photosystem I where they are activated by light, transferred via ferredoxin to NADP reductase (FNR in Fig. 4) and used there to reduce NADP to NADPH. The released H<sup>+</sup> form a gradient across the membrane that drives ATP synthesis, and both, NADPH and ATP, are used to convert CO<sub>2</sub> to carbohydrates in the Calvin cycle (not shown).

The here described three-dimensional structure of cyanobacterial PSII has provided more details than any of the previous PSII structures and has corrected several misinterpretations of lower resolution electron density maps. The number of 14 lipids is the highest yet found in any protein complex and suggests structural and functional roles. The flexible hydrophobic lipids may promote the assembly and rearrangement of the 20 protein subunits in the PSII complex and the diffusion of plastoquinone/plastoquinol between photo-

system II and the quinone pool in the thylakoid membrane.

The carotenoids, distributed uniformly at the periphery of PSII or clustered at the monomer-monomer interface, protect the complex from photodamage.

Most of the cations in the water-oxidizing Mn<sub>4</sub>Ca-cluster in "3+1" Mn configuration are bridged in bidentate mode by carboxylate groups that probably play functional roles during Kok-cycle reactions. The novel insights into PSII structure and function suggest mutational studies that will deepen our understanding of PSII function.

## References

- [1] B. Loll, J. Kern, W. Saenger, A. Zouni, J. Biesiadka, *Nature* 438, 1040-1044 (2005).

## The oxygen that we breathe — photosynthetic O<sub>2</sub>-production followed in X-ray absorption experiments

*M. Haumann, P. Liebisch, C. Müller, M. Grabolle, M. Barra, P. Loja, H. Dau*

*Freie Universität Berlin, Institut für Experimentalphysik*

### Atmosphere and biosphere shaped by photosynthetic O<sub>2</sub>-production

In photosynthetic organisms, solar energy drives the conversion of CO<sub>2</sub> into energy-rich carbohydrates (sugar, starch). The spreading of early photosynthetic organisms was restricted by limited availability of suitable substrate molecules that could provide the needed reducing equivalents (electrons). About three billion years ago, however, nature invented—by evolutionary trial and error—a fascinating machinery for using the ubiquitous water as a substrate. Thereby the previous limitations were removed and in the next 3 billion years a dramatic change in atmosphere and biosphere took place. In the process of photosynthetic water-splitting, dioxygen (O<sub>2</sub>) is produced and released (Fig. 1). Within about 2 billion years the previously negligibly oxygen level in the atmosphere increased to 21%. The sensitivity of early organisms to reactive dioxygen has led to a reshaping of the bacterial world.

Perhaps more important, the presence of dioxygen enabled the evolution of a respiratory machinery that can account for the energetic needs of higher life forms—including human beings. But how is—driven by light—water split and dioxygen produced? This question is a focus points of research with synchrotron radiation of groups at the FU Berlin (see also contribution of Loll et al. in the group of W. Saenger).

### Atomic structure of the oxygen-evolving complex by synchrotron experiments

The unknown territory in photosynthesis research is rapidly shrinking, but access to the 'inner sanctum' still represents a special challenge. (The mechanism of water splitting has been denoted as the 'inner sanctum' or 'holy grail' of photosynthesis research.) We know that water is split (or oxidized) at a manganese-calcium complex bound to the proteins of Photosystem II (PSII) [1]. This huge protein-cofactor complex is found in

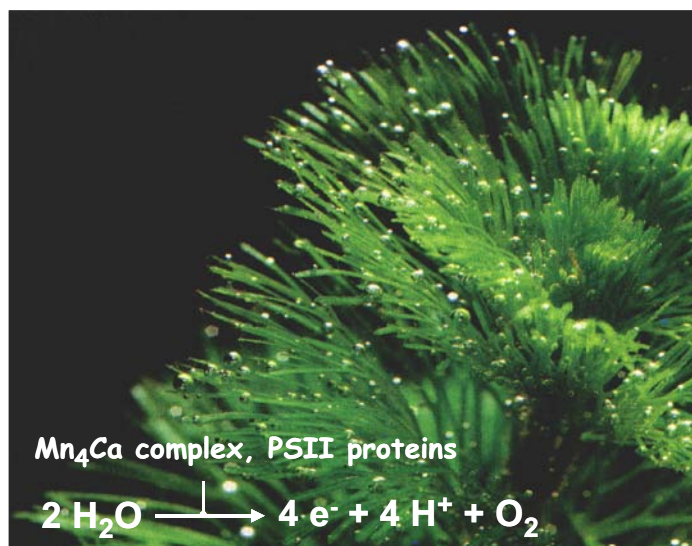


**Fig. 1.** Sum equation of photosynthetic water oxidation and dioxygen formation at the manganese complex of Photosystem II (PSII). Water-splitting by PSII also is denoted as water oxidation because formally electrons are extracted from the oxygen of two water molecules and thus the water-oxygen is oxidized. The water plant in the background was illuminated and produced bubbles of dioxygen as clearly visible in this photo.

the lipid bilayer membranes of plants, green algae and cyanobacteria (blue-green algae). Recently a highly-resolved structural model has been presented [2] that includes the location of several thousand atoms of the PSII proteins and of numerous cofactors (chlorophyll and carotenoid molecules, quinones acting as electron acceptor and carrier molecules, iron of still unknown function, the manganese complex, and others). The basis for this model had been the three dimensional electron density map obtained by protein crystallography with synchrotron radiation. The crystallographic model represents a long-awaited breakthrough, but it does not suffice to answer the question how water is split. Recent progress comes from a complementary approach: X-ray absorption spectroscopy on suspensions of isolated PSII particles or on multilayers of membrane particles with PSII almost in its native environment (see [3-5] and refs. therein).

### Reaction intermediates studied by X-ray absorption experiments

One cycle of O<sub>2</sub> production is driven by the absorption of four photons that can be provided by short Laser flashes. By application of a sequence of saturating Laser flashes it is possible to step trillions of PSII synchronously through the reaction cycle; four semi-stable states of the oxygen-formation cycle (S-states) are formed. We have studied these four S-states by X-ray absorption spectroscopy (XAS). Therefore we stabilized the S-states by freezing the protein samples at -200 °C (temperature of liquid nitrogen) prior to the X-ray experiment at even lower temperature (~20 K). We also have developed techniques to study the semi-stable S-states at room temperature—thereby avoiding the ambiguities of low-temperature experiments on proteins that function only above the freezing point of water (see [4] and refs. therein). These experiments involve the illumination of protein samples by Laser flashes of nanosecond duration. The samples are simultaneously exposed to the X-ray beam provided at the synchrotron radiation source; the excited X-ray fluorescence is recorded (Fig. 2). Eventually we have obtained a picture on the changes in structure and oxidation state of the PSII manganese complex in the catalytic cycle (Fig. 3).

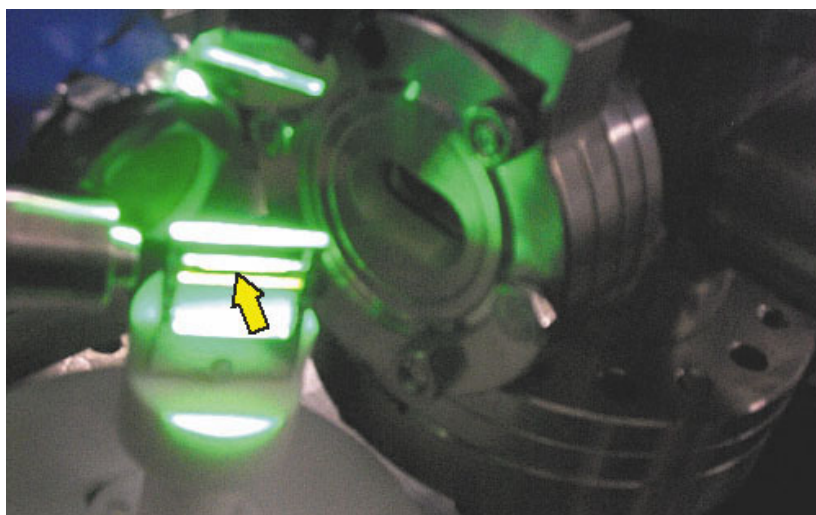


**Fig. 2.** Sample simultaneously exposed to the X-ray beam and to visible light which drives photosynthetic water oxidation. In the photograph, the X-ray beam enters from the upper right edge and passes through an ion chamber before it hits the PSII sample (marked by the yellow arrow). The X-ray fluorescence is detected at right angles by a photodiode (the round device behind the sample). The temperature of the sample is controlled by a stream of nitrogen delivered by the metallic pipe in the left part of the photograph. To drive the photoenzyme through its catalytic cycle, samples are illuminated with a sequence of nanosecond flashes of green laser-light.

### Watching biological function—at the atomic level—in real time

Very recently we could go a step further. An experiment long thought to be impossible was successfully completed [5]. We monitored, in a time-resolved X-ray experiment, the S-state transitions of the PSII manganese complex in real time. The temporal resolution was 10 microseconds, which is by a factor of 100 faster than in all previous XAS-experiments on protein-bound metal centers. But even more exciting than the methodical progress, is the discovery of a novel reaction intermediate in the O<sub>2</sub>-formation step [5]. The identification of this reaction step as a deprotonation process rather than the expected electron transfer bears important mechanistic implications. This time-resolved synchrotron experiment also takes us a step closer towards a vision in structural biology: watching biological function in real time.

#### Acknowledgement

We thank the staff scientists at BESSY in Berlin (KMC1, Dr. F. Schäfers; KMC2, Prof. A. Erko), DESY in Hamburg (EMBL

beamline, Dr. W. Meyer-Klaucke), ESRF in Grenoble (ID 26, Dr. P. Glatzel) for their support. We explicitly thank J. Wichmann, B. Süß and Dr. R. Krivanek who contributed by complementary experiments not involving synchrotron radiation. We acknowledge support by the BMBF (05KS1KEA/6), the Volkswagen Foundation (Haumann/Dau) and the DFG (C6 and C8 in the Sfb 498).

#### References

- [1] J. Nugent (ed.) *Biochim. Biophys. Acta* **1503**, Special Issue on Photosynthetic Water Oxidation (2001).
- [2] B. Loll, J. Kern, W. Saenger, A. Zouni, and J. Biesiadka, *Nature* **438**, 1040-1044 (2005).
- [3] H. Dau, P. Liebisch, and M. Haumann, *Anal. Bioanal. Chem.* **376**, 562-583 (2003).
- [4] M. Haumann, C. Müller, P. Liebisch, L. Iuzzolino, J. Dittmer, M. Grabolle, T. Neisius, W. Meyer-Klaucke, H. Dau, *Biochemistry* **44**, 1894-1908 (2005).
- [5] M. Haumann, P. Liebisch, C. Müller, M. Barra, M. Grabolle, and H. Dau, *Science* **310**, 1019-1021 (2005).

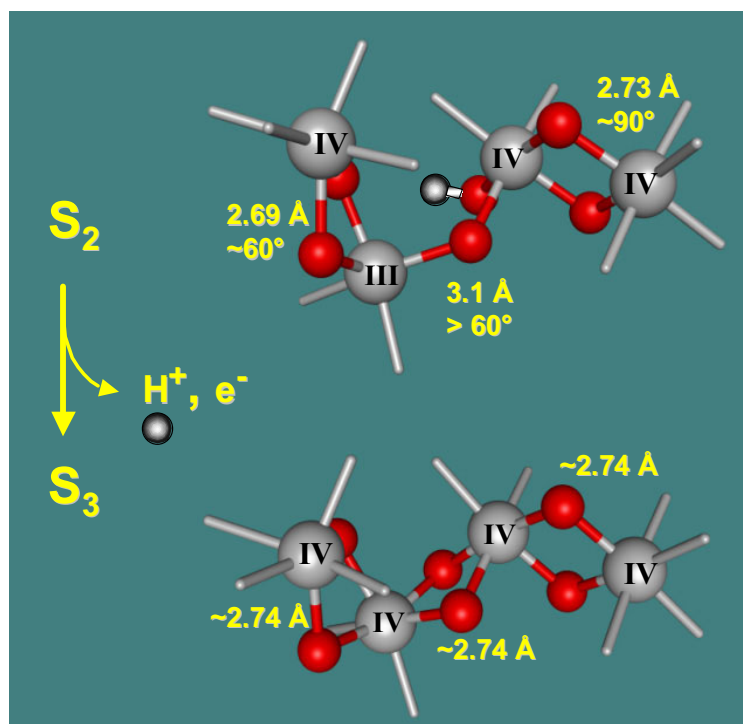


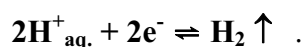
**Fig. 3.** Structural changes of the PSII manganese complex in the S<sub>2</sub>→S<sub>3</sub> transition (ball-and-stick representation, red balls, oxygen; grey balls, manganese; small grey ball, proton). A five-coordinated Mn(III) is transformed into a six-coordinated Mn(IV). This involves the coupled removal of an electron and a proton. The newly formed bridging oxide can serve as a proton acceptor in the O<sub>2</sub>-formation transition. The changes in structure and oxidation state have been inferred from X-ray absorption data collected at 10 K and at room temperature. Distances between Mn atoms are indicated in Å (=10<sup>-10</sup> m).

## Hydrogen is the fuel: Catalysis at nickel-iron active sites of hydrogenases tracked by X-ray absorption spectroscopy

S. Löscher, H. Dau and M. Haumann

Freie Universität Berlin, Institut für Experimentalphysik

Enzymes denoted as hydrogenases catalyze the production of molecular hydrogen. They are widespread among microorganisms such as bacteria. Understanding the mechanism of this biological hydrogen production may pave the road for the design of bio-mimetic and biotechnological applications for the generation of H<sub>2</sub>-gas as a fuel [1]. Hydrogenases reversibly and effectively catalyze the following reaction at a protein-bound dinuclear transition-metal center of the Fe-Fe or Ni-Fe type (Fig. 1):



Frequently, hydrogenases are rapidly inactivated by poisoning of their active site by dioxygen. However, for the efficient biotechnological employment of these biological catalysts, resistance against inhibition by O<sub>2</sub> is highly advantageous.

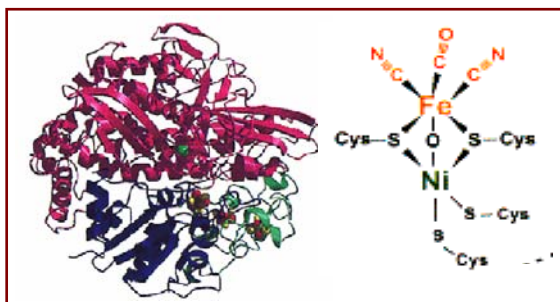


**Fig. 1.** Left, crystal structure of prototypic Ni-Fe hydrogenase protein derived from X-ray crystallography [2]; right, scheme of the Ni-Fe active site; Cys, cysteine residues of the protein.

(i) In fuel-cell applications for the generation of electricity two enzyme-covered electrodes may be operated in parallel [3]

catalyzing two half-cell reactions to produce electrical energy (Fig. 2):

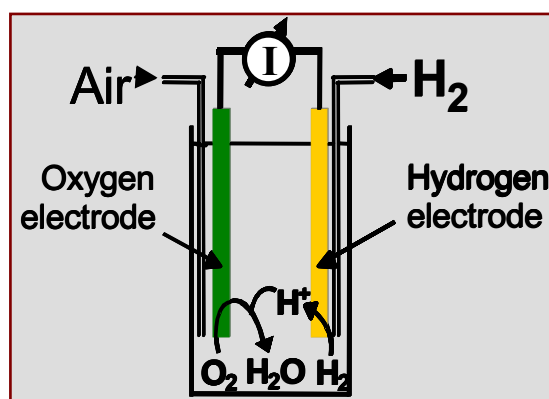
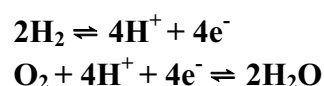


**Fig. 2.** Schematic biological fuel-cell. Electrodes may be covered with hydrogenases and O<sub>2</sub>-consuming enzymes [3].

(ii) A further prospect for energy generation is coupling of the sunlight-powered photosynthetic water oxidation reaction producing O<sub>2</sub> gas to the generation of H<sub>2</sub> gas by hydrogenases.

Both reaction sequences involve H<sub>2</sub> turnover in parallel to dioxygen conversion so that resistance of the hydrogenase to O<sub>2</sub> is a prerequisite for effective operation.

In nature in a particular organism, the bacterium *Ralstonia eutropha* (Fig. 3), three different hydrogenases of the Ni-Fe type are found (Fig. 4) which all are operative in the presence of O<sub>2</sub> [4]. Understanding their mechanism of H<sub>2</sub> catalysis and the reasons for O<sub>2</sub>-tolerance of the active site at the atomic level is the primary goal of our research.

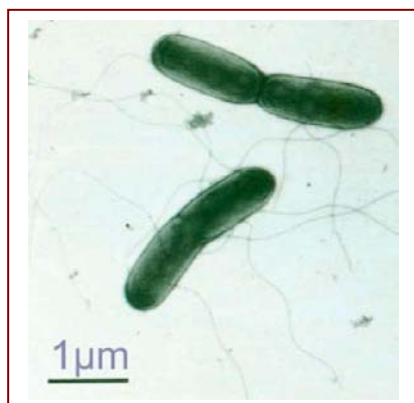


**Fig. 3.** Cells of the proteobacterium *Ralstonia eutropha*.

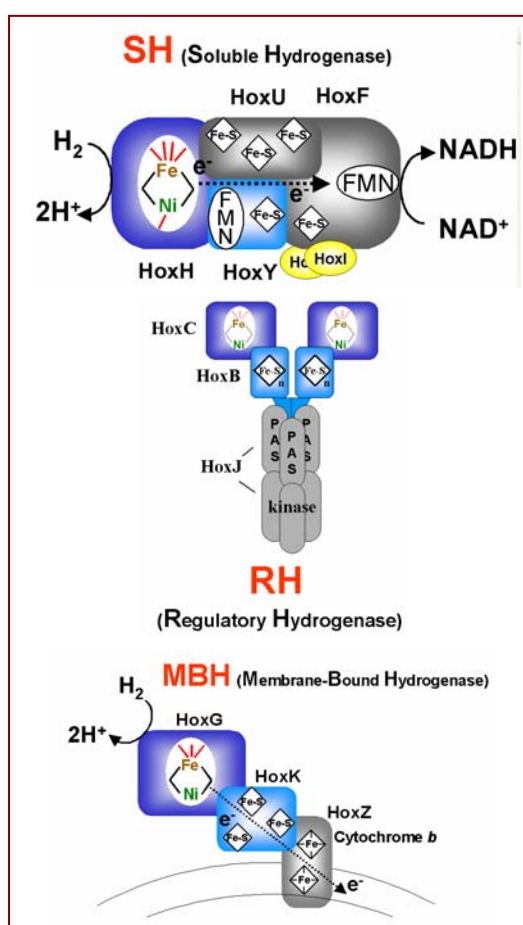


**Fig. 4.** Organisation of the three different Ni-Fe hydrogenases from *Ralstonia eutropha* (courtesy of AG Prof. B. Friedrich, HU-Berlin).

Evidently, knowledge of the atomic structure of the Ni-Fe active site is important for understanding the mechanism of  $H_2$ -conversion. We employ X-ray absorption spectroscopy (XAS) at the Ni and Fe K-edges to obtain information on the interactions between the amino acid residues

of the protein and the metal atoms, on the binding of hydrogen to the active site, and on redox processes occurring during catalysis. XAS on biological samples frequently is denoted as BioXAS [5].

The BioXAS technique relies on the absorption of X-ray photons by the metal atoms under investigation. This process leads to generation of photoelectrons which are backscattered at the surrounding matrix atoms whereby interference of outgoing and backscattered electron waves occurs. Interference causes an oscillatory behaviour of the X-ray absorption if plotted versus the excitation energy. To extract structural information, XAS spectra are simulated according to the well-known “EXAFS formula” [6] :

$$\chi(k) = \frac{S_0^2}{k} \sum_{i=1}^p N_i \frac{|f_{\text{eff},i}(k, R_i)|}{R_i^2} e^{-2k^2\sigma_i^2 - 2R_i/\lambda(k)} \sin(2kR_i + \phi_i(k))$$

XAS data analysis yields information on the number and chemical identity of metal ligands, on metal-to-metal distances, on the oxidation state of the metal ions, and on changes of these parameters during catalysis.

XAS measurements were performed at BESSY-II, at the European Molecular Biology Laboratory Outstation (EMBL at HASYlab, DESY, Hamburg), and at the European Synchrotron Radiation Facility (ESRF, Grenoble, France). At these synchrotrons, brilliant and stable X-ray beams in combination with high-resolution monochromators, cryostat devices for measurements at liquid-helium temperatures, and efficient X-ray detectors have been made available (Fig. 5) so that XAS on ultra-dilute and fragile biological samples now is an established and exceptionally powerful tool to study protein-bound metal centers.

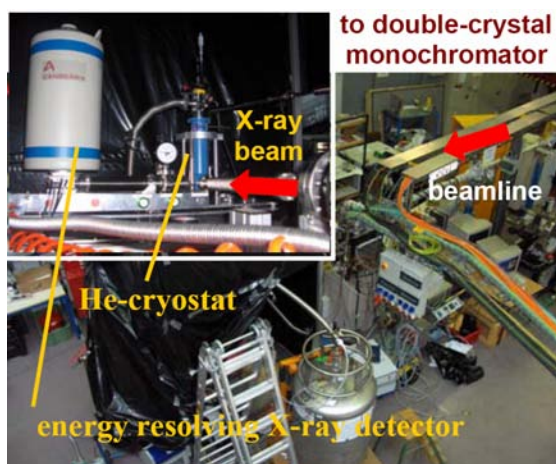


**Fig. 5.** Experimental setup for BioXAS measurements at KMC-1 at BESSY-II.

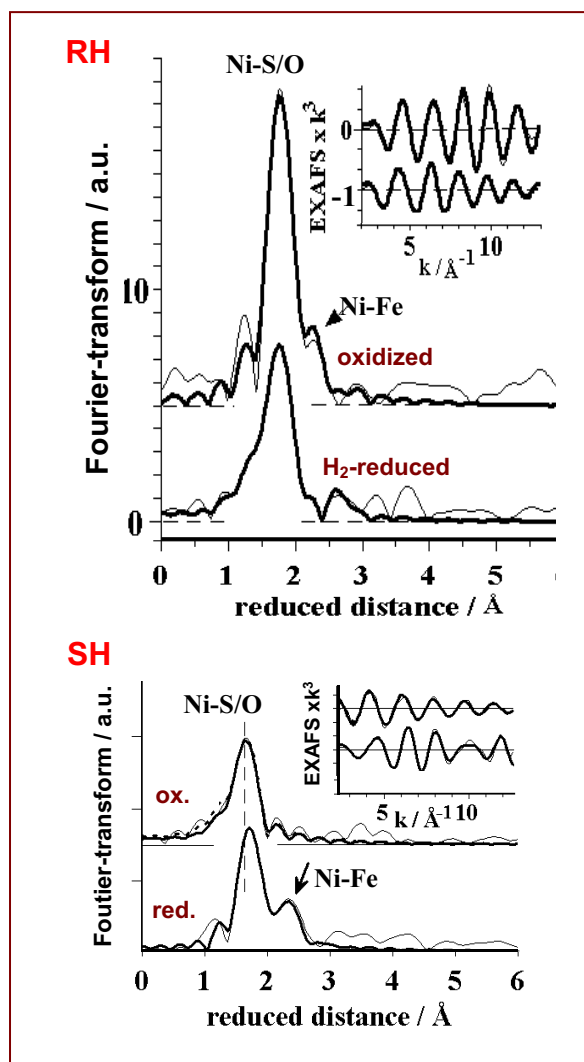


**Fig. 6.** EXAFS spectra of isolated Ni-Fe hydrogenases in oxidized and reduced states. Thick lines, simulations [7,8].

To obtain structural information on their Ni-Fe site, the isolated and purified hydrogenases of *Ralstonia eutropha* were studied *in vitro* by XAS at the Ni K-edge. It is believed that at the Ni atom most of the hydrogen chemistry occurs. Selected Ni EXAFS (extended X-ray absorption fine structure) spectra of the regulatory Ni-Fe hydrogenase (RH) and of the nicotinamid-adenine-dinucleotide-reducing soluble enzyme (SH) are shown in Fig. 6.

The RH belongs to a specific type of Ni-Fe hydrogenase; it acts as a hydrogen sensor. Upon H<sub>2</sub>-cleavage by the RH, a complex signal-transduction cascade is initiated in the cell which finally leads to the expression of the other two hydrogenases [4], which use H<sub>2</sub> to provide reducing equivalents for live-sustaining cell reactions such as carbon dioxide (CO<sub>2</sub>) fixation and respiration.

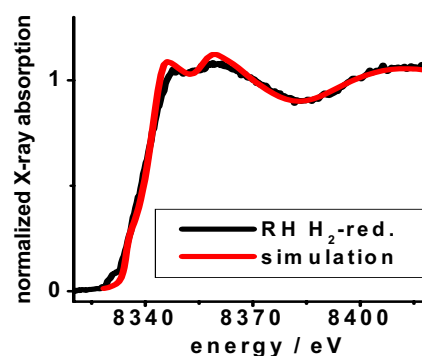


**Fig. 7.** Ni XANES spectrum of a RH preparation under H<sub>2</sub> and simulation (red).

Simulations both of XANES spectra (Fig. 7) using a novel approach [9] and of EXAFS spectra has lead to the formulation of structural models of the Ni-Fe active sites and to important insights into the binding properties of H<sub>2</sub> (Fig. 8).

Besides the Ni-Fe active site, all hydrogenases contain a further type of metal center, namely iron-sulfur clusters (Fe-S), which are involved in electron transfer reactions during H<sub>2</sub>-turnover. Structural

information on these cofactors was derived from XAS measurements at the Fe K-edge

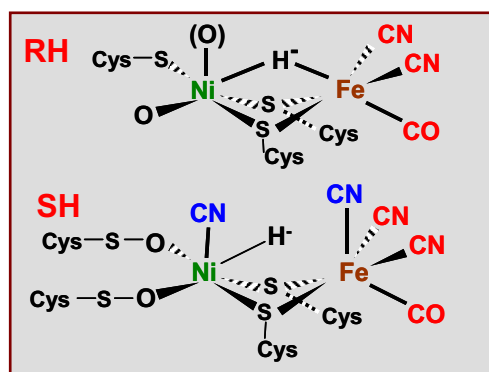


**Fig. 8.** Structural models of the Ni-Fe active sites of the hydrogen sensor (RH) and of the NAD-reducing hydrogenase (SH) during  $H_2$ -turnover derived on basis of XAS, EPR, and FTIR investigations [7,8].

Interestingly, there is evidence for the presence of unusual types of Fe-S clusters in the  $O_2$ -tolerant hydrogenases which are not found in the prototypic enzymes [10]. As revealed by shifts of the K-edge position to lower energies, these Fe-S clusters accept electrons during  $H_2$ -turnover at the Ni-Fe site.

BioXAS techniques successfully were employed to unravel structural and functional features of the Ni-Fe active sites and of Fe-S clusters in hydrogenases. There are remarkable differences between the  $O_2$ -tolerant Ni-Fe hydrogenases and the prototypic enzymes at the atomic level. Unique strategies seem to be implemented which allow for the use of hydrogen as an energy source in the presence of oxygen. In the near future, adaptation of biological systems for technological  $H_2$ -production may be within reach.

## References

- [1] R. Cammack, R. Robson, and M. Frey, Eds. *Hydrogen as a fuel: learning from nature*. Taylor & Francis, London, UK (1997)
- [2] A. Volbeda, M. H. Charon, C. Piras, S. Hatchikian, M. Frey, and J. Fontecilla-Camps, *Nature* **373**, 556-557 (1995).
- [3] K. A. Vincent, J. A. Cracknell, O. Lenz, I. Zebger, B. Friedrich, and F. A. Armstrong *Proc. Natl. Acad. Sci. USA* **102**, 16951-16954 (2005).
- [4] O. Lenz and B. Friedrich, *Proc. Natl. Acad. Sci. USA* **95**, 12474-12479 (1998).
- [5] H. Dau, P. Liebisch, and M. Haumann, *Anal. Bioanal. Chem.* **376**, 562-583 (2003).
- [6] D. E. Sayers, E. A. Stern, and F. W. Lytle, *Phys. Rev. Lett.* **27**, 1204-1207 (1971).
- [7] M. Haumann, A. Porthun, T. Buhrke, P. Liebisch, W. Meyer-Klaucke, B. Friedrich, and H. Dau, *Biochemistry* **42**, 11004-11015 (2003).
- [8] T. Burgdorf, S. Löscher, P. Liebisch, E. van der Linden, M. Galander F. Lenzian, S. P. Albracht, W. Meyer-Klaucke, B. Friedrich, H. Dau, and M. Haumann, *J. Am. Chem. Soc.* **127**, 576-592 (2005).
- [9] H. Dau, P. Liebisch, and M. Haumann, *Phys. Scripta* **T115**, 844-846 (2005).
- [10] T. Buhrke, S. Löscher, E. Schlodder, I. Zebger, L. K. Andersen, P. Hildebrandt, W. Meyer-Klaucke, H. Dau, B. Friedrich, and M. Haumann, *J. Biol. Chem.* **280**, 19488-19495 (2005).

## Acknowledgement

We thank the beamline scientists at BESSY-II (Dr. F. Schäfers, M. Mertin) and at the EMBL outstation Hamburg (Dr. W. Meyer-Klaucke) for excellent support, the workgroup of Prof. B. Friedrich (HU-Berlin, Microbiology) for an exciting collaboration.

## Enigmatic manganese volcanoes at the cell wall of a green alga: Microfocus X-ray spectroscopy relates microscopic and atomic-level structure

Peter Liebisch<sup>1</sup>, Andreas Schöler<sup>1</sup>, Claudia Müller<sup>1</sup>, Christoph Plieth<sup>2</sup>,  
Alexej Erko<sup>3</sup>, Holger Dau<sup>1</sup>

<sup>1</sup> Freie Universität Berlin, Institut für Experimentalphysik

<sup>2</sup> Christian-Albrechts-Universität Kiel, Zentrum für Biochemie und Molekularbiologie

<sup>3</sup> BESSY GmbH, Berlin

Manganese is an essential trace element in plants and crucial for photosynthetic oxygen evolution [1] as well as for other enzymatic reactions. Manganese toxicity has long been recognized as a factor limiting growth when organisms are exposed to high concentrations of Mn. Possibly related to a detoxification mechanism, cells of the green alga *Chara corallina* develop brown deposits on the outer cell wall when cultured in alkaline water with a Mn-containing sediment. Are these volcano-shaped brown deposits a distinct form of manganese dioxide (Braunstein)?

To address the questions of spatial distribution and chemical speciation of metals on

the alga cell wall, we performed microfocus XAS experiments. Elemental 2D-mapping by means of characteristic X-ray fluorescence as well as X-ray absorption measurements on selected spots on the cell wall were employed. The used microfocus technique facilitates an exciting combination of microscopy ( $\mu\text{m}$  resolution) and structural studies at atomic resolution (resolution of  $0.02 \text{ \AA}$ ).

For data collection two types of samples were used: (1) Cell walls of unicellular alga placed between 25  $\mu\text{m}$  layers of cellophane and then dried. These samples were particularly flat and easy to handle. (2) Fresh alga cells were cut and placed between two

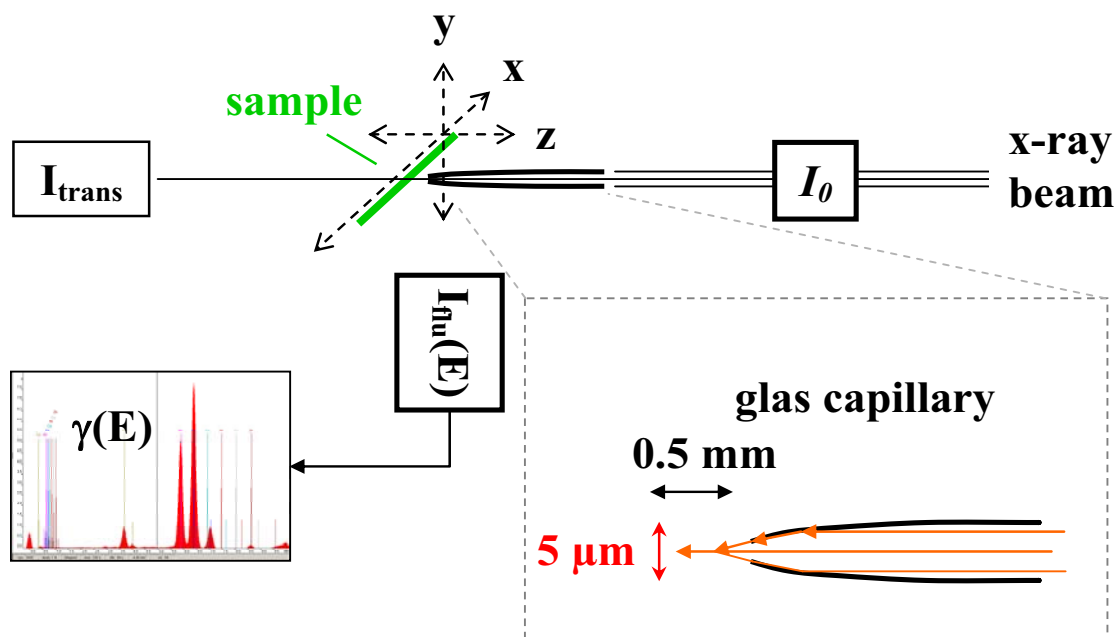


**Figure 1.** Experimental setup for micro-focus XAS experiment (KMC-2, BESSY).

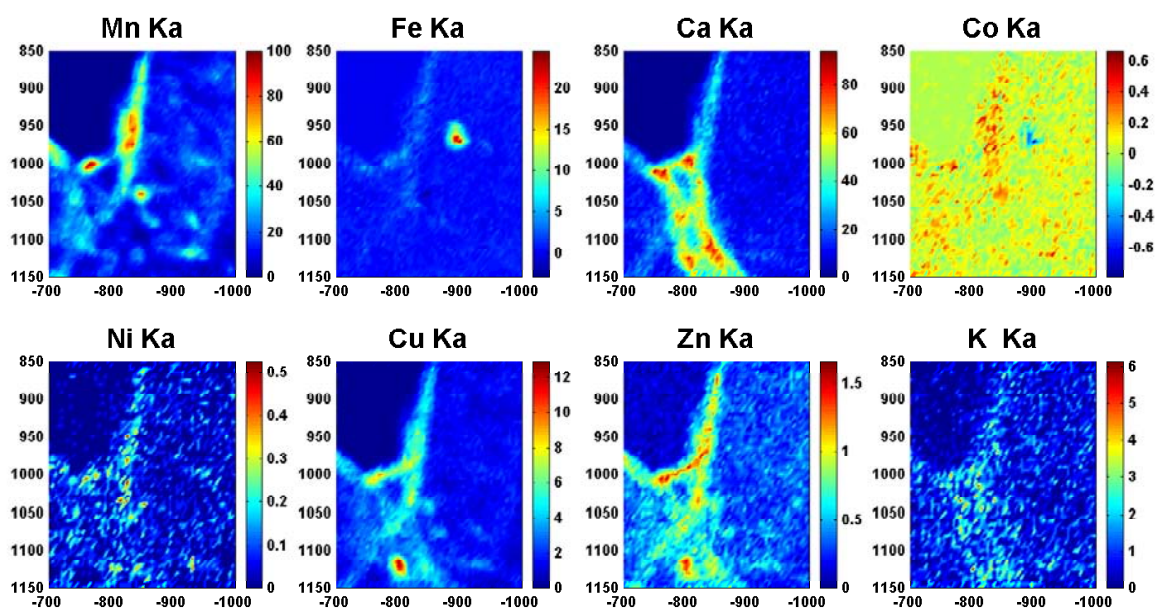


**Fig. 2:** 2D-map of x-ray emission intensity for different elements (*Chara corallina* cell). The  $x$ - and  $y$ -dimensions are given in  $\mu\text{m}$  and the intensity represents the number of counts for each characteristic fluorescence line normalized to the maximum of  $\text{Mn-K}_{\alpha}$  counts and weighted by a calibration factor obtained for a stoichiometric standard.

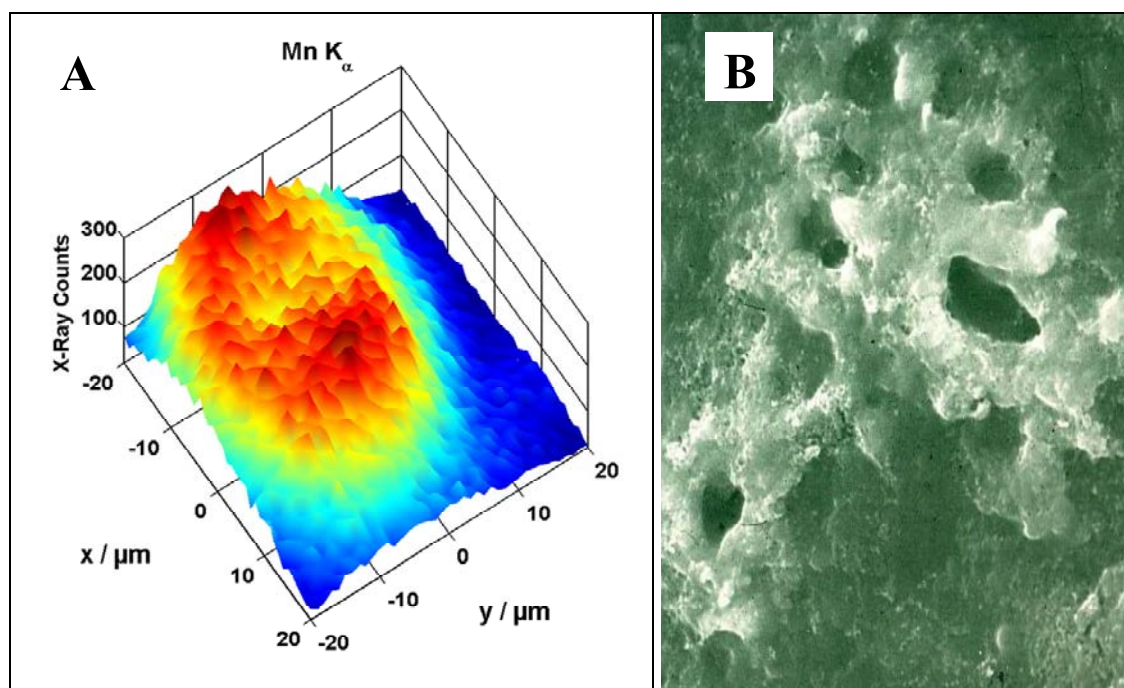


**Fig. 3:** Crater structure on alga cell surface. (A) 2D-map of  $\text{Mn K}_{\alpha}$  fluorescence, (B) electron microscopy (EM) image. Manganese is found in craters (or volcano-like) structures. While their existence and shape was known from EM images, their elemental composition now was mapped in the microfocus experiment. The resolution is sufficiently high to resolve the crater structure, i.e. as good as  $5 \mu\text{m}$ .

stretched  $12.5 \mu\text{m}$  layers of Kapton foil contrast to (1), these samples remained wet immediately before the measurements. In and thus “chemically intact” for about 8

hours.

For selected elements (Mn, Fe, Ca, Co, Ni, Cu, Zn, K) the intensity of their characteristic x-ray fluorescence lines was measured across a 2D-mesh. The data was normalized and weighted according to factors gained from standard measurements with a sample of known element stoichiometry. For Fe and Co, the  $K_{\alpha}$  intensity was further corrected for contributions of Mn- $K_{\beta}$  and Fe- $K_{\beta}$ , respectively. While Fig. 2 shows a representative map for all measured elements, Fig. 3 shows a Mn- $K_{\alpha}$  map of a crater structure on the cell surface. Those structures are of special interest in the light of Mn-sedimentation and detoxification strategies of cells. Detailed analysis of the element composition of the deposits is in progress.

For selected spots on typical Mn-containing deposits, XAS measurements were performed. Figure 4 shows XANES spectra of

the Mn K-edge for a dried and a freshly prepared sample. As a first step of the chemical speciation, alga data is compared with reference spectra measured for known Mn oxides. Clearly one can assign the intact bio-sediment to a form of  $MnO_2$  with an Mn oxidation state close to IV. The preliminary analysis of the elemental mapping suggests a Mn:Ca stoichiometry of 5:1. The analysis of microfocus EXAFS measurements (not shown) may lead to a structural model of these biogenic manganese deposits at the atomic level (work in progress).

## References

- [1] H. Dau, P. Liebisch, and M. Haumann, *Anal. Bioanal. Chem.* **376**, 562 (2003).
- [2] J. D. Hem and C. J. Lind, *Geochimica et Cosmochimica Acta* **58**, 1601 (1994).
- [3] F. M. M. Morel and N. M. Price, *Science* **300**, 944 (2003).

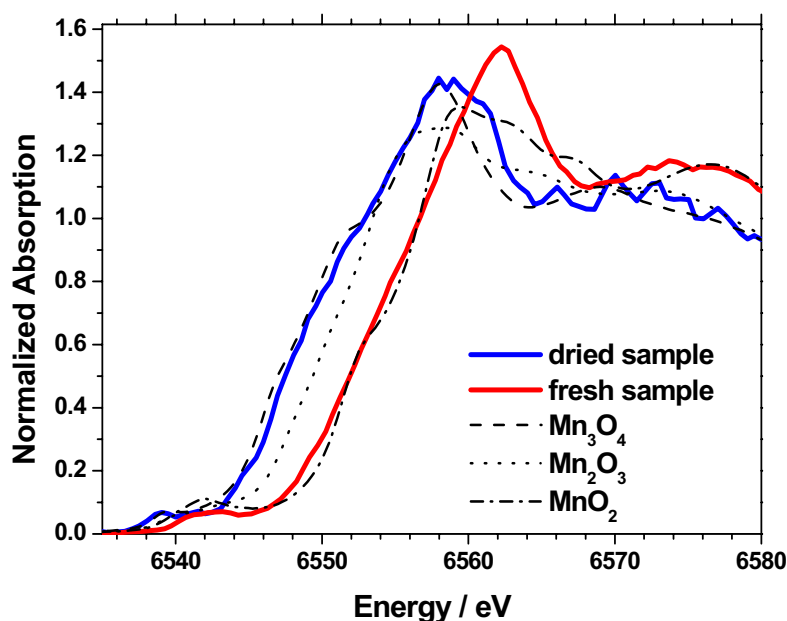


**Fig. 4:** XAS measurement on Mn-containing spot. By comparison with reference substances, determination of the Mn oxidation state and eventually detailed chemical speciation can be achieved. Also complete EXAFS spectra were collected on a single Mn crater.

# Synchrotron Radiation Circular Dichroism (SRCD) reveals structural changes in the photoreceptors phytochrome and photoactive yellow protein (PYP)

Berthold Borucki, Harald Otto, Sven Seibeck, Maarten P. Heyn

Freie Universität Berlin, Institut für Experimentalphysik

## 1. Introduction

### Why Circular Dichroism (CD)?

CD is the difference in absorption of left and right circularly polarized light by a chiral molecule.

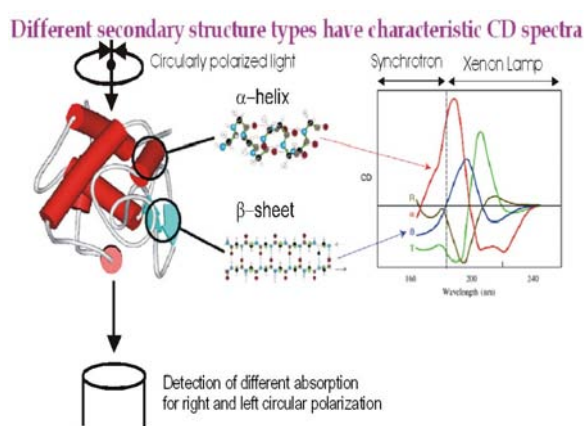


**Fig. 1:** The CD of the amide chromophores of proteins in the UV region (160-240 nm) depends characteristically on their secondary structure ( $\alpha$ -helices,  $\beta$ -sheets, random coil etc.). This is shown schematically. (From introduction to SRCD, Daresbury).

The CD spectrum of the protein is a superposition of the fractions of the pure motif spectra of Fig 1. Therefore we can study:

- secondary structure of proteins that cannot be crystallized.
- structural changes of photoreceptors in the signaling state.
- environmental effects on the structure of proteins (pH, salt, temperature etc.)
- protein folding / unfolding, chromophore assembly.

- ligand binding or dimerization effects. The proteins can be investigated in aqueous solutions at low concentrations. Time resolutions up to microseconds are possible.

### Why synchrotron radiation for CD?

- the wavelength region 160 to 190 nm is only accessible by synchrotron radiation providing more precise secondary structure information (see Fig. 1).
- much higher intensity in the UV, therefore shorter collection times for the spectra with much higher signal to noise ratio.
- stopped-flow CD measurements require fewer combined shots to provide good data over a wide wavelength range.

## 2. Light induced changes of secondary structure of photoactive yellow protein (PYP)

### What is PYP?

PYP is a bacterial 14 kD blue-light photoreceptor ( $\lambda_{\max} = 446$  nm) whose putative function is phototaxis. PYP is the prototype of a superfamily of more than 1000 PAS- domain signal proteins that act as light sensors of bacteria and plants, redox sensors, serine / threonine kinases, voltage gated channels and much more.

### Structural changes:

Upon illumination with blue light the hydroxycinnamoyl chromophore isomerizes

and becomes protonated, absorbing in the signaling state  $I_2$  at 355 nm (see Fig. 2A). The isomerization is associated with a change of sign of the CD (Fig. 2B) and induces big secondary structural changes (Fig. 2C). These measurements are carried out at the BESSY CD beamline and show a much smaller  $\alpha$ -helical fraction in the signaling state.

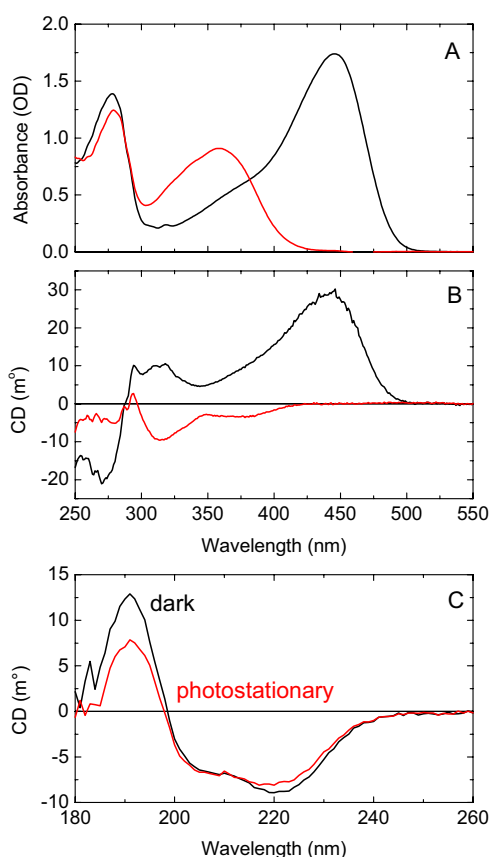


**Fig. 2:** In panel A the spectral shift from 446 to 355 nm is shown. In panel B we see the big CD change caused by the chromophore isomerisation [1]. In panel C the large secondary structural changes are monitored by the CD of the protein backbone. The sample was illuminated at 470 nm leading to a photostationary state of  $\sim 50\%$   $I_2$  accumulation.

High resolution X-ray crystallography (up to 0.8 Å) can follow the early structural changes up to milliseconds but probably not

the large structural change in the signaling state  $I_2$ . A very recent NMR structure of a 25 aminoacids smaller PYP mutant is shown in Fig 3.

The structure is quite different to native PYP but beside of the tennis racket like chromophor motion we can see the much smaller  $\alpha$ -helical content in the signaling state  $I_2$ .

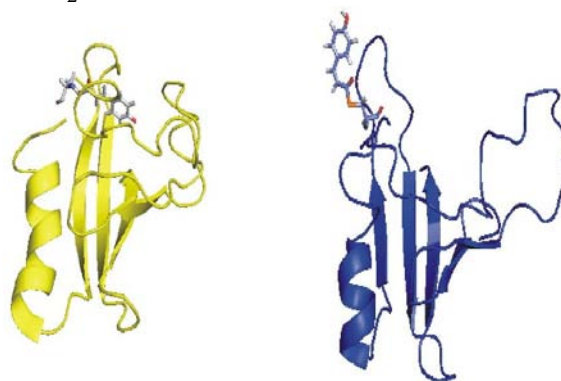


**Fig. 3:** NMR structure of D25 PYP [2] in the ground state P (left 1XFN.pdb) and the signaling state  $I_2$  (right 1XFQ.pdb).

### 3. Changes of the secondary structure in phytochrome

Phytochromes are red-light photoreceptors initially found in higher plants but recently also discovered in a variety of bacteria and fungi. The autocatalytic assembly of the photochromic holoprotein from apoprotein and bilin chromophores is associated with absorbance changes (see Fig. 4A). A substantial increase of the  $\alpha$ -helical content has been reported for the assembly of Cph1 phytochrome [3]. In contrast to these results, our measurements reveal smaller differences in the far-UV CD spectra of apo- and holoprotein of Cph1 and Agp1, respectively (see Fig. 4B).

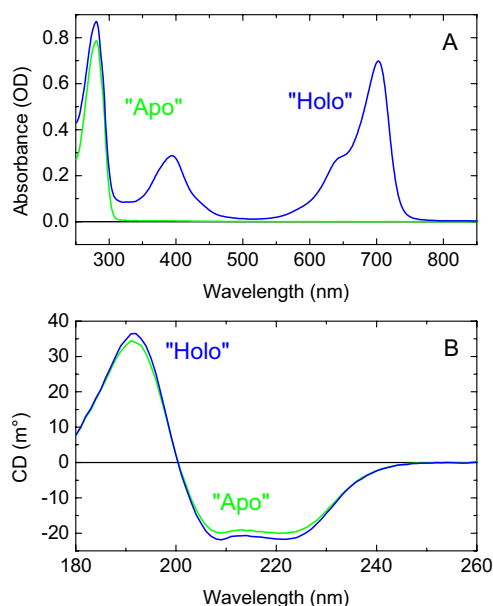


**Fig. 4:** UV-Vis Absorption spectra (A) and far-UV CD spectra (B) of Apo- and Holo-phytochrome Agp1.

Far-UV CD is also a valuable tool to determine the fractions of secondary structures quantitatively. Fig. 5 shows that the CD spectra of the related phytochromes Cph1 and Agp1 differ significantly.

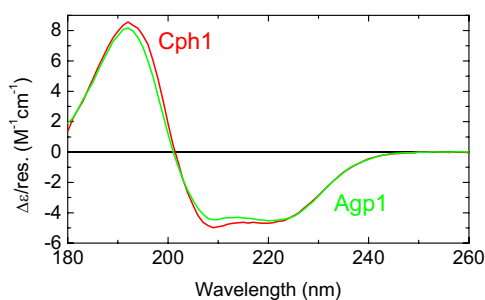


**Fig. 5:** Far-UV CD spectra of two phytochromes (Cph1 and Agp1) from different bacterial organisms (*Synechocystis* and *Agrobacterium tumefaciens*).

Analysis using the software package CDPro (CDSSTR) yields the following fractions of secondary structure:

	Cph1	Agp1
$\alpha$ -Helix	41.7 %	39.0 %
3/10 Helix	9.5 %	8.9 %
$\beta$ -Sheet	7.2 %	8.0 %
poly(Pro)II Struct.	2.7 %	3.4 %
Turns	12.7 %	12.7 %
Unordered	27.3 %	28.7 %

#### 4. Future experiments

Kinetic CD measurements of the auto-assembly of phytochromes will be performed in the near- and far-UV, similar to our recent absorption measurements (see Fig. 6). The stopped-flow technique allows rapid mixing of the apoprotein and the chromophore within 1 millisecond.

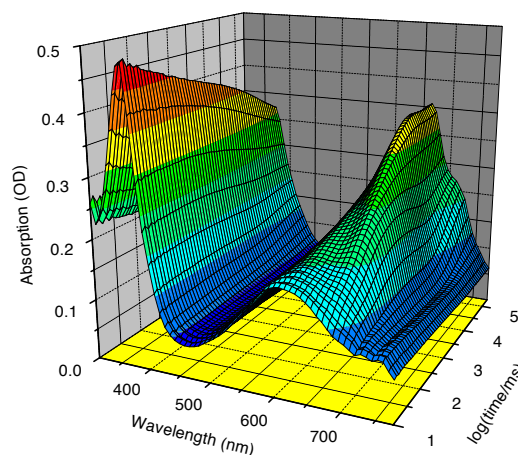


**Fig. 6:** Stopped-Flow measurement of the assembly of Cph1 phytochrome from the apoprotein and the chromophore phycocyanobilin. The absorbance is shown as a function of wavelength and time after mixing.

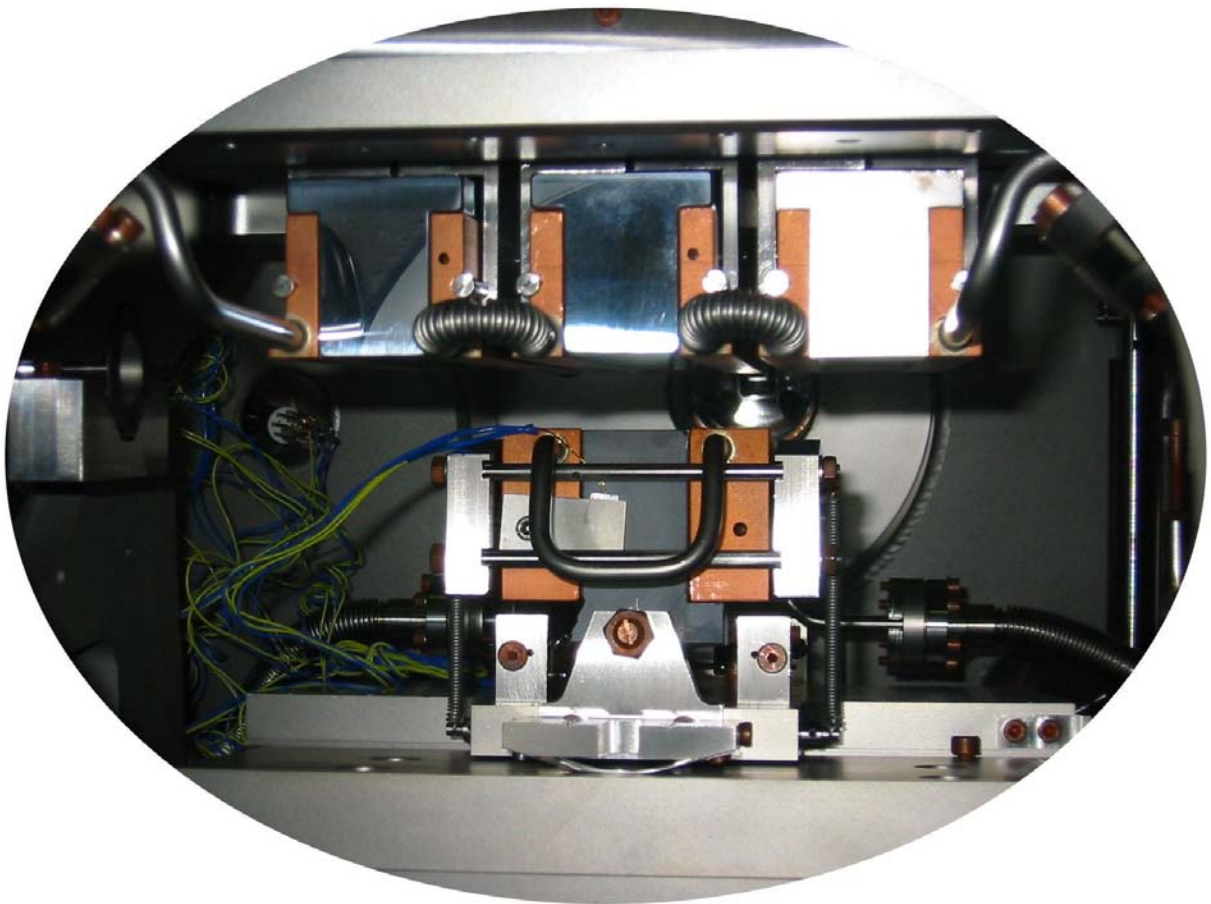
#### References

- [1] B. Borucki, H. Otto, T. E. Meyer, M. A. Cusanovich, and M. P. Heyn, *J. Phys. Chem. B* **109**, 629 (2005).
- [2] C. Bernard et al., *Structure* **13**, 953 (2005).
- [3] C. M. Park, J.Y. Shim, S. S. Yang, J. G. Kang, J. I. Kim, Z. Luka, and P. S. Song, *Biochemistry* **39**, 6349 (2000).



---

# Instrumentation



Previous page: Interior view of the grating chamber of the BUS-beamline. The three T-shaped areas in the upper part of the figure are the gable ends of the three gratings. The grooves are on the not visible lower side. The inverted T-shaped area in the lower part is the gable end of the pre-mirror  $M_2$ . The copper parts provide cooling for the optical elements. The original size of the parts in the foreground (background) is approximately 1.5 times (2 times) larger than on the picture.

## Instrumentation

The high photon flux and brilliance as well as the unique time structure provided by state-of-the-art 3<sup>rd</sup> generation synchrotron-radiation facilities, such as BESSY II in Berlin-Adlershof, allow to perform experiments on a previously not feasible level. However, to make full use of these properties of synchrotron radiation, special efforts have to be devoted to developments in instrumentation. This covers the design, setup and operation of both beamlines that provide photons with well-defined properties and user experiments that make use of these photons.

The Freie Universität Berlin has a long experience with the setup and operation of beamlines; this goes back to the late 80's of the last century and started with the very successful operation of the beamline SX700/II at BESSY. Currently, the Freie Universität Berlin is involved in four beamline projects covering the energy range from UV to soft X-ray radiation. The contribution of Püttner *et al.* describes three of these beamlines. The fourth beamline project, namely the Russian-German beamline, and its substantial impact on the international cooperation between scientists, is described by Molodtsov *et al.*

Two recent developments in the field of user experiments are described in the second part of this chapter. The setup described by Miguel *et al.* synchronizes Laser pulses with the X-ray pulses created in the single-bunch mode of the BESSY II storage ring with the aim to study the dynamic response of magnetic multilayers under the influence of ultrafast magnetic pulses. The experiment is expected to shine light on the magnetization processes relevant for modern magnetic storage devices. The successful setup of a X-ray absorption experiment dedicated to measure dilute biological samples is described by Loja *et al.*. This new instrument will allow to obtain information on the nuclear geometry at the atomic level as well as the oxidation state of the metalcenters in biological metalloenzymes – the catalysts in biological systems – during the process of catalysis.



## VUV and Soft X-ray beamline activities of the Freie Universität Berlin at BESSY II

R. Püttner,<sup>1</sup> G. Reichardt,<sup>2</sup> M. Martins,<sup>1</sup> N. Schwentner,<sup>1</sup> and G. Kaindl<sup>1</sup>

<sup>1</sup>*Institut für Experimentalphysik, Freie Universität Berlin, Berlin, Germany*

<sup>2</sup>*BESSY GmbH, Berlin, Germany*

The operation of beamlines by the Freie Universität Berlin at BESSY has a long tradition since the late 80's of the last century, when the then high-resolution beamline SX700/II was assembled at BESSY in Wilmersdorf. Currently, the Freie Universität Berlin is involved in three beamline projects for the VUV and soft X-ray region which cover the energy region from 3 to  $\cong 1000$  eV. This involvement in the setup, design, and operation of beamlines allows to plan and perform long-term projects and guarantees a certain amount of beamtime.

The two beamlines U125/2-NIM and U125/2-SGM cover the lower energy region from 3 to  $\cong 400$  eV and are installed at the quasiperiodic undulator U125/2. This undulator is provided by BESSY and possesses a unique arrangement of the magnets that allows – in combination with the above mentioned beamlines – a highly effective suppression of higher-order light. Standard undulators generate light at integer multiples (higher harmonics) of a basic energy (1<sup>st</sup> harmonic). All these energies fulfill the grating equation, pass the monochromator, and lead to unwanted higher-order light that can disturb an experiment, particularly with low-energy photons. As shown in Fig. 1, the higher harmonics of the quasi-periodic undulator U125/2 are shifted to energies that are non-integer multiples of the 1<sup>st</sup> harmonic, i.e. they cannot pass the monochromator.

The U125/2-NIM (normal incidence monochromator), also called 10m-NIM, covers the lower end of the energy region

from 3 to 40 eV. The design was optimized with respect to the following goals: (i) very high spectral resolution; (ii) high transmission and high brilliance; (iii) flexibility in scanning, precision in reading; (iv) versatile connection of large experimental chambers. The optical layout of this beamline is given in Figure 2.

The 10m-NIM beamline was realized in a joint effort of the University of Kaiserslautern (Schmoranzner group), caring for construction and manufacturing of the monochromator, BESSY (G. Reichardt), taking responsibility for the connection to the undulator, drive unit, refocusing, and installation, and the Freie Universität Berlin (Schwentner group), contributing the vacuum system as well as a Laser assisted grating controller.

To enhance resolution, a 10-m arm length monochromator in an off-Rowland-circle mount with a deflection angle of  $2^\circ$  was chosen. The instrument is worldwide unique in this respect on SR sources, and comparable ones are the 6.5-m eagle mounted at the ALS and LURE. Fig. 3 demonstrates the resolving power beyond

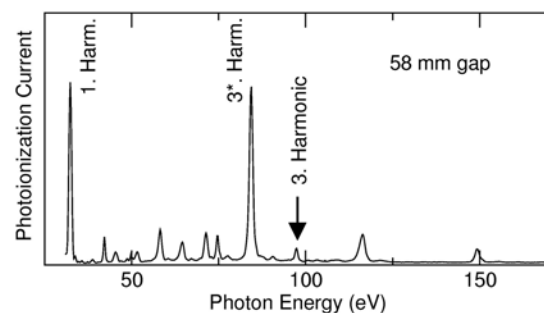


**Fig. 1:** Spectrum of the quasiperiodic undulator U125/2 using a gap of 58 mm.

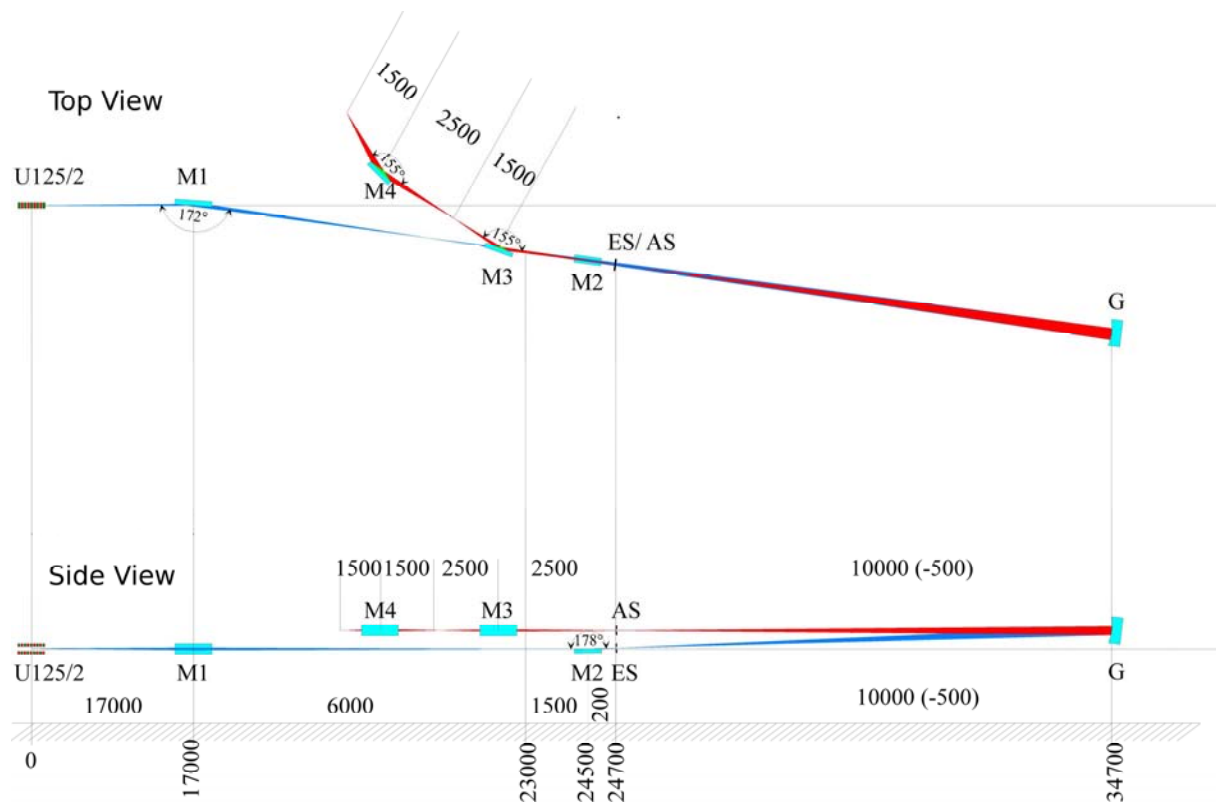


**Fig. 2:** The optical layout of beamline U125/2-NIM.

$10^5$ , which was achieved with a 1200 l/mm grating in second order. Higher order and/or a more densely ruled grating could lead to further improvements.

The installation at the U125/2 undulator provides a high brilliance source. The demagnification by the two pre-mirrors M1 and M2 in Fig. 2 is optimized with respect to photon flux by accepting the full divergence above 15-eV photon energy. Details of the demanding specifications are presented in Ref. [1]. Three spherical gratings can be interchanged in situ and allow a quick adaptation of resolution and photon flux.

Continuous improvements extend the long-wavelength limit to the ultraviolet, and at present a spectral range from 400 nm to 30 nm (from 3eV to 40 eV) is covered. The high resolving power requires a

small step size and a slow scanning speed, while the large spectral range calls for fast scanning. Therefore, a new type of grating drive, with an ultrasonic vacuum piezo motor (Nanomotion) has been employed for the first time at this beamline fulfilling the contradicting demands in an excellent way. Furthermore mechanical feedthroughs to the grating unit become obsolete. The necessary

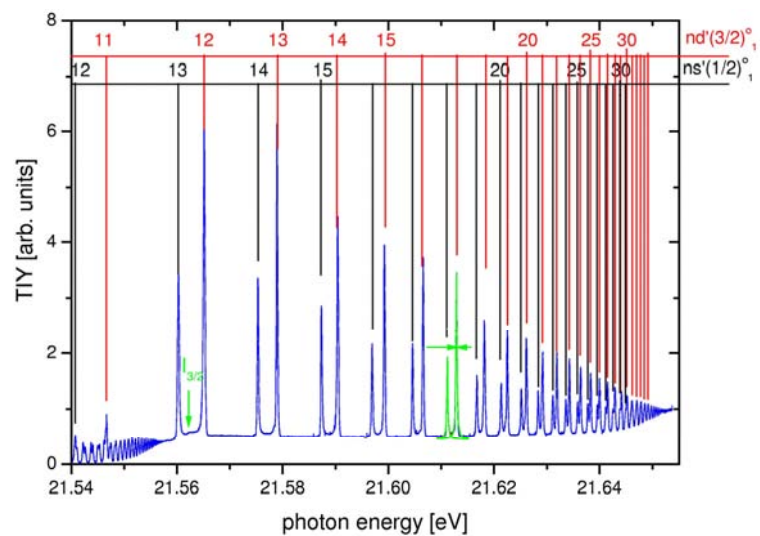


**Fig. 3:** The photoionization spectrum of Neon below the Ne 2p threshold. The resonance at 21.62 eV, indicated in green, exhibits a total width of 187  $\mu\text{eV}$  (FWHM).

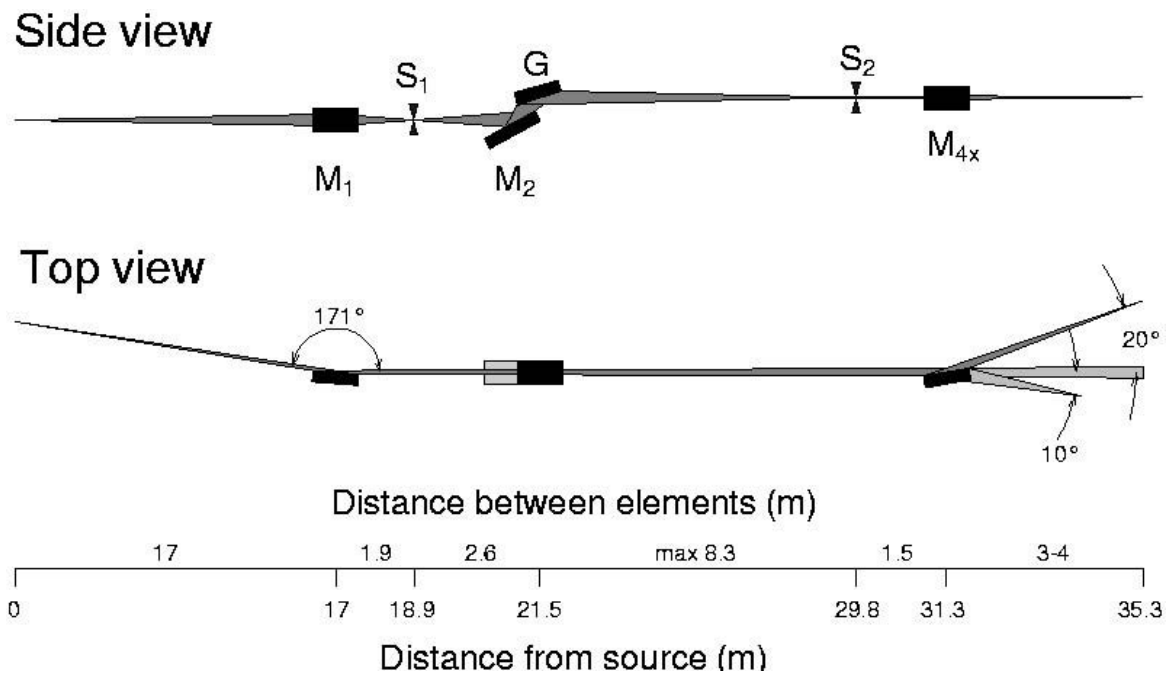


**Fig. 4:** Optical layout of the beamline U125/2-SGM (BUS).

high precision in absolute wavelengths reading is achieved by a combination of techniques. Standard readout works with an in-vacuum angle encoder with a resolution of 0.01 arcsec (Heidenhain RON), mounted on the rotation axis of the grating. Ultimate precision of the grating angle reading delivers a Laser interferometer centered between entrance and exit slit. The beam behind the exit slit is spatially separated from the other two beamlines of the undulator by the mirrors M3 and M4 to provide ample room for spacious experiments. In addition the beam is refocused to  $100 \times 120 \mu\text{m}^2$  and  $5.5 \times 12 \text{ mrad}^2$  in horizontal and vertical direction, respectively. An area of  $4 \times 3 \text{ m}^2$  is available and a platform on air bearings supports the interchange of experiments.

The U125/2-SGM, also called BUS beamline (BUS = Berliner Universitätsverbund Synchrotronstrahlung), was designed for high resolution in the energy range from 30 to 400 eV. It is a spherical-grating monochromator equipped with a movable pre-mirror and a movable exit slit. From its spectral range it complements the 10 m-NIM monochromator which is installed at the same undulator (see

above). The BUS-beamline was financed and is operated by the ‘Berliner Universitätsverbund Synchrotronstrahlung’, which is a cooperation between the three universities in Berlin. It was designed at the Freie Universität Berlin by Dr. Michael Martins and set up in a joint effort by the three involved universities. The beamline became operational in July 2001 and is operated by the Freie Universität Berlin (Kaindl group).

The design of this beamline is displayed in Fig. 4. It is equipped with two exchangeable focusing mirrors,  $M_{4x}$ , which allow to set up two experiments on two separate exit ports. The  $10^\circ$  exit port (lower exit port in Fig. 4) is available for mounting various experimental

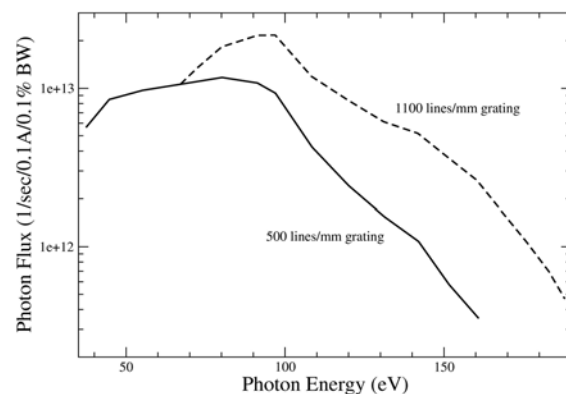


**Fig. 5:** Photon flux of the BUS-beamline in the energy region from 30 to 180 eV.

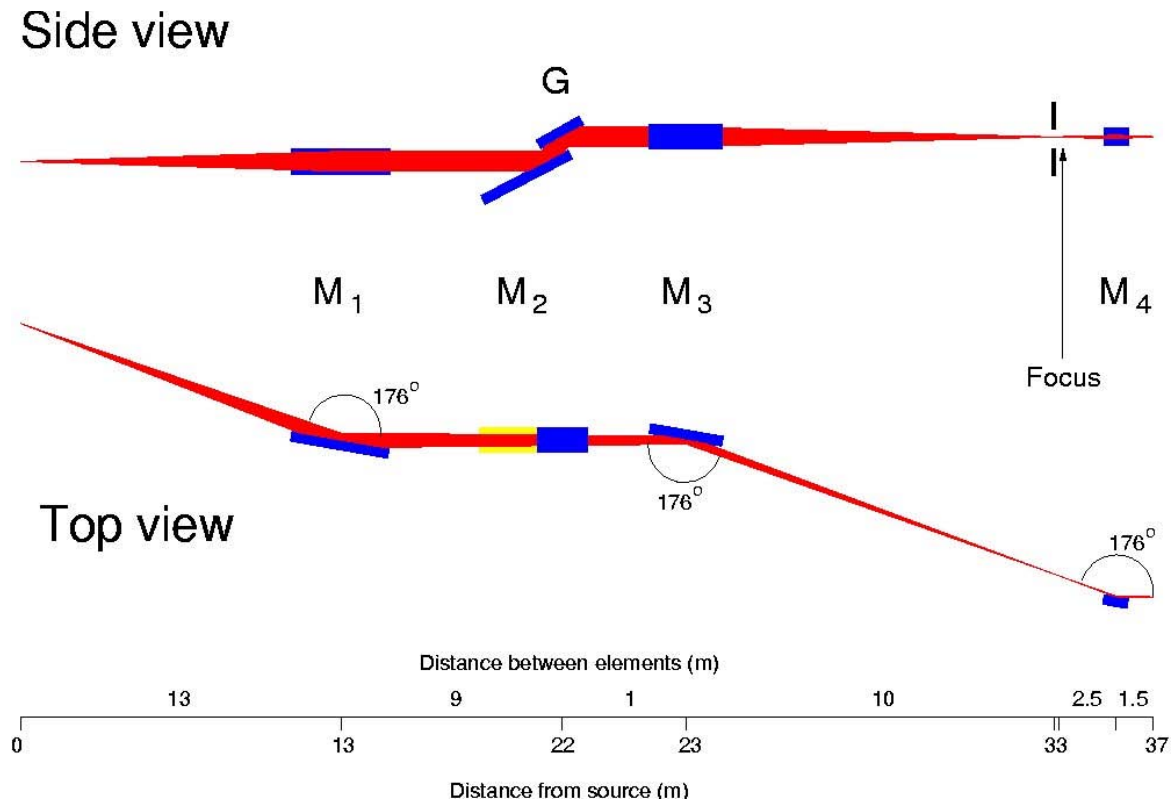


**Fig. 6:** Optical layout of the plane-grating monochromator PM2.

user chambers. At the  $20^\circ$  exit port (upper exit port in Fig. 4) a permanent setup of a high-resolution photoemission chamber for solid state and material science studies equipped with a Scienta SES 200 analyzer is planned for the near future. In addition, at the  $0^\circ$  exit port an unfocused beam is available for diagnostic purposes. The beamline is equipped with three mirrors, with groove densities of 500 l/mm, 1100 l/mm, and 2200 l/mm to provide high energy resolution (e.g. less than 1 meV at 64 eV) over a broad spectral range from 30 to 400 eV. The different gratings deliver a high photon flux of several  $10^{12}$  to  $10^{13}$  photons/ in the energy region from 30 to 180 eV. A more detailed description of the design and the performance is given in Ref. [2].

The PM2 is a beamline equipped with a plane-grating monochromator designed for the energy region from 50 to 1000 eV in order to complement the beamlines U125/2-NIM and U125/2-SGM. It was successfully operated under the name SX700/II at

BESSY. Currently it is rebuilt at a bending magnet at BESSY II. For this purpose, the design was modified in order to adjust it to the new storage-ring parameters. In addition, a focussing mirror was implemented. The new design of this beamline is very similar to that of the Russian-German beamline, which is operated successfully at a bending magnet and provides high resolving power and high beam stability. Therefore, one can expect a comparable high performance for the PM2.

## References

- [1] G. Reichardt, J. Bahrdt, J.-S. Schmidt, W. Gudat, A. Ehresmann, R. Müller-Albrecht, H. Molter, H. Schmoranzer, M. Martins, N. Schwentner, and S. Sasaki, Nucl. Instr. and Meth. A, **467-468**, 462 (2001).
- [2] M. Martins, G. Kaindl, and N. Schwentner, J. Electron Spectrosc. Rel. Phenom. **101-103**, 965 (1999).

## The Russian-German Beamline at BESSY II

G. Kaindl,<sup>1</sup> S.L. Molodtsov,<sup>2</sup> and V.K. Adamchuk<sup>3</sup>

<sup>1</sup>*Institut für Experimentalphysik, Freie Universität Berlin, Berlin, Germany*

<sup>2</sup>*Institut für Festkörperphysik, Technische Universität Dresden, Dresden, Germany*

<sup>3</sup>*Institut of Physics, St. Petersburg State University, St. Petersburg, Russia*

The idea to build a dedicated beamline for Russian-German scientific collaboration in the field of applications of synchrotron radiation at the 'Berliner Elektronenspeicherring für Synchrotronstrahlung' (BESSY II) came up in 1994, and was formulated in a letter by G. Kaindl to the then Bundesminister für Forschung und Technologie, Dr. Paul Krüger. It was strongly supported by leading scientists from both countries, who gathered at BESSY in Nov. 1995 on the occasion of the Russian-German Workshop on "Perspectives of Synchrotron Radiation in Atomic, Molecular, and Materials Science", and again in May 1996 on the occasion of the "Russian-German Seminar on XPS and XRS" in Voronezh, Russia.

The construction of the beamline began in

the fall of 1999 after the "Stiftung Deutsche Klassenlotterie Berlin" (DKBL-Stiftung) had decided to support it with DM 710.000,-, in addition to a substantial commitment of the Russian side in form of major beamline components. The time between submission of the project proposal and the positive decision of the DKBL-Stiftung had been used to complete the optical design of the high-resolution plane-grating monochromator to be installed at the bending magnet D16-1A of BESSY II. In this design study, which was supported by BMBF and by BESSY GmbH, the idea was realized to build a high-resolution monochromator for the energy region from about 30 eV to 1500 eV with the best possible energy resolution. It was shown that this could be

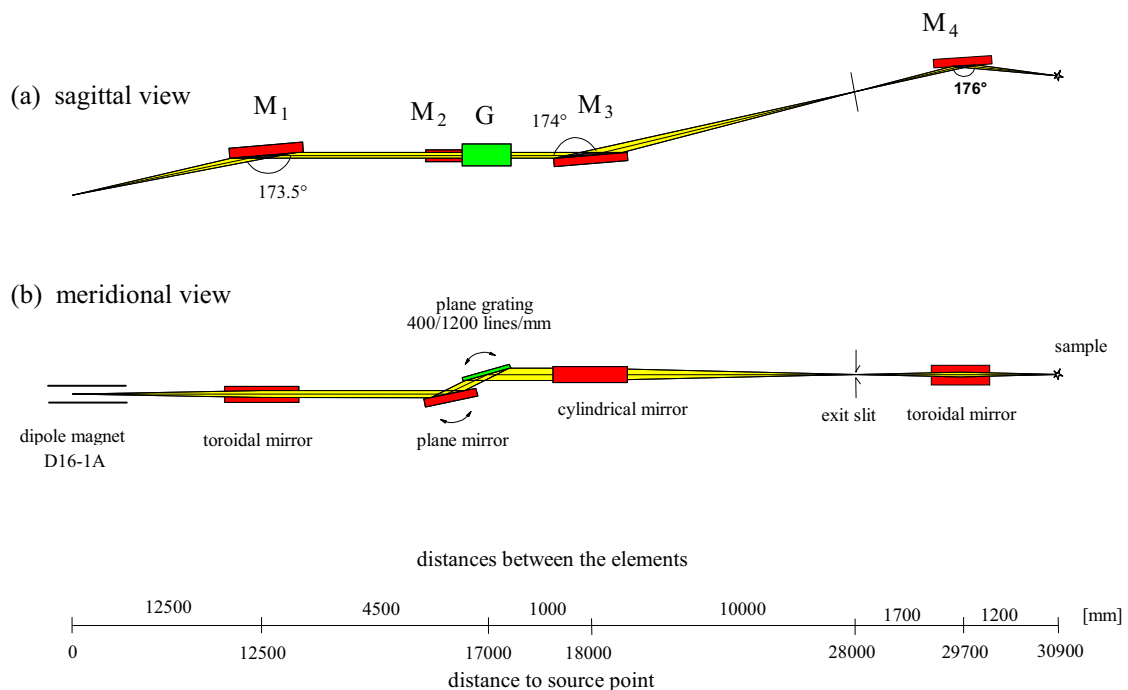


**Fig. 1:** Optical layout of the Russian-German Beamline at BESSY II (from Ref. [2]).

best realized with a Petersen-type plane-grating monochromator operated with collimated light [1]. As shown in Fig. 1, the beamline consists of a toroidal mirror  $M_1$ , focusing the source horizontally with almost no magnification onto the exit slit, while the sagittal radius collimates the beam vertically. The collimated light is then diffracted from a plane grating  $M_2$ , while a cylindrical mirror  $M_3$  focuses the diffracted light vertically onto the exit slit. Finally, the toroidal mirror  $M_4$  refocuses the diffracted light onto the sample position in the experimental chamber.

Two gratings are used (400 groves/mm and 1200 groves/mm) to cover the desired photon-energy range. The incidence angles on the Pt-covered mirrors  $M_1$  and  $M_3$  were chosen to be  $87^\circ$  to give reasonable reflectivities over the whole energy range. Only the first toroidal mirror  $M_1$  has to be water cooled during operation.

The beamline is in operation at BESSY II since Nov. 2001, and already during commissioning it became clear that it provides superior energy resolution as well as excellent stability [2]. This is obvious from the photoionization spectrum of  $N_2$  shown in Fig. 2 as well as from the double-excitation spec-

trum of He in the region of the  $2_{-1}3$  and  $2_{,1}4$  resonances around 64.125 eV, shown in Fig. 3. The energy resolving power is comparable to that of the very best undulator beamlines, with  $E/\Delta E \cong 100.000$  at  $h\nu \cong 64$  eV. This is the best resolving power achieved up to now anywhere at a bending-magnet beamline.

The Russian-German Beamline (RGLB) is operated by a senior scientist (at present PD Dr. S.L. Molodtsov, TU Dresden) with the assistance of doctoral students and graduated scientists from Technical University Dresden, Freie Universität Berlin, and BESSY. Beamtime at the RGLB is assigned on the basis of the scientific values of submitted project proposals by a bilateral steering committee with presently 7 members that meets twice per year. 70% of the beamtime is assigned to Russian groups and 30% to the general BESSY user. At present, 7 leading universities and research institutes from Russia and Germany support the RGLB as part of the Russian-German Laboratory at BESSY. These include on the Russian side: St. Petersburg State University, Shubnikov Institute of Crystallography (Moscow), Kurchatov Institute (Moscow), Ioffé Physico-Technical Institute (St. Petersburg); from the

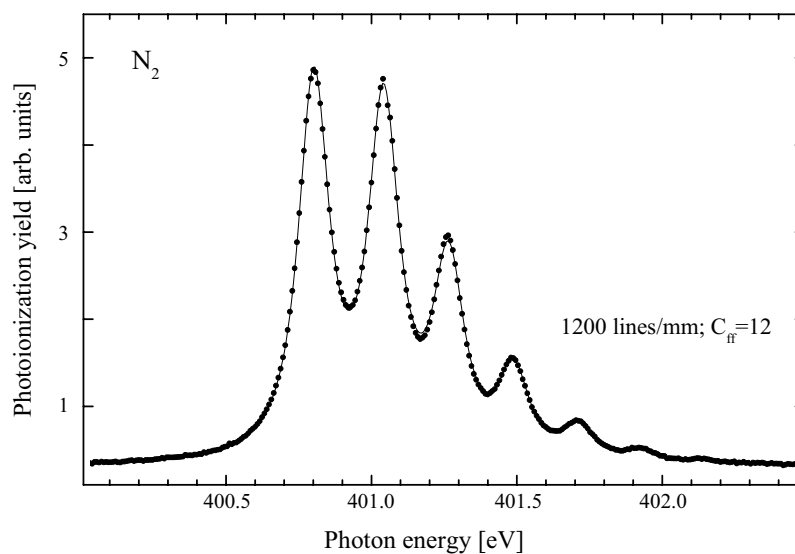


**Fig. 2:** Photoionization spectrum of molecular nitrogen in the region of the  $N_2 1s^{-1}\pi^*$  excitation (from Ref. [2]).

German side: Freie Universität Berlin, BESSY GmbH, Technical University Dresden. Each partner institution can delegate one scientist as a member to the steering committee.

Since the inauguration of the RGLB on Nov. 20, 2001, 34 different groups from 16 different institutions in Russia have used the RGLB at BESSY II. These institutions are spread all over Russia: Moscow, St. Petersburg, Novosibirsk, Chernogolovka, Izhevsk, Voronezh, Yekaterinburg, Krasnoyarsk, Chelyabinsk, and Syktyvkar. The success of the RGLB can be measured most objectively by the scientific results that have been published up to now (Jan. 2006): 59 articles have already appeared in refereed international scientific magazines, including high-impact journals like Phys. Rev. Letters, Applied Physics Letters, Phys. Rev. A and B; 16 more are in print, and 10 more have been submitted. In addition, there are 137 contributions

to international conferences as well as 56 scientific reports to the BESSY Annual Report. This is a remarkable scientific output in the 4 years that have passed since inauguration of the beamline. Of the many excellent results that have been achieved at the RGLB up to now, just three highlights will be briefly mentioned:

D.V. Vyalikh *et al.*, from the TU Dresden, studied the electronic structure of the regular surface of *Bacillus Sphaericus* that is widely used as a template for the fabrication of metallic nanostructures. In this study, they found (see Fig. 4) a semiconductor-like electronic structure with a gap of  $\cong 3$  eV and the Fermi level close to the bottom of the lowest unoccupied molecular orbital [3].

A.S. Vinogradov *et al.*, in a collaboration between St. Petersburg State University, the Freie Universität Berlin, the University Leipzig, BESSY, and MAX-Lab, studied the low-lying unoccupied electronic structure of  $3d$

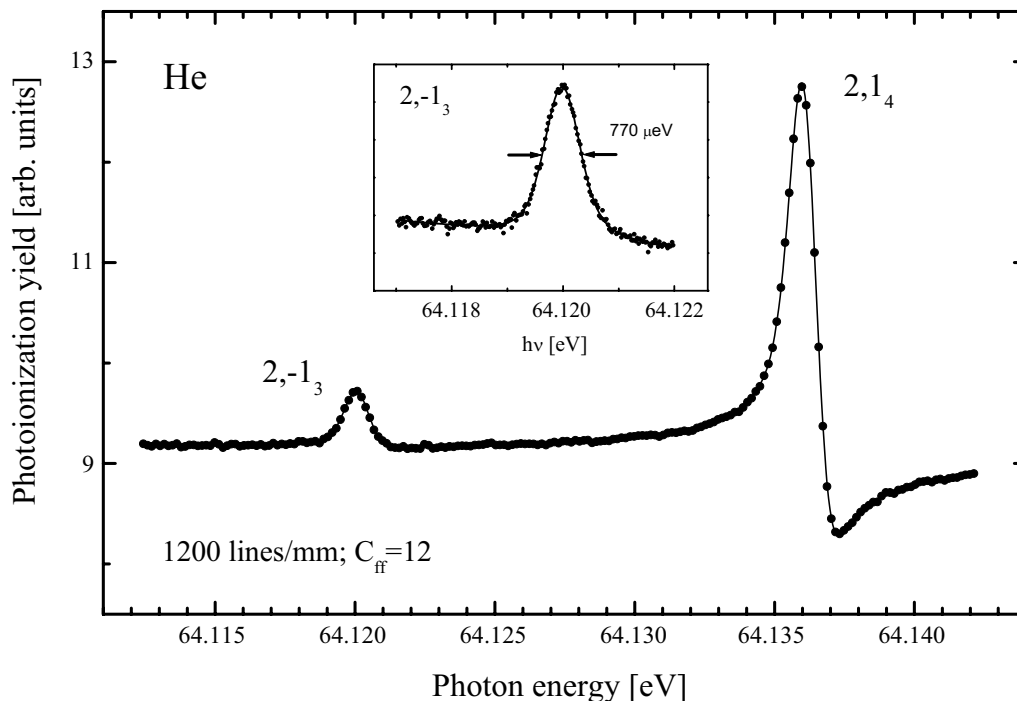


**Fig. 3:** The  $2,-1_3$  and  $2,1_4$  autoionizing resonances of doubly excited He; the inset shows the vicinity of the resonance  $2,-1_3$ . Solid lines through the data points represent fits of Fano-like profiles convoluted with a Gaussian (from Ref. [2]).

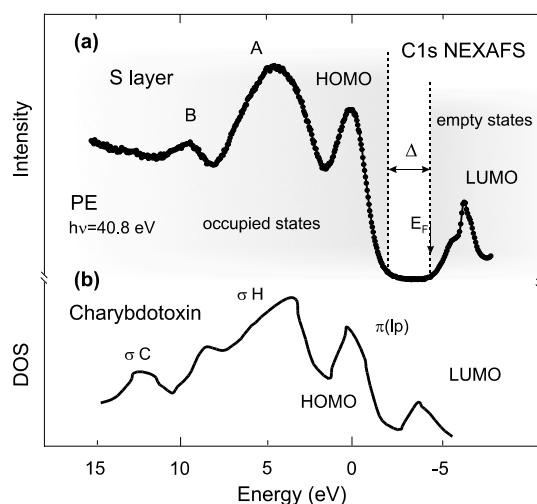


**Fig. 4:** (a) Valence-band and LUMO originating structure of the S layer of *Bacillus Sphaericus*. (b) DOS calculated for charybdotoxin; (from Ref. [3]).

transition-metal (TM) fluorides in a systematic way by NEXAFS at the F  $1s$  threshold. It was found that even in these most ionic  $3d$  TM compounds, the low-lying empty electronic states are formed by covalent mixing of TM  $3d$  with fluorine  $2p$  electronic states, with covalent mixing decreasing along the series of  $3d$  TM fluorides from Ti to Cu [4].

A. Varykhalov et al., in a collaboration between St. Petersburg State University, BESSY, the University of Potsdam, and the Consiglio Nazionale delle Ricerche, Trieste/Italy, studied the ground-state electronic structure of strongly correlated Ni metal via the observation of quantum-well states in thin Ag films on Ni(111). This is of particular interest for a highly correlated metal, like Ni, where the results of photoemission experiments deviate considerably from the calculated ground-state properties. By analyzing the quantum-well states in the Ag/Ni(111) films with the so-called phase accumulation model, the bottom of the  $\Lambda_1$  band of Ni metal could be determined as  $2.6 \pm 0.15$  eV, in good agreement with early local-density calculations of Ni. These results bear interesting implications for the interpretation of photoemission spectra of highly correlated materials [5].

There is no doubt that the creation of the RGLB at BESSY II, with the leading role of the Freie Universität Berlin, has tremendously stimulated in general the Russian-German scientific collaboration in the field of synchrotron-radiation research and in particular the long-lasting partnership between the Freie Universität and St. Petersburg State University.

## References

- [1] S.A. Gorovikov, S.L. Molodtsov, and R. Follath, . Nucl. Instr. and Meth. in Phys. Res. A **411**, 506 (1998).
- [2] S.I. Fedoseenko, D.V. Vyalikh, I.E. Iossifov, R. Follath, S.A. Gorovikov, R. Püttner, J.-S. Schmidt, S.L. Molodtsov, V.K. Adamchuk, W. Gudat, and G. Kaindl, Nucl. Instr. and Meth. in Phys. Res. A **505**, 718 (2003).
- [3] D.V. Vyalikh, S. Danzenbächer, M. Mertig, A. Kirchner, W. Pompe, Yu.S. Dedkov, and S.L. Molodtsov, Phys. Rev. Lett. **93**, 238103 (2004).
- [4] A.S. Vinogradov, S.I. Fedoseenko, S.A. Krasnikov, A.B. Preobrajenski, V.N. Sivkov, D.V. Vyalikh, S.L. Molodtsov, V.K. Adamchuk, C. Laubschat, and G. Kaindl, Phys. Rev. B **71**, 045127 (2005).
- [5] A. Varykhalov, A. M. Shikin, W. Gudat, P. Moras, C. Grazioli, C. Carbone, and O. Rader, Phys. Rev. Lett. **95**, 247601 (2005).

## Magnetic field pulse creation by synchronized laser pulses for magnetization dynamics studies of multilayered systems

J. Miguel,<sup>1</sup> K. Fukumoto,<sup>1</sup> M. Bernien,<sup>1</sup> W. Kuch,<sup>1</sup> D. Bayer,<sup>2</sup> M. Aeschlimann,<sup>2</sup>  
B. Heitkamp,<sup>3</sup> L. Heyne,<sup>3</sup> N. Höfer,<sup>3</sup> J. Sanchez-Barriga,<sup>3</sup> and H. Dürr<sup>3</sup>

<sup>1</sup>*Institut für Experimentalphysik, Freie Universität Berlin, Berlin, Germany*

<sup>2</sup>*Technische Universität Kaiserslautern, Kaiserslautern, Germany*

<sup>3</sup>*BESSY GmbH, Berlin, Germany*

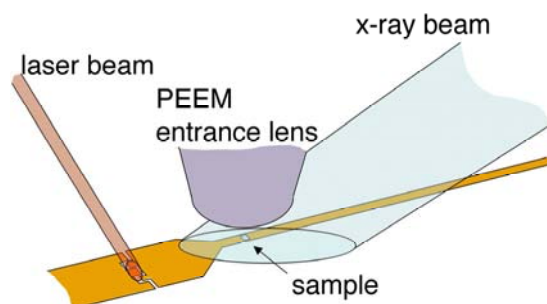
An important development in the search for new ultra-small information recording technologies are magnetic random access media devices, with the key feature of the non-volatility of the stored information. These devices generally comprise a stack of two thin magnetic layers separated by a non-magnetic spacer layer. For a fast operation, the magnetization direction of one of the magnetic layers has to be reversed with maximum speed. A fundamental understanding of the processes occurring during the fast magnetization reversal in coupled multilayered magnetic systems is indispensable for achieving optimum operation speed of such devices.

We aim at setting up a synchrotron radiation experiment to study magnetization

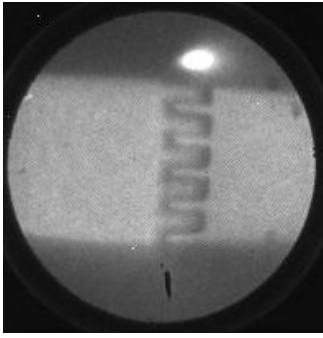
dynamics in multi-layered magnetic structures with highest time, lateral, and layer resolution. We use a pulsed laser system synchronized to the X-ray pulses in single bunch mode to trigger current pulses through a metallic wire, the so-called strip line, onto which the sample is placed. These current pulses then induce magnetic field pulses at the sample position. The strip line and sample on it are lithographically fabricated on a GaAs substrate.

Fig. 1 shows a sketch of the experimental set-up. Magnetic information from the sample is obtained by photoelectron emission microscopy (PEEM) with x-ray magnetic circular dichroism (XMCD) as magnetic contrast mechanism [1, 2]. This technique provides both the layer selectivity and the necessary spatial information, with a maximum resolution of about 100 nm. In the time-resolved variant (TR-PEEM), it is thus possible to correlate the transient magnetic domain patterns of the different ferromagnetic layers to the excitation by the magnetic field pulse.

The laser irradiates a finger-shaped photoconductive switch close to the sample. This is a region where the strip line is interrupted. During the laser pulse, charge carriers are created in the underlying semiconducting substrate, leading to a short current pulse [3]. The current pulse thus produced travels along the strip line and creates a magnetic field at



**Fig. 1:** Sketch of the experimental set-up. A short laser pulse, synchronized to the x-ray pulse frequency, triggers a current pulse through a lithographic strip line in a photoconductive switch. The resulting magnetic field pulse is used to excite the sample, the magnetic properties of which are imaged with lateral and elemental resolution by a PEEM.



**Fig. 2:** PEEM image of the photoconductive switch together with the laser spot. The switch is imaged by photoelectrons excited by a Hg discharge lamp, while the laser spot becomes visible due to multiphoton photoemission. The switching area is  $100\ \mu\text{m}$  wide and consists of 10 fingers of  $5\ \mu\text{m}$  width and  $10\ \mu\text{m}$  length.

the position of the sample, a multilayered magnetic microstructure.

A PEEM image of this switch is shown in Fig. 2. The laser spot is focused down to a size smaller than  $\cong 20\ \mu\text{m}$  by a lens inside of

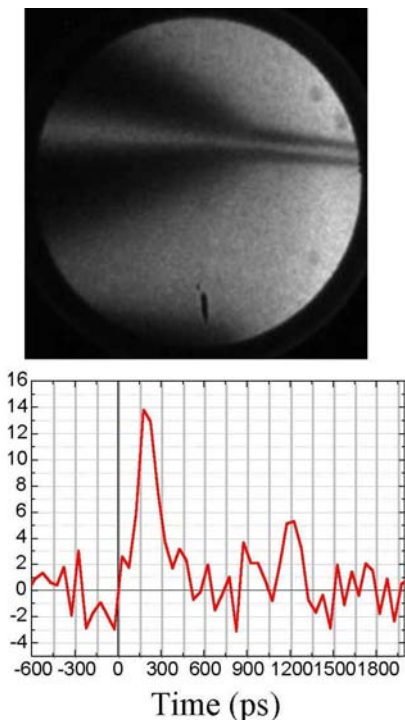


**Fig. 3:** Top: PEEM image of the strip line taken during the laser pulse. Bottom: Temporal evolution of the contrast of the area around the strip-line in the top panel, representing the temporal evolution of the magnetic field pulse.

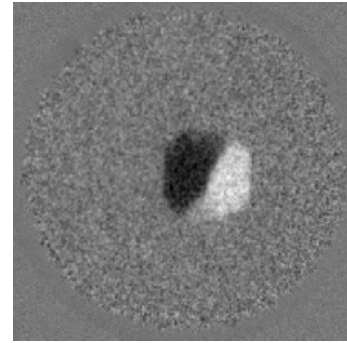


**Fig. 4:** Magnetic domains present in square  $\text{Fe}_{20}\text{Ni}_{80}$  magnetic microstructures grown onto the strip line, as seen by XMCD-PEEM.

the ultrahigh vacuum system. In this figure, the laser spot (moved out of the photoconductive switch for better visibility) appears as a bright spot due to multiphoton photoemission induced by the laser pulse.

In order to test the synchronization between the BESSY x-ray pulse and the laser pulse, PEEM images of the strip line were taken before, during, and after the laser pulse with  $50\ \text{ps}$  time increments. One of them is shown in the top panel of Fig. 3. The switch is located left of the imaged area. The current pulse induces a transient image distortion in the PEEM image of the strip-line due to its electric and magnetic fields. This can be followed as a change of contrast between the strip-line and the surrounding ground pads. The temporal evolution of the contrast in the area of the strip-line is shown in the bottom panel. The magnetic pulse is characterized by an initial rise time of  $150\ \text{ps}$  and a decay time of about  $200\ \text{ps}$ . Taking into account the dimensions of the strip line and the distance to the FeNi layer, a peak field of  $8\ \text{Oe}$  at the magnetic microstructure position is calculated. The laser pulse thus creates a magnetic pulse in the sample plane with a total width of  $350\ \text{ps}$ .

Magnetic microstructures of different sizes and shapes were grown onto the strip line, and characterized by XMCD-PEEM. Fig. 4 shows a magnetic domain pattern in a

---

$10 \times 10 \mu\text{m}^2$   $\text{Fe}_{20}\text{Ni}_{80}$  microstructure on top of the stripline, obtained by subtracting the two PEEM images acquired with left and right circularly polarized x-rays under static conditions.

In upcoming experiments we aim at studying the magnetic response of one of the magnetic layers in a trilayered structure under ultrafast magnetic pulses as a function of the domain configuration of the other magnetic layer.

## References

- [1] J. Stöhr, Y. Wu, B. D. Hermsmeier, M. G. Samant, G. R. Harp, S. Koranda, D. Dunham, and B. P. Tonner, *Science* **259**, 658 (1993).
- [2] W. Kuch, *Appl. Phys. A* **76**, 665 (2003).
- [3] D. H. Auston, *Appl. Phys. Lett.* **26**, 101 (1974).

## X-ray spectroscopy to study catalytic metal centers: A new BioXAS experiment at BESSY beamline KMC-1

*P. Loja<sup>1</sup>, M. Barra<sup>1</sup>, S. Löscher<sup>1</sup>, O. Kirilenko<sup>1</sup>, P. Liebisch<sup>1</sup>, M. Mertin<sup>2</sup>,  
F. Schäfers<sup>2</sup>, M. Haumann<sup>1</sup>, H. Dau<sup>1</sup>*

<sup>1</sup>*Freie Universität Berlin, Fachbereich Physik*  
<sup>2</sup>*BESSY GmbH, Berlin*

X-ray absorption spectroscopy (XAS) has become one of the most important techniques to analyze the nuclear geometry at the atomic level (by EXAFS) and oxidation state (by XANES) of metal centers in biological metalloenzymes during catalysis. At the bending-magnet, crystal-monochromator beamline KMC-1 at BESSY-II we installed and tested a new setup for XAS on biological samples (BioXAS [1-3]).

XAS measurements were performed on synthetic model compounds and on the metal complexes of metalloenzymes. The properties of the beamline KMC-1 and of the

newly purchased equipment (Figs. 1, 2) are well suited for BioXAS experiments on ultra-dilute samples.

An energy-resolving Ge detector (reset type, Canberra, maximal count rate of  $\sim 300$  kcps), a digital signal processor (DXP multichannel analyzer from XIA), and a helium cryostat plus electronics (Oxford) had been purchased and appropriately modified (by the workshop of the FB Physik, FU-Berlin). The cryostat was flanged to the detector so that the retractable Ge element was at a distance of only  $\sim 2$  cm to the sample, for maximal X-ray fluorescence

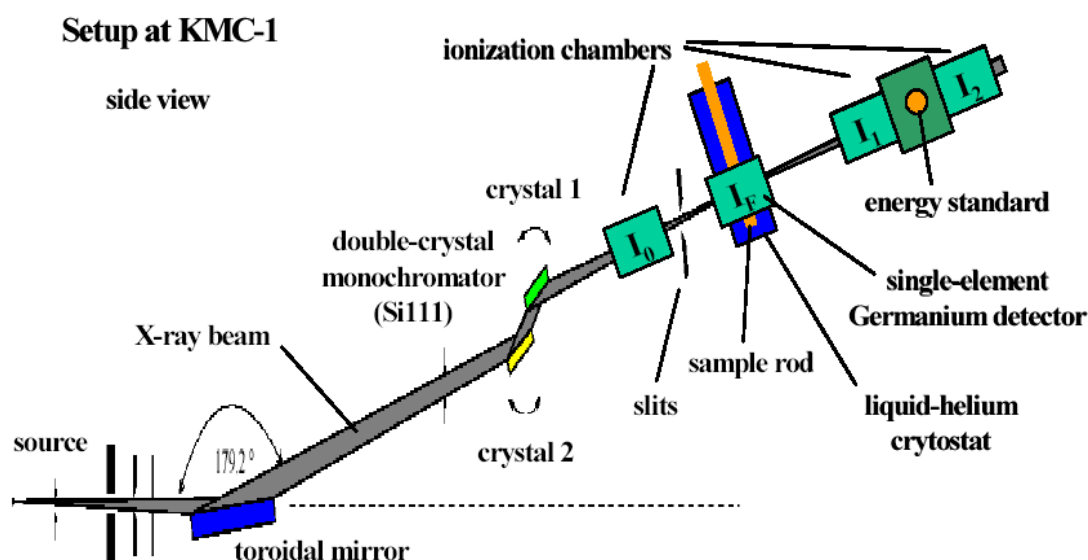


**Fig. 1:** Scheme of the experimental setup at beamline KMC-1 (not drawn to scale). The liquid helium cryostat (Optistat, Oxford) with the sample was placed about in the beam focus (spot size  $\sim 0.5$  mm<sup>2</sup>;  $\sim 10^{11}$  photons s<sup>-1</sup> mm<sup>-2</sup> at  $\sim 6$  KeV; energy resolution (FWHM) with Si111 crystal better than 3 eV). For X-ray fluorescence detection at right angle to the incident beam, an energy-resolving single-element large-area Germanium detector (Canberra, active area 100 mm<sup>2</sup>) was used. To obtain an absolute energy calibration, reference samples were used as standards and placed behind the sample in a separate vacuum chamber.

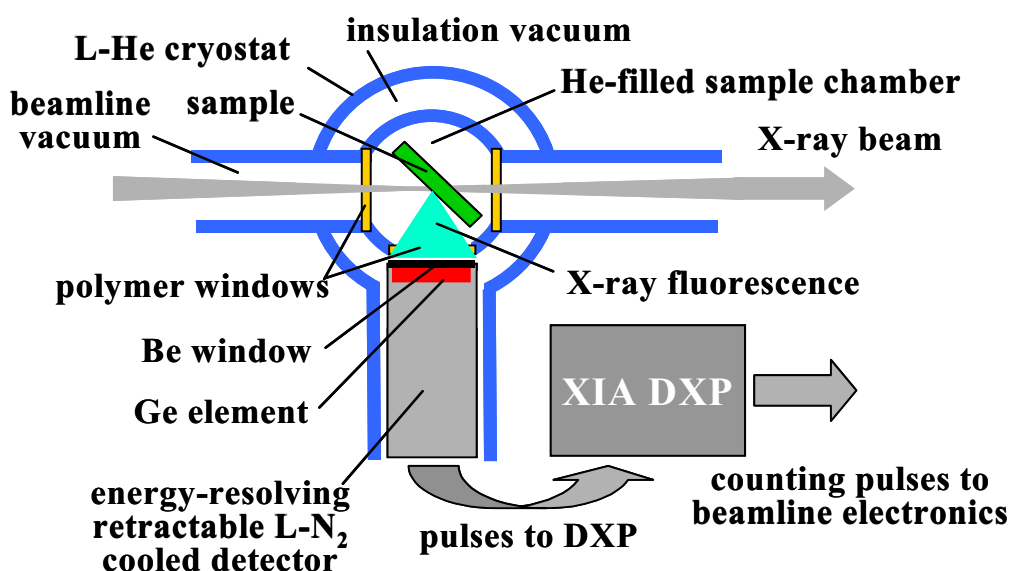


Fig. 2: Details of the cryostat and detector setup.

count rates (Fig. 2). Cryostat and detector were mounted on a home-built stage permitting for vertical and horizontal movement of the setup to measure separate spots on the same sample. By the DXP, pulses were shaped, selected, and converted to TTL pulses for counting by the beamline electronics. The energy resolution of the detector system was better than 200 eV at a total count rate of 50 kcps allowing for highly efficient suppression of scattered X-rays and for the collection of EXAFS spectra with negligible background (Fig. 3). EXAFS scans were performed using the beamline software by scanning of the Si111 monochromator at the Mn K-edge (scan range 6400-7200 eV, the monochromator driving and ion-chamber electrometer readout times were optimized so that the deadtime was smaller than 0.5 s at 1.5 s acquisition time per data point). An energy calibration of XAS spectra was obtained by simultaneous measurement of the absorption spectra of standards with known features placed behind the sample (Figs. 1).

Measurements on ultra-dilute biological samples (e.g. manganese complex of a photosystem-II-protein preparation) revealed that

the setup was suited to obtain high-quality EXAFS spectra (Fig. 3).

#### Outlook

The performance of the XAS setup at KMC-1 was comparable to, e.g., the BioXAS station of the EMBL at HASYLAB, DESY, Hamburg. In the future, it is intended to improve the setup so that routine collection of BioXAS data becomes possible for X-ray energies ranging from 2.5 to about 10 keV. This energy range allows for XAS measurements on the most important metals (e.g. Ca, V, Mn, Fe, Ni, Cu, Zn) in biological and synthetic biomimetic systems.

#### References

- [1] H. Dau, P. Liebisch, and M. Haumann, *Anal. Bioanal. Chem.* **376**, 562-583.
- [2] H. Dau and M. Haumann, *J. Synchrotron. Radiat.* **10**, 76-85.
- [3] M. Haumann, C. Müller, P. Liebisch, L. Iuzzolino, J. Dittmer, M. Grabolle, T. Neisius, W. Meyer-Klaucke, and H. Dau, *Biochemistry* **44**, 1894-1908.



---

## Publications

### 2000:

- [1] D. Arvanitis, N. Haack, G. Ceballos, H. Wende, K. Baberschke, A. L. Ankudinov, and J. J. Rehr  
Shape resonances of oriented molecules  
J. Electron Spectr. Relat. Phenom. **113**, 57 (2000).
- [2] G. Ceballos, N. Haack, H. Wende, R. Püttner, K. Baberschke, and D. Arvanitis  
Vibrational fine structure in the N 1s  $\rightarrow$   $\pi^*$  resonance of the N<sub>2</sub> molecule physisorbed on the Cu(100) surface  
Surf. Sci. **448**, 261 (2000).
- [3] K. Decanniere, A. M. Babu, K. Sandman, J. N. Reeve, and U. Heinemann  
Crystal structures of recombinant histones HMfA and HMfB from the hyperthermophilic archaeon *Methanothermus fervidus*  
J. Mol. Biol. **303**, 35 (2000).
- [4] M. Dickgießer and N. Schwentner  
Penetration depth of energetic F atoms from F<sub>2</sub> dissociation in layered rare gas samples  
J. Chem. Phys. **113**, 8260 (2000).
- [5] M. Dickgießer and N. Schwentner  
Optimization of Exciton-Induced Detection of Atoms at Interfaces  
J. Phys. Chem. **104**, 3743 (2000).
- [6] M. Dickgießer and N. Schwentner  
Set-up combining Synchrotron radiation-induced photochemistry with IR probing: (HCl)<sub>n</sub> in Kr Matrix  
Nucl. Instr. Meth. B, **168**, 252 (2000).
- [7] A. V. Grinberg, F. Hannemann, B. Schiffler, J. J. Müller, U. Heinemann, and R. Bernhardt  
Adrenodoxin: Structure, stability and electron transfer properties  
Proteins: Struct. Funct. Genet. **40**, 590 (2000).
- [8] N. Haack, G. Ceballos, H. Wende, K. Baberschke, D. Arvanitis, A. L. Ankudinov, and J. J. Rehr  
Shape resonances of oriented molecules: ab initio theory and experiments on hydrocarbon molecules  
Phys. Rev. Lett. **84**, 614 (2000).
- [9] U. Heinemann, J. Frevert, K.-P. Hoffmann, G. Illing, H. Oschkinat, W. Saenger, and R. Zettl  
Linking Structural Biology with Genome Research  
In: *Genomics and Proteomics: Functional and Computational Aspects* (S. Suhai, ed.) Kluwer Academic/Plenum Publishing, New York (2000), p. 179–189.
- [10] U. Heinemann, J. Frevert, K. P. Hofmann, G. Illing, H. Oschkinat, W. Saenger, and R. Zettl  
Linking Structural Biology with Genome Research: the Berlin "Protein Structure Factory" Initiative  
In: *Genomics and Proteomics: Functional and Computational Aspects* (S. Suhai, ed.) Kluwer Academic/Plenum Publishing, New York (2000), p. 179–189.
- [11] U. Heinemann  
Structural genomics in Europe: Slow start, strong finish?  
Nature Struct. Biol. **7**, 940 (2000).
- [12] U. Heinemann, J. Frevert, K.-P. Hofmann, G. Illing, C. Maurer, H. Oschkinat, and W. Saenger  
An integrated approach to structural genomics  
Prog. Biophys. Mol. Biol. **73**, 347 (2000).
- [13] U. Heinemann, U. Mueller, H. Heumann, and M. Sprinzl  
Structural studies of model RNA helices with relevance to aminoacyl-tRNA synthetase specificity and HIV reverse transcription  
J. Biomol. Struct. Dyn. **C11**, 39 (2000).
- [14] J. Hunter Dunn, D. Arvanitis, K. Baberschke, A. Hahlin, O. Karis, R. Carr, and N. Mårtensson  
A comparative study of x-ray absorption spectroscopy at various synchrotron facilities and the effect of transverse source coherence  
J. Electron Spectr. Relat. Phenom. **113**, 67 (2000).
- [15] P. J. Jensen, K. H. Bennemann, K. Baberschke, P. Pouloupoulos, and M. Farle  
Magnetization and susceptibility of coupled ferromagnetic trilayers calculated with a Green's function type theory  
J. Appl. Phys. **87**, 6692 (2000).

- [16] J. Lindner, P. Pouloupoulos, F. Wilhelm, M. Farle, and K. Baberschke  
Atomic exchange processes at the interface and their role on the magnetic moments of ultrathin Ni/Cu(001) films  
Phys. Rev. B **62**, 10431 (2000).
- [17] C. Meinke, A. V. Solé, P. Pospisil, and H. Dau  
Does the structure of the water-oxidizing photosystem II–manganese complex at room temperature differ from its low-temperature structure? A comparative X-ray absorption study  
Biochemistry **39**, 7033 (2000).
- [18] U. Mueller, D. Perl, F. X. Schmid, and U. Heinemann  
Thermal stability and atomic-resolution crystal structure of the *Bacillus caldolyticus* cold shock protein  
J. Mol. Biol. **297**, 975 (2000).
- [19] A. I. Nesvizhskii, A. L. Ankudinov, J. J. Rehr, and K. Baberschke  
Interpretation of X-ray magnetic circular dichroism and X-ray near-edge structure in Ni  
Phys. Rev. B **62**, 15295 (2000).
- [19] P. Orth, D. Schnappinger, W. Hillen, W. Saenger, and W. Hinrichs  
The Crystal Structure of the Tet Repressor/Operator Complex Reveals Detailed Function of a Gene Regulating Molecular Switch  
Nature Struct. Biol. **7**, 215 (2000).
- [20] D. Perl, U. Mueller, U. Heinemann, and F.X. Schmid  
Two exposed amino acid residues confer thermostability on a cold shock protein  
Nature Struct. Biol. **7**, 380 (2000).
- [21] I. Przylas, K. Tomoo, Y. Terada, T. Takaha, S. Okada, W. Saenger, and N. Sträter  
Crystal Structure of Amylomaltase from *Thermus aquaticus*, a Glycosyltransferase Catalyzing the Production of Large Cyclic Glucans  
J. Mol. Biol. **296**, 873 (2000).
- [22] I. Przylas, Y. Terada, K. Fuji, T. Takaha, W. Saenger, and N. Sträter  
X-Ray Structure of Acarbose bound to Amylomaltase from *Thermus aquaticus*. Implications for the synthesis of Large Cycloamyloses  
Eur. J. Biochem. **267**, 6903 (2000).
- [23] H. Raaf, M. Groen, and N. Schwentner  
Amplification in Light-Induced Reactions of Cu with Cl<sub>2</sub> in the VUV  
Appl. Surf. Science **154–155**, 536 (2000).
- [24] W. Saenger, P. Orth, C. Kisker, W. Hillen, and W. Hinrichs  
The Tetracycline Repressor - A Paradigm for a Biological Switch  
Angew. Chem. Int. Ed. **39**, 2042–2052 (2000); Angew. Chem. **112**, 2122 (2000).
- [25] C. Schüßler-Langeheine, E. Weschke, R. Meier, A. Yu. Grigoriev, H. Ott, C. Mazumdar, D. V. Vyalikh, C. Sutter, D. Abernathy, G. Grübel, and G. Kaindl  
Resonant magnetic x-ray scattering from in situ grown holmium-metal films  
Nuclear energy agency organisation for economic co-operation and development  
Proceedings of Workshop "Speciation, Techniques and Facilities for Radioactive Materials at Synchrotron Light Sources", Grenoble, France 10-12 September 2000. p. 295.
- [26] M. Shikin, D. V. Vyalikh, Yu. S. Dedkov, G. V. Prudnikova, V. K. Adamchuk, E. Weschke, and G. Kaindl  
Extended energy range of Ag quantum-well states in Ag(111)/Au(111)/W(110)  
Phys. Rev. B **62**, R2303 (2000).
- [27] P. Srivastava and K. Baberschke  
New opportunities in soft-X-ray absorption to characterize the adsorbate bonding  
Topics in Catalysis **10**, 199 (2000).
- [28] K. Starke  
Magnetic Dichroism in Core-Level Photoemission  
Springer Tracts in Modern Physics **159**, Springer, Berlin, Heidelberg (2000).
- [29] J. Tebbe, P. Orth, E. Küster, W. Hillen, W. Saenger, W. Hinrichs  
Crystallization and Preliminary X-ray Analyses of Catabolite Control Protein A, Free and in Complex with its DNA-Binding Site  
Acta Cryst. **D56**, 67 (2000).
- [30] H. Wende, R. Chauvistré, N. Haack, G. Ceballos, F. Wilhelm, K. Baberschke, P. Srivastava, and D. Arvanitis  
Surface EXAFS study of the p4g (2x2) reconstruction of C on Ni(100) and C on Ni films  
Surf. Sci. **465**, 187 (2000).

- [31] H. Wende, F. Wilhelm, P. Pouloupoulos, K. Baberschke, J. W. Freeland, Y. U. Idzerda, A. Rogalev, D. L. Schlagel, T. A. Lograsso, and D. Arvanitis  
On the Temperature Dependence of Multiple- and Single-Scattering Contributions in Magnetic EXAFS  
in "*Theory and computation for synchrotron radiation spectroscopy*", edited by M. Benfatto, C.R. Natoli and E. Pace, AIP Proceedings **514**, 140 (2000).
- [32] F. Wilhelm, U. Bovensiepen, A. Scherz, P. Pouloupoulos, A. Ney, H. Wende, G. Ceballos, and K. Baberschke  
Manipulation of the Curie temperature and the magnetic moments of ultrathin Ni and Co films by Cu-capping  
J. Magn. Magn. Mat. **222**, 163 (2000).
- [33] F. Wilhelm, P. Pouloupoulos, P. Srivastava, H. Wende, M. Farle, K. Baberschke, M. Angelakeris, N. K. Flevaris, W. Grange, J.-P. Kappler, G. Ghiringhelli, and N. B. Brookes  
Magnetic anisotropy and the anisotropy of the orbital moment of Ni in Ni/Pt multilayers  
Phys. Rev. B **61**, 8647 (2000).
- [34] F. Wilhelm, P. Pouloupoulos, G. Ceballos, P. Srivastava, H. Wende, K. Baberschke, D. Benea, H. Ebert, M. Angelakeris, N. K. Flevaris, D. Niarchos, A. Rogalev, and N. B. Brookes  
Layer-resolved magnetic moments in Ni/Pt multilayers  
Phys. Rev. Lett. **85**, 413 (2000).
- [35] M. Wühn, Y. Joseph, P. S. Bagus, A. Niklewski, R. Püttner, S. Reiß, W. Weiss, M. Martins, G. Kaindl, and Ch. Wöll  
The electronic structure and orientation of styrene adsorbed on FeO(111) and Fe<sub>3</sub>O<sub>4</sub>(111) - A spectroscopic investigation  
J. Phys. Chem. B **104**, 7694 (2000).

**2001:**

- [36] K. Baberschke  
Anisotropy in Magnetism  
Lecture Notes in Physics **580**, Springer, Berlin (2001), p. 27.
- [37] G. Ceballos, N. Haack, H. Wende, R. Püttner, D. Arvanitis, and K. Baberschke  
High-resolution X-ray absorption spectra of the  $\pi^*$  resonance of N<sub>2</sub>, directly physisorbed on metallic Cu (100)  
Nucl. Instrum. Meth. Phys. A **467-468**, 1560 (2001).
- [38] G. Ceballos, H. Wende, K. Baberschke, and D. Arvanitis  
Molecular Geometry Modifications upon Adsorption for N<sub>2</sub>O: N and O K-edge NEXAFS  
Surf. Sci. **482-485**, 15 (2001).
- [39] H. Delbrück, U. Mueller, D. Perl, F. X. Schmid, and U. Heinemann  
Crystal structures of mutant forms of the *Bacillus caldolyticus* cold shock protein differing in thermal stability  
J. Mol. Biol. **313**, 359 (2001).
- [40] F. Heigl, O. Krupin, A. Vollmer, and K. Starke  
X-Ray magneto-optics at rare-earth 4d-4f thresholds  
Appl. Phys. A **73**, 707 (2001).
- [41] U. Heinemann, G. Illing, and H. Oschkinat  
High-throughput three-dimensional protein structure determination  
Curr. Opin. Biotechnol. **12**, 348 (2001).
- [42] R. C. Hillig, P. G. Coulie, V. Stroobant, W. Saenger, A. Ziegler, and M. Hülsmeier  
High-resolution Structure of HLA-A\*0201 in Complex with a Tumour-specific Antigenic Peptide Encoded by the MAGE-A4 Gene  
J. Mol. Biol. **310**, 1167 (2001).
- [43] P. Jordan, P. Fromme, H. T. Witt, O. Klukas, W. Saenger, and N. Krauß  
Three dimensional structure of cyanobacterial photosystem I at 2.5 Å resolution  
Nature **411**, 909 (2001).
- [44] C. Kolczewski, R. Püttner, O. Plashkevych, H. Ågren, V. Staemmler, M. Martins, G. Snell, A. S. Schlachter, M. M. Sant'Anna, G. Kaindl, and L. G. M. Pettersson  
Detailed study of pyridine at the C 1s and N 1s ionization thresholds: The influence of the vibrational fine structure  
J. Chem. Phys. **115**, 6426 (2001).
- [45] A. Meinhart, C. Alings, N. Sträter, A. G. Camacho, J. C. Alonso, and W. Saenger  
Crystallization and preliminary X-ray diffraction studies on the  $\epsilon$   $\zeta$  addition system encoded by *Streptococcus pyogenes* plasmid pSM19035  
Acta Cryst **D57**, 745 (2001).

- [46] J. J. Müller, A. Lapko, G. Bourenkov, K. Ruckpaul, and U. Heinemann  
Adrenodoxin reductase – adrenodoxin complex structure suggests electron transport path in steroid biosynthesis  
*J. Biol. Chem.* **276**, 2786 (2001).
- [47] J. J. Müller, E.-C. Müller, T. Montag, N. Zyto, B. Löschner, H. Klein, U. Heinemann, and A. Otto  
Characterization and crystallization of a novel *Sarcocystis muris* lectin, SML-2  
*Acta Crystallogr. D* **57**, 1042 (2001).
- [48] K. Murayama, P. Orth, A. B. de la Hoz, J. C. Alonso, and W. Saenger  
Crystal Structure of  $\omega$  Transcriptional Repressor Encoded by *Streptococcus pyogenes* Plasmid pSM19035 at 1.5 Å Resolution  
*J. Mol. Biol.* **314**, 789 (2001).
- [49] A. Ney, P. Pouloupoulos, F. Wilhelm, A. Scherz, M. Farle, and K. Baberschke  
Absolute determination of the magnetic moments of Co monolayers: A combination of UHV magnetometries  
*J. Magn. Magn. Mater.* **226**, 1570 (2001).
- [50] T. Niedenzu, D. Röleke, G. Bains, E. Scherzinger, and W. Saenger  
Prototype Crystal Structure of the Hexameric Replicative Helicase RepA of Plasmid RSF1010  
*J. Mol. Biol.* **306**, 479 (2001).
- [51] O. Nimz, K. Geßler, I. Uson, and W. Saenger  
An orthorhombic crystal form of cyclohexaicosaoose, CA26 32.59 H<sub>2</sub>O: comparison with the triclinic form  
*Carbohydr. Res.* **336**, 141 (2001).
- [52] P. Pouloupoulos, F. Wilhelm, H. Wende, G. Ceballos, K. Baberschke, D. Benea, H. Ebert, M. Angelakeris, N.K. Flevaris, A. Rogalev, and N.B. Brookes  
X-ray magnetic circular dichroic magnetometry on Ni/Pt multilayers  
*J. Appl. Phys.* **89**, 3874 (2001).
- [53] P. Pouloupoulos and K. Baberschke  
Phase Transitions in Coupled Two-Dimensional Ferromagnetic Layers  
*Lecture Notes in Physics* **580**, Springer, Berlin (2001), p. 283.
- [54] R. Püttner, B. Grémaud, D. Delande, M. Domke, M. Martins, A. S. Schlachter, and G. Kaindl  
Statistical properties of inter-series mixing in helium: From integrability to chaos  
*Phys. Rev. Lett.* **86**, 3747 (2001).
- [55] H. Raaf and N. Schwentner  
Efficiencies above unity in light-induced reaction of Cu with Cl<sub>2</sub>: Excitation, amplification and diffusion processes  
*Appl. Surf. Sci.* **174**, 13 (2001).
- [56] G. Reichardt, J. Bahrtdt, J.-S. Schmidt, W. Gudat, A. Ehresmann, R. Mueller Albrecht, H. Molter, H. Schmoranzner, M. Martins, N. Schwentner, and S. Sasaki  
A 10m-normal incidence monochromator at the quasi-periodic undulator U125-2 at BESSYII  
*Nucl. Instrum. Meth. Phys. A* **467/468**, 462 (2001).
- [57] A. Scherz, F. Wilhelm, P. Pouloupoulos, H. Wende, and K. Baberschke  
Element-specific Magnetization Curves and Crossover in Co/Cu/Ni/Cu(001) Trilayers Studied by XMCD  
*J. Synch. Rad.* **8**, 472 (2001).
- [58] A. Scherz, F. Wilhelm, U. Bovensiepen, P. Pouloupoulos, H. Wende, and K. Baberschke  
Separate Curie temperatures in magnetic trilayers and the effect of spin fluctuations  
*J. Magn. Magn. Mater.* **236**, 1 (2001).
- [59] A. Scherz, H. Wende, P. Pouloupoulos, J. Lindner, K. Baberschke, P. Blomquist, R. Wäppling, F. Wilhelm, and N.B. Brookes  
Induced V and reduced Fe moment at the interface of Fe/V(001) superlattices  
*Phys. Rev. B* **64**, R 180407 (2001).
- [60] K. J. Schmidt and K. Christmann  
The adsorption of xenon on a Ru(10-10) surface  
*Surf. Sci.* **492**, 167 (2001).
- [61] C. Schüßler-Langeheine, E. Weschke, A. Yu. Grigoriev, H. Ott, A. Möller, R. Meier, Chandan Mazumdar, and G. Kaindl  
Magnetic effects in the band structure of ferromagnetic and antiferromagnetic lanthanide metal films  
*J. Electron Spectrosc. Relat. Phenom.* **114–116**, 795 (2001).
- [62] C. Schüßler-Langeheine, E. Weschke, A. Yu. Grigoriev, H. Ott, R. Meier, D.V. Vyalikh, Chandan Mazumdar, C. Sutter, D. Abernathy, G. Grübel, and G. Kaindl  
Resonant magnetic x-ray scattering from ultrathin Ho-metal films down to a few atomic layers  
*J. Electron Spectrosc. Relat. Phenom.* **114–116**, 953 (2001).

- [63] T. Schwartz, J. Behlke, K. Lowenhaupt, U. Heinemann, and A. Rich  
Structure of the DLM-1-Z-DNA complex reveals a conserved family of Z-DNA-binding proteins  
*Nature Struct. Biol.* **8**, 761 (2001).
- [64] K. Starke, F. Heigl, A. Vollmer, M. Weiss, G. Reichardt, and G. Kaindl  
X-ray Magneto-Optics in Lanthanides  
*Phys. Rev. Lett.* **86**, 3415 (2001).
- [65] K. Starke, F. Heigl, J. E. Prieto, O. Krupin, A. Vollmer, G. Reichardt, F. Senf, R. Follath, N. B. Brookes, and G. Kaindl  
X-ray Magneto-Optics  
*Adv. Solid State Phys.* **41**, 161 (2001).
- [66] K. Starke, F. Heigl, A. Vollmer, and G. Kaindl  
X-ray Magneto-Optics in Lanthanide Materials  
*Mat. Res. Soc. Conf. Proc.* **678**, EE7.7 (2001).
- [67] H. Wende, F. Wilhelm, P. Pouloupoulos, A. Rogalev, D.L. Schlagel, T.A. Lograsso, and K. Baberschke  
Magnetic EXAFS at Gd L-Edges: The Spin-Pair-Distribution Function of Gd Neighbors  
*J. Synch. Rad.* **8**, 419 (2001).
- [68] H. Wende, F. Wilhelm, P. Pouloupoulos, A. Rogalev, J. Goulon, D.L. Schlagel, T.A. Lograsso, and K. Baberschke  
Temperature-Dependent Magnetic EXAFS Investigation of Gd  
*Nucl. Instrum. Meth. Phys. A* **467-468**, 1426 (2001).
- [69] E. Weschke and G. Kaindl  
Magnetic exchange splitting in lanthanide metals  
*J. Phys.: Cond. Matter* **13**, 11133 (2001).
- [70] F. Wilhelm, P. Pouloupoulos, H. Wende, A. Scherz, K. Baberschke, M. Angelakeris, N. K. Flevaris, and A. Rogalev  
Systematics of the induced magnetic moments in 5d layers and the violation of the third Hund's rule  
*Phys. Rev. Lett.* **87**, 207202 (2001).
- [71] H. T. Witt, A. Zouni, J. Kern, P. Fromme, N. Krauß, W. Saenger, and P. Orth  
Crystal structure of photosystem II and aspects of its function  
In: PS2001 proceedings: 12<sup>th</sup> International Congress on Photosynthesis, Brisbane, Australia, PL-001, CSIRO Publishing, Collingwood, Australia (2001).
- [72] A. Zouni, H. T. Witt, J. Kern, N. Krauß, W. Saenger, and P. Orth  
Crystal structure of photosystem II from *Synechococcus elongatus* at 3.8 Å resolution  
*Nature* **409**, 739 (2001).
- [73] A. Zouni, J. Kern, B. Loll, P. Fromme, H. T. Witt, P. Orth, N. Krauß, W. Saenger, and J. Biesiadka  
Biochemical characterization and crystal structure of water oxidizing photosystem II from *Synechococcus elongatus*  
In: PS2001 proceedings: 12<sup>th</sup> International Congress on Photosynthesis, Brisbane, Australia, PL-001, CSIRO Publishing, Collingwood, Australia (2001)

**2002:**

- [74] P. Fromme, J. Kern, B. Loll, J. Biesiadka, W. Saenger, H. T. Witt, N. Krauß, and A. Zouni  
Functional implications on the mechanism of the function of photosystem II including water oxidation based on the structure of photosystem II  
*Phil. Trans. R. Soc. Lond. B* **357**, 1337-1345 (2002).
- [75] H. Delbrück, G. Ziegelin, E. Lanka, and U. Heinemann  
An Src homology 3-like domain is responsible for dimerization of the repressor protein KorB encoded by the promiscuous IncP plasmid RP4  
*J. Biol. Chem.* **277**, 4191 (2002).
- [76] M. Haumann, P. Pospisil, M. Grabolle, C. Müller, P. Liebisch, V.A. Solé, T. Neisius, J. Dittmer, L. Iuzzolino, and H. Dau  
First steps towards time-resolved BioXAS at room temperature: state transitions of the manganese complex of oxygenic photosynthesis  
*J. Synch. Rad.* **9**, 304 (2002).
- [77] M. Haumann, M. Grabolle, T. Neisius, and H. Dau  
The first room-temperature X-ray absorption spectra of higher oxidation states of the tetra-manganese complex of photosystem II  
*FEBS Letters* **512**, 116 (2002).

- [78] F. Heigl, O. Krupin, A. Vollmer, G. Kaindl, and K. Starke  
Two-axis rotatable UHV-compatible magnet  
*Rev. Sci. Instr.* **73**, 369 (2002).
- [79] U. Heinemann  
Establishing a structural genomics platform: The Berlin-based Protein Structure Factory  
*Gene Funct. Dis.* **3**, 25 (2002).
- [80] M. Hülsmeier, R. C. Hillig, A. Volz, M. Ruhl, W. Schröder, W. Saenger, A. Ziegler, and B. Uchanska-Ziegler  
HLA-B27 subtypes differentially associated with disease exhibit subtle structural alterations  
*J. Biol. Chem.* **277**, 47844 (2002).
- [81] G. Koellner, A. Bzowska, B. Wielgus-Kutrowska, M. Luic, T. Steiner, W. Saenger, and J. Stepinski  
Open and Closed Conformation of the *E. coli* Purine Nucleoside Phosphorylase Active Center and Implications for the Catalytic Mechanism  
*J. Mol. Biol.* **315**, 351 (2002).
- [82] M. Krüer, M. Haumann, W. Meyer-Klaucke, R. Thauer, and H. Dau  
Methanol:coenzyme M methyltransferase from *Methanosarcina barkeri*: The role of zinc in the methylation of the coenzyme M thiol group – new insights from X-ray absorption spectroscopy  
*Eur. J. Biochem.* **269**, 2117 (2002).
- [83] T. Matila, R. Püttner, A. Kivimäki, H. Aksela, and S. Aksela  
Auger decay widths of the ligand-field split Br 3d components in the HBr molecule  
*J. Phys. B* **35**, 4607 (2002).
- [84] A. Ney, A. Scherz, P. Pouloupoulos, K. Lenz, H. Wende, K. Baberschke, F. Wilhelm, and N. B. Brookes  
Clarification of contesting results for the total magnetic moment of Ni/Cu(001)  
*Phys. Rev. B* **65**, 024411 (2002).
- [85] P. Pouloupoulos, A. Scherz, F. Wilhelm, H. Wende, and K. Baberschke  
Direct probe of induced magnetic moments at interfaces via x-ray magnetic circular dichroism  
*phys. stat. sol. (a)* **189**, 293 (2002).
- [86] J. E. Prieto, F. Heigl, O. Krupin, G. Kaindl, and K. Starke  
Prediction of huge X-ray Faraday rotation at Gd N<sub>4,5</sub>  
*Phys. Rev. B* **66**, 172408 (2002).
- [87] R. Püttner, Y.-F. Hu, E. Nömmiste, G. M. Bancroft, and S. Aksela  
Angular resolved photoabsorption spectra of HBr below the Br 3d ionization thresholds  
*Phys. Rev. A* **65**, 032513 (2002).
- [88] R. Püttner, V. Pennanen, T. Matila, A. Kivimäki, M. Jurvansuu, H. Aksela, and S. Aksela  
Refinement in the analysis of molecular Auger electron spectra: The 2p<sup>-1</sup> → 3pπ<sup>-2</sup> Spectra of HCl and DCI  
*Phys. Rev. A* **65**, 042505 (2002).
- [89] W. Saenger, P. Jordan, and N. Krauß  
The assembly of protein subunits and cofactors in photosystem I  
*Curr. Opin. Struct. Biol.* **12**, 244 (2002).
- [90] A. Scherz, P. Pouloupoulos, H. Wende, G. Ceballos, K. Baberschke, and F. Wilhelm  
Thickness dependence of the V induced magnetic moment in Fe/V/Fe(110) trilayers  
*J. Appl. Phys.* **91**, 8760 (2002).
- [91] A. Scherz, H. Wende, K. Baberschke, J. Minar, D. Benea, and H. Ebert  
Relation between L<sub>2,3</sub> XMCD and the magnetic ground-state properties for the early 3d element V  
*Phys. Rev. B* **66**, 184401 (2002).
- [92] C. Schüßler-Langeheine, H. Ott, A. Yu. Grigoriev, A. Möller, R. Meier, Z. Hu, Chandan Mazumdar, G. Kaindl, and E. Weschke  
Oxygen-induced magnetic surface states on the (0001) surfaces of heavy lanthanide metals  
*Phys. Rev. B* **65**, 214410 (2002).
- [93] K. Starke, F. Heigl, A. Vollmer, and G. Kaindl  
X-Ray Magneto-optics in Lanthanides and Perspectives for Studying Actinides  
Nuclear Science, OECD Nuclear Energy Agency, Conference proceedings  
(Issy-les-Moulineaux, 2002), p. 137.
- [94] H. Wende, Z. Li, A. Scherz, G. Ceballos, K. Baberschke, A. Ankudinov, J. J. Rehr, F. Wilhelm, A. Rogalev, D. L. Schlagel, and T. A. Lograsso  
Quadrupolar and Dipolar Contributions to XMCD at the Tb L<sub>3,2</sub>-edges: Experiment versus Theory  
*J. Appl. Phys.* **91**, 7361 (2002).

- [95] E. Werner, W. Wende, A. Pingoud, and U. Heinemann  
High resolution crystal structure of domain I of the *Saccharomyces cerevisiae* homing endonuclease PI-SceI  
Nucleic Acids Res. **30**, 3962 (2002).
- [96] E. Werner, M. Ziegler, F. Lerner, M. Schweiger, Y. A. Muller, and U. Heinemann  
Crystallization and preliminary X-ray analysis of human nicotinamide adenyltransferase (NMNAT)  
Acta Crystallogr. D **58**, 140 (2002).
- [97] E. Werner, M. Ziegler, F. Lerner, M. Schweiger, and U. Heinemann  
Crystal structure of human nicotinamide mononucleotide adenyltransferase in complex with NMN  
FEBS Letters **516**, 239 (2002), Corrigendum: FEBS Letters **523**, 254 (2002).

**2003:**

- [98] K. Baberschke  
Ferromagnetic Monolayers: A Fresh Look at Fundamentals  
phys. stat. sol. (b) **236**, 233 (2003).
- [99] M. Bargheer and N. Schwentner  
Particle transport phenomena in low temperature solids  
Low Temp. Phys. **29**, 165 (2003).
- [100] H. Dau and M. Haumann  
X-ray absorption spectroscopy to watch catalysis by metalloenzymes: status and perspectives discussed for the water-splitting manganese complex of photosynthesis  
J. Synch. Rad. **10**, 76 (2003).
- [101] H. Dau, P. Liebisch, and M. Haumann  
X-ray absorption spectroscopy to analyze nuclear geometry and electronic structure of biological metal centers – Potential and questions examined with special focus on the tetra-nuclear manganese complex of oxygenic photosynthesis  
Anal. Bioanal. Chem. **376**, 562 (2003).
- [102] V. Dietz and N. Schwentner  
Online measurement of photochemical reaction rates in the VUV with a quartz microbalance: Cl<sub>2</sub> and Cu  
Surf. Sci. **528**, 215 (2003).
- [103] S. I. Fedoseenko, D. V. Vyalikh, I. E. Iossifov, R. Follath, S. A. Gorovikov, R. Püttner, J.-S. Schmidt, S. L. Molodtsov, V. K. Adamchuk, W. Gudat, and G. Kaindl  
Commissioning results and performance of the high-resolution Russian–German beamline at BESSY II  
Nucl. Instr. Meth. in Phys. Res. A **505**, 718 (2003).
- [104] J. M. Gottfried, N. Elghobashi, S. L. M. Schröder, and K. Christmann  
Oxidation of Gold by Oxygen-ion Sputtering  
Surf. Sci. **523**, 89 (2003).
- [105] J. M. Gottfried, K. J. Schmidt, S. L. M. Schröder, and K. Christmann  
Oxygen Chemisorption on Au(110)-(1x2). II. Spectroscopic Measurements  
Surf. Sci. **525**, 197 (2003).
- [106] M. Haumann, A. Porthun, T. Buhrke, P. Liebisch, W. Meyer-Klaucke, B. Friedrich, and H. Dau  
Hydrogen-induced structural changes at the nickel site of the regulatory [NiFe] hydrogenase from *Ralstonia eutropha* detected by X-ray absorption spectroscopy  
Biochemistry **42**, 11004 (2003).
- [107] U. Heinemann, K. Büssow, U. Mueller, and P. Umbach  
Facilities and methods for the high-throughput crystal structure analysis of human proteins  
Acc. Chem. Res. **36**, 157 (2003).
- [108] F. Hübing, A. S. Shulakov, K. Starke, A. Y. Grigoriev, and G. Kaindl  
Surface X-ray Emission from Lanthanide Metals  
Surf. Sci. Lett. **526**, L137 (2003).
- [109] O. Krupin, J. E. Prieto, S. Gorovikov, K. Starke, and G. Kaindl  
Ferrimagnetic 4f spin order in O/Gd surface monoxide  
Thin Solid Films **428**, 98 (2003); *ibid.* **437**, 309 (2003).

- [110] J. Lindner, A. Scherz, P. Pouloupoulos, C. Rüdert, A. N. Anisimov, H. Wende, K. Baberschke, P. Blomquist, R. Wäppling, F. Wilhelm, and N. B. Brookes  
 Ultrathin Fe-limit in Fe/V (001) superlattices  
*J. Magn. Magn. Mater.* **256**, 404 (2003).
- [111] B. Loll, G. Raszewski, W. Saenger, and J. Biesiadka  
 Functional Role of C<sup>α</sup>-H...O Hydrogen Bonds Between Transmembrane  $\alpha$ -Helices in Photosystem I  
*J. Mol. Biol.* **328**, 737 (2003).
- [112] T. Maier, N. Sträter, Ch. G. Schütte, R. Klingenstein, K. Sandhoff, and W. Saenger  
 The X-ray crystal structure of human  $\beta$ -hexosaminidase B provides new insight into Sandhoff disease  
*J. Mol. Biol.* **328**, 669 (2003).
- [113] A. Meinhart, J. C. Alonso, N. Sträter, W. Saenger  
 Crystal Structure of the Plasmid Maintenance System  $\epsilon/\zeta$ : Functional Mechanism of Toxin  $\zeta$  and Inactivation by  $\epsilon_2\zeta_2$  Complex Formation  
*Proc. Natl. Acad. Sci. (US)* **100**, 1661 (2003).
- [114] A. Melnikov, I. Radu, U. Bovensiepen, O. Krupin, K. Starke, E. Matthias, and M. Wolf  
 Coherent Optical Phonons and Parametrically Coupled Magnons Induced by Femtosecond Laser Excitation of the Gd(0001) Surface  
*Phys. Rev. Lett.* **91**, 227403 (2003).
- [115] J. J. Müller, A. Lapko, K. Ruckpaul, and U. Heinemann  
 Modeling of electrostatic recognition processes in the mammalian mitochondrial steroid hydroxylase system  
*Biophys. Chem.* **100**, 281 (2003).
- [116] O. Nimz, K. Geßler, I. Uson, S. Lättig, H. Welfle, G.M. Sheldrick, and W. Saenger  
 X-ray structure of the cyclomaltohexaicosaoose triiodide inclusion complex provides a model for amylose-iodine at atomic resolution  
*Carbohydr. Res.* **328**, 977 (2003).
- [117] R. Nünthel, T. Gleitsmann, P. Pouloupoulos, A. Scherz, J. Lindner, E. Kosubek, Ch. Litwinski, Z. Li, H. Wende and K. Baberschke, S. Stolbov, and T. S. Rahman  
 Epitaxial growth of Ni on Cu(001) with the assistance of O-surfactant and its magnetism compared to Ni/Cu(001)  
*Surf. Sci.* **531**, 53 (2003).
- [118] P. Pospíšil, M. Haumann, J. Dittmer, V. A. Solé, and H. Dau  
 Stepwise transition of the tetra-manganese complex of photosystem II to a binuclear Mn<sub>2</sub>( $\mu$ -O)<sub>2</sub> complex in response to a temperature jump: a time-resolved structural investigation employing X-ray absorption spectroscopy  
*Biophys. J.* **84**, 1370 (2003).
- [119] J. E. Prieto, F. Heigl, O. Krupin, G. Kaindl, and K. Starke  
 Quantitative magneto-optics of Gd and Tb in the soft x-ray region  
*Phys. Rev. B* **68**, 134453 (2003).
- [120] R. Püttner, Y. F. Hu, G. M. Bancroft, A. Kivimäki, M. Jurvansuu, H. Aksela, and S. Aksela  
 Relating the 4s<sup>-1</sup> inner-valence photoelectron spectrum of HBr with the Br 3d<sup>-1</sup>5l<sub>λ</sub> resonant Auger spectra: An approach to the assignments  
*Phys. Rev. A* **68**, 032705 (2003).
- [121] S. Rüttinger, H. Magnan, H. Wende, P. Le Fèvre, K. Baberschke, and D. Chandesris  
 EXAFS study of Co growth on Pt(997): from atomic chains to two monolayers  
*Surf. Sci.* **548**, 138 (2003).
- [122] A. Scherz, P. Pouloupoulos, R. Nünthel, J. Lindner, H. Wende, F. Wilhelm, and K. Baberschke  
 Direct probe of interdiffusion effects on the induced V spin-polarization at Fe/V interfaces  
*Phys. Rev. B* **68**, 140401(R) (2003).
- [123] K. J. Schmidt and K. Christmann  
 The Adsorption of Xenon on Ru(10-10): An Angle-resolved UV Photoemission Study  
*Surf. Sci.* **525**, 159 (2003).
- [124] K. Starke, F. Heigl, J. E. Prieto, O. Krupin, and G. Kaindl  
 Soft X-ray magneto-optics in lanthanids at the N<sub>4,5</sub> and M<sub>4,5</sub> thresholds  
*Nucl. Instr. Meth. Phys. Res. B* **199**, 313 (2003).
- [125] H. Wende, A. Scherz, F. Wilhelm, and K. Baberschke  
 Induced magnetism at thin-film interfaces probed by x-ray magnetic circular dichroism  
*J. Phys.: Cond. Matter* **15**, S547 (2003).

- [126] H. Wende, Ch. Litwinski, A. Scherz, T. Gleitsmann, Z. Li, C. Sorg, K. Baberschke, A. Ankudinov, J. J. Rehr, and Ch. Jung  
A systematic study of embedded atom EXAFS: The (2x1)O/Cu(110) reconstruction as an ideal prototype system  
*J. Phys.: Condens. Matter* **15**, 5197 (2003).
- [127] F. Wilhelm, P. Pouloupoulos, A. Scherz, H. Wende, K. Baberschke, M. Angelakeris, N. K. Flevaris, J. Goulon, and A. Rogalev  
Interface magnetism in 3d/5d multilayers probed by X-ray magnetic circular dichroism  
*phys. stat. sol. (a)* **196**, 33 (2003).
- [128] H. Xu, N. Sträter, W. Schröder, Ch. Böttcher, K. Ludwig, and W. Saenger  
Structure of DNA helicase RepA in complex with sulfate at 1.95 Å resolution implicates structural changes to an 'open' form  
*Acta Cryst.* **D59**, 815 (2003).

**2004:**

- [129] A. L. Ankudinov, J. J. Rehr, H. Wende, A. Scherz, and K. Baberschke  
Spin-dependent sum rules for x-ray absorption spectra  
*Europhys. Lett.* **66**, 441 (2004).
- [130] K. Baberschke  
The magnetism of ultrathin trilayers: A playground to study fundamentals  
*J. Magn. Magn. Mater.* **272–276**, 1130 (2004).
- [131] V. Berghof, M. Gudipati and N. Schwentner  
Photochemistry in the charge transfer and neutral excited States of HCl in Xe and Kr matrices  
*J. Chem. Phys.* **120**, 1414 (2004).
- [132] R. Bienert, M. Zeeb, L. Dostál, A. Feske, C. Magg, K. Max, H. Welfle, J. Balbach, and U. Heinemann  
Single-stranded DNA bound to bacterial cold-shock proteins: Preliminary crystallographic and Raman analysis  
*Acta Crystallogr. D* **60**, 755 (2004).
- [133] W. D. Brewer, A. Scherz, C. Sorg, H. Wende, K. Baberschke, P. Bencok, and S. Frota-Pessoa  
Direct observation of orbital magnetism in cubic solids  
*Phys. Rev. Lett.* **93**, 077205 (2004).
- [134] U. Christmann, H. Dau, M. Haumann, E. Kiss, P. Liebisch, D. Rehder, G. Santoni, and C. Schulzke  
Substrate binding to vanadate-dependent bromoperoxidase from *Ascophyllum nodosum*: a vanadium K-edge XAS approach  
*Dalton Transactions* **16**, 2534 (2004).
- [135] H. Dau, P. Liebisch, and M. Haumann  
The structure of the manganese complex of photosystem II in its dark-stable  $S_1$ -state – EXAFS results in relation to recent crystallographic data  
*Phys. Chem. Chem. Phys.* **6**, 4781 (2004).
- [136] R. C. Hillig, M. Hülsmeier, W. Saenger, K. Welfle, R. Misselwitz, H. Welfle, C. Kozerski, A. Volz, B. Uchanska-Ziegler, and A. Ziegler  
Thermodynamic and Structural Analysis of Peptide- and Allele-dependent Properties of Two HLA-B27 Subtypes Exhibiting Differential Disease Association  
*J. Biol. Chem.* **279**, 652 (2004).
- [137] M. Hülsmeier, M.T. Fiorillo, F. Bettosini, R. Sorrentino, W. Saenger, A. Ziegler, and B. Uchanska-Ziegler  
Dual, HLA-B27 Subtype-dependent Conformation of a Self-peptide  
*J. Exp. Med.* **199**, 271 (2004).
- [138] Y. H. Jiang, R. Püttner, R. Hentges, J. Viefhaus, M. Poiguine, U. Becker, J. M. Rost, and G. Kaindl  
Partial cross sections of doubly excited helium below the ionization threshold  $I_7$   
*Phys. Rev. A* **69**, 042706 (2004).
- [139] Y. H. Jiang, R. Püttner, M. Martins, R. Follath, J. M. Rost, and G. Kaindl  
Isotope shifts of double-excitation states in helium  
*Phys. Rev. A* **69**, 052703 (2004).
- [140] D. Khare, G. Ziegelin, E. Lanka, and U. Heinemann  
Sequence-specific DNA binding determined by contacts outside the helix-turn-helix motif of the ParB homolog KorB  
*Nature Struct. Mol. Biol.* **11**, 656 (2004).

- [141] B. A. Manjasetty, H. Delbrück, D.-T. Pham, U. Müller, M. Fieber-Erdmann, C. Scheich, V. Sievert, K. Büssow, F. H. Neisen, W. Weihofen, B. Loll, W. Saenger, and U. Heinemann  
Crystal Structure of *Homo sapiens* Protein hp 14.5  
PROTEINS: Structure, Function, and Bioinformatics **54**, 797 (2004).
- [142] B. A. Manjasetty, J. Hennecke, R. Glockshuber, and U. Heinemann  
Crystal structure of circularly permuted DsbA<sub>Q100T99</sub>: Preserved global fold and local structural adjustments  
Acta Crystallogr. D **60**, 304 (2004).
- [143] B. A. Manjasetty, F. H. Niesen, H. Delbrück, F. Götz, V. Sievert, K. Büssow, J. Behlke, and U. Heinemann  
X-ray structure of fumarylacetoacetate hydrolase family member: *Homo sapiens* FLJ36880  
Biol. Chem. **385**, 935 (2004).
- [144] B. A. Manjasetty, C. Quedenau, V. Sievert, K. Büssow, F. Niesen, H. Delbrück, and U. Heinemann  
X-ray structure of human gankyrin, the product of a gene linked to hepatocellular carcinoma  
Proteins: Struct. Funct. Bioinf. **55**, 214 (2004).
- [145] A. Melnikov, U. Bovensiepen, I. Radu, O. Krupin, K. Starke, E. Matthias, and M. Wolf  
Picosecond magnetization dynamics of the Gd(0001) surface  
J. Magn. Magn. Mater. **272–276**, 1001 (2004).
- [146] P. Pouloupoulos, F. Wilhelm, Z. Li, A. Scherz, H. Wende, K. Baberschke, M. Angelakeris, N. K. Flevaris, A. Rogalev, and N. B. Brookes  
Element-specific hysteresis loops and the anisotropy of the orbital moment of Pt in Ni/Pt multilayers  
J. Magn. Magn. Mater. **272–276**, 317 (2004).
- [147] R. Püttner, C. Kolczewski, M. Martins, A. S. Schlachter, G. Snell, M. Sant'Anna, J. Viehhaus, K. Hermann, and G. Kaindl  
The C 1s NEXAFS spectrum of benzene below threshold: Rydberg or valence character of the unoccupied  $\sigma$ -type orbitals  
Chem. Phys. Lett. **393**, 361 (2004).
- [148] Y. Roske, A. Sunna, W. Pfeil, and U. Heinemann  
High-resolution crystal structures of *Caldicellulosiruptur* strain Rt8B.4 carbohydrate-binding module CBM27-1 and its complex with mannohexaose  
J. Mol. Biol. **340**, 543 (2004).
- [149] A. Scherz, H. Wende, and K. Baberschke  
Fine structure of X-ray Magnetic Circular Dichroism for early 3d transition metals  
Appl. Phys. A **78**, 843 (2004).
- [150] C. Sorg, N. Ponpandian, A. Scherz, H. Wende, R. Nünthel, T. Gleitsmann, and K. Baberschke  
The magnetism of ultrathin Ni films grown with O surfactant  
Surf. Sci. **565**, 197 (2004).
- [151] T. Tolinski, K. Lenz, J. Lindner, E. Kosubek, C. Sorg, M. Bernien, A. Scherz, H. Wende, and K. Baberschke  
Interlayer exchange coupling and damping processes in coupled trilayer systems  
Molec. Phys. Rep. **40**, 164 (2004).
- [152] D. V. Vyalikh, S. I. Fedoseenko, I. E. Iossifov, R. Follath, S. A. Gorovikov, S. L. Molodtsov, J.-S. Schmidt, R. Püttner, V. K. Adamchuk, W. Gudat, and G. Kaindl  
The Russian-German Soft X-Ray Beamline at BESSY II  
AIP Conference Proceedings **705**, 309 (2004).
- [153] J. Wang, W. Kuch, L. I. Chelaru, F. Offi, M. Kotsugi, and J. Kirschner  
Exchange coupling between ferro- and antiferromagnetic layers across a non-magnetic interlayer: Co/Cu/FeMn on Cu(100)  
J. Phys.: Cond. Matter **16**, 9181 (2004).
- [154] W. Weihofen, J. Liu, W. Reutter, W. Saenger, and H. Fan  
Crystal Structure of CD26/Dipeptidylpeptidase IV in Complex with Adenosine Deaminase Reveals a Highly Amphiphilic Interface  
J. Biol. Chem. **279**, 43330 (2004).
- [155] H. Wende  
Recent advances in X-ray absorption spectroscopy  
Rep. Prog. Phys. **67**, 2105 (2004).
- [156] E. Weschke, H. Ott, E. Schierle, C. Schüßler-Langeheine, D. V. Vyalikh, G. Kaindl, V. Leiner, M. Ay, T. Schmitte, H. Zabel, and P. J. Jensen  
Finite-Size Effect on Magnetic Ordering Temperatures in Long-Period Antiferromagnets: Holmium Thin Films  
Phys. Rev. Lett. **93**, 157204 (2004).

**2005:**

- [157] A. L. Ankudinov, J. J. Rehr, H. Wende, and K. Baberschke  
Information in Magnetic EXAFS  
*Physica Scripta* **T115**, 651 (2005).
- [158] Yu. Babanov, S. Kiryanov, A. Sidorenko, L. Romashev, D. Vyalikh, S. Molodtsov, G. Güntherodt, U. Ruediger, Yu. Dedkov, M. Fonine, K. Baberschke, H. Wende, and Y. U. Idzerda  
Overlapping XAFS L Spectra of 3d Metals: A new Application of the Regularization Method  
*Physica Scripta* **T115**, 194 (2005).
- [159] K. Baberschke  
X-ray Magnetic Dichroism: The technique of choice to study magnetism element specifically  
*Physica Scripta* **T115**, 49 (2005).
- [160] T. Bührke, S. Löscher, E. Schlodder, I. Zebger, L. K. Andersen, P. Hildebrandt, W. Meyer-Klaucke, H. Dau, B. Friedrich, and M. Haumann  
Reduction of unusual iron-sulfur clusters in the H<sub>2</sub>-sensing regulatory Ni-Fe hydrogenase from *Ralstonia eutropha*  
*J. Biol. Chem.* **280**, 19488 (2005).
- [161] T. Burgdorf, S. Löscher, P. Liebisch, E. van der Linden, M. Galander, F. Lenzian, W. Meyer-Klaucke, S. P. J. Albracht, B. Friedrich, H. Dau, and M. Haumann  
Structural and oxidation-state changes at its nonstandard Ni-Fe site during activation of the NAD-reducing hydrogenase from *Ralstonia eutropha* detected by X-ray absorption, EPR, and FTIR spectroscopy  
*J. Am. Chem. Soc.* **127**, 576 (2005).
- [162] A. Chassé, W. Kuch, M. Kotsugi, Xingyu Gao, F. Offi, S. Imada, S. Suga, H. Daimon, and J. Kirschner  
Magnetism-induced symmetry breaking in photoelectron diffraction patterns  
*Phys. Rev. B* **71**, 014444 (2005).
- [163] V. Chevelkov, K. Faelber, A. Diehl, U. Heinemann, H. Oschkinat, and B. Reif  
Detection of water molecules in a microcrystalline sample of the SH3 domain of  $\alpha$ -spectrin by MAS solid-state NMR  
*J. Biomol. NMR* **31**, 295 (2005).
- [164] H. Dau and M. Haumann  
Considerations on the mechanism of photosynthetic water oxidation: dual role of oxo-bridges between Mn ions in (i) redox-potential maintenance and (ii) proton abstraction from substrate water  
*Photosynth. Res.* **84**, 325 (2005).
- [165] H. Dau, P. Liebisch, and M. Haumann  
The manganese complex of oxygenic photosynthesis conversion of five-coordinated Mn(III) to six-coordinated Mn(IV) in the S<sub>2</sub>-S<sub>3</sub> transition is implied by XANES simulations  
*Physica Scripta* **T115**, 844 (2005).
- [166] M. T. Fiorillo, C. Rückert, M. Hülsmeier, R. Sorrentino, W. Saenger, A. Ziegler, and B. Uchanska-Ziegler  
Allele-dependent Similarity Between Viral and Self-peptide Presentation by HLA-B27 Subtypes  
*J. Biol. Chem.* **280**, 2962 (2005).
- [167] K. Fukumoto, W. Kuch, J. Vogel, J. Camarero, S. Pizzini, F. Offi, Y. Pennec, M. Bonfim, A. Fontaine, and J. Kirschner  
Mobility of domain wall motion in the permalloy layer of a spin-valve-like Fe<sub>20</sub>Ni<sub>80</sub>/Cu/Co trilayer  
*J. Magn. Magn. Mater.* **293**, 863 (2005).
- [168] X. Gao, Hai Xu, A. T. S. Wee, W. Kuch, C. Tieg, and Shouguo Wang  
Magnetic circular dichroism study of Fe/Co/Cu(001) using electron yield x-ray absorption spectroscopy with different probe depths  
*J. Appl. Phys.* **97**, 103527 (2005).
- [169] M. Haumann, C. Müller, P. Liebisch, M. Barra, M. Grabolle, and H. Dau  
Photosynthetic O<sub>2</sub> formation tracked by time-resolved X-ray experiments  
*Science* **310**, 1019 (2005).
- [170] M. Haumann, C. Müller, P. Liebisch, L. Iuzzolino, J. Dittmer, M. Grabolle, T. Neisius, W. Meyer-Klaucke, and H. Dau  
Structural and oxidation state changes of the photosystem II manganese complex in four transitions of the water oxidation cycle (S<sub>0</sub>→S<sub>1</sub>, S<sub>1</sub>→S<sub>2</sub>, S<sub>2</sub>→S<sub>3</sub>, and S<sub>3,4</sub>→S<sub>0</sub>) characterized by X-ray absorption spectroscopy at 20 K and room temperature  
*Biochemistry* **44**, 1894 (2005).
- [171] M. Haumann, C. Müller, P. Liebisch, T. Neisius, and H. Dau  
A novel BioXAS technique with sub-millisecond time resolution to track oxidation state and structural changes at biological metal centers  
*J. Synch. Rad.* **12**, 35 (2005).

- [172] F. Heigl, J. E. Prieto, O. Krupin, G. Kaindl, K. Starke, and M. Bode  
Annealing-induced extension of the helical phase in terbium films  
*Phys. Rev. B*, **72**, 035417 (2005).
- [173] A. Heinz, F. Hannemann, J. J. Müller, U. Heinemann, and R. Bernhardt  
The interaction domain of the redox protein adrenodoxin is mandatory for binding of the electron acceptor CYP11A1, but is not required for binding of the electron donor adrenodoxin reductase  
*Biochem. Biophys. Res. Commun.* **338**, 491 (2005).
- [174] M. Hülsmeier, P. Chames, R.C. Hillig, R. L. Stanfield, G. Held, P.G. Coulie, C. Alings, G. Wille, W. Saenger, B. Uchanska-Ziegler, H. R. Hoogenboom, and A. Ziegler  
A Major Histocompatibility Complex • Peptide-restricted Antibody and T Cell Receptor Molecules Recognize Their Target by Distinct Binding Modes  
*J. Biol. Chem.* **280**, 2872 (2005).
- [175] M. Hülsmeier, K. Welfle, T. Pöhlmann, R. Misselwitz, U. Alexiev, H. Welfle, W. Saenger, B. Uchanska-Ziegler, and A. Ziegler  
Thermodynamic and Structural Equivalence of Two HLA-B27 Subtypes complexed with a Self-Peptide  
*J. Mol. Biol.* **346**, 1367–1369 (2005).
- [176] P. J. Jensen, C. Sorg, A. Scherz, M. Bernien, K. Baberschke, and H. Wende  
Comment on: „Magnetic phase transition in Co/Cu/Ni/Cu(100) and Co/Fe/Ni/Cu(100)“  
*Phys. Rev. Lett.* **94**, 039703 (2005).
- [177] J. Kern, B. Loll, A. Zouni, K.-D. Irrgang, W. Saenger, and J. Biesiadka,  
Cyanobacterial Photosystem II at 3.2 Å resolution – the plastoquinone binding pockets  
*Photosynth. Res.* **84**, 153 (2005).
- [178] O. Krupin, G. Bihlmayer, K. Starke, S. Gorovikov, J. E. Prieto, K. Döbrich, S. Blügel, and G. Kaindl  
Rashba Effect at Magnetic Metal Surfaces  
*Phys. Rev. B* **71**, 201403(R) (2005).
- [179] D. Kümmel, J. J. Müller, Y. Roske, R. Misselwitz, K. Büssow, and U. Heinemann  
The structure of the TRAPP subunit TPC6 suggests a model for a TRAPP subcomplex  
*EMBO Rep.* **6**, 787 (2005).
- [180] P. Liebisch, M. Haumann, and H. Dau  
Simulations of XANES spectra for protein-bound metal centers: Analysis of linear dichroism data  
*Physica Scripta* **T115**, 859 (2005).
- [181] B. Loll, J. Kern, A. Zouni, W. Saenger, J. Biesiadka, and K.-D. Irrgang  
Antenna system of Photosystem II from *Thermosynechococcus elongatus* at 3.2 Å resolution  
*Photosynth. Res.* **86**, 175 (2005).
- [182] B. Loll, J. Kern, W. Saenger, A. Zouni, and J. Biesiadka  
Towards complete cofactor arrangement in the 3.0 Å resolution structure of photosystem II  
*Nature* **483**, 1040 (2005).
- [183] S. Löscher, I. Zebger, P. Hildebrandt, W. Meyer-Klaucke, and M. Haumann  
The structure of the Ni-Fe site in the isolated HoxC subunit of the hydrogen-sensing hydrogenase from *Ralstonia eutropha*  
*FEBS Letters* **579**, 4287 (2005).
- [184] B. A. Manjasetty, F. H. Niesen, C. Scheich, Y. Roske, F. Götz, J. Behlke, V. Sievert, U. Heinemann, and K. Büssow  
X-ray structure of engineered human aortic preferentially expressed protein-1 (APEG-1)  
*BMC Struct. Biol.* **5:21**, 1 (2005).
- [185] T. Maier, I. Przytylska, N. Sträter, P. Herdewijn, and W. Saenger  
Reinforced HNA backbone hydration in the crystal structure of a decameric HNA/RNA hybrid  
*J. Amer. Chem. Soc.* **127**, 2937 (2005).
- [186] C. Müller, P. Liebisch, M. Barra, H. Dau, and M. Haumann  
The location of calcium in the manganese complex of oxygenic photosynthesis studied by X-ray absorption spectroscopy at the Ca K-edge  
*Physica Scripta* **T115**, 847 (2005).
- [187] J. E. Prieto, O. Krupin, K. Döbrich, F. Heigl, G. Kaindl, and K. Starke  
X-ray magneto-optics in lanthanides principles and applications  
*Appl. Phys. A* **80**, 1021 (2005).

- [188] J. E. Prieto, O. Krupin, S. Gorovikov, K. Döbrich, G. Kaindl, and K. Starke  
The Sm/Co(0001) interface  
*Phys. Rev. B* **72**, 092409 (2005).
- [189] M. Rossocha, R. Schultz-Heienbrok, H. von Moeller, J. P. Coleman, and W. Saenger  
Conjugated bile acid hydrolase is a tetrameric N-terminal thiol hydrolase with specific recognition of its cholyly but not of its tauryly product  
*Biochemistry* **44**, 5739 (2005).
- [190] A. Scherz, E. K. U. Gross, H. Appel, C. Sorg, K. Baberschke, H. Wende, and K. Burke  
Measuring the Kernel of Time-Dependent Density Functional Theory with X-Ray Absorption Spectroscopy of 3d Transition Metals  
*Phys. Rev. Lett.* **95**, 253006 (2005).
- [191] A. Scherz, H. Wende, C. Sorg, K. Baberschke, J. Minár, D. Benea, and H. Ebert  
Limitations of integral XMCD sum-rules for the early 3d elements  
*Physica Scripta* **T115**, 586 (2005).
- [192] A. Scherz, C. Sorg, M. Bernien, N. Ponpandian, K. Baberschke, and H. Wende  
Importance of giant spin fluctuations in two-dimensional magnetic trilayers  
*Phys. Rev. B* **72**, 054447 (2005).
- [193] A. S. Schlachter, S. W. J. Scully, R. A. Phaneuf, E. D. Emmons, A. Aguilar, D. Leitner, M. S. Lubell, A. M. Covington, R. Püttner, A. Müller, and B. M. McLaughlin  
K-shell photoionization of  $C^{2+}$  ions: experiment and theory  
*J. Electron Spectrosc. Rel. Phenom.* **144–147**, 53 (2005).
- [194] J. Schmalhorst, M. Sacher, A. Thomas, H. Brückl, G. Reiss, and K. Starke  
X-ray absorption and magnetic-circular-dichroism studies of annealed magnetic tunnel junctions  
*J. Appl. Phys.* **97**, 123711 (2005).
- [195] C. Schüßler-Langeheine, J. Schlappa, A. Tanaka, Z. Hu, C.-F. Chang, E. Schierle, M. Benomar, H. Ott, E. Weschke, G. Kaindl, O. Friedt, G. A. Sawatzky, H.-J. Lin, C. T. Chen, M. Braden, and L. H. Tjeng  
Spectroscopy of stripe order in  $La_{1.8}Sr_{0.2}NiO_4$  using resonant soft x-ray diffraction  
*Phys. Rev. Lett.* **95**, 156402 (2005).
- [196] S. W. J. Scully, A. Aguilar, E. D. Emmons, R. A. Phaneuf, M. Halka, D. Leitner, J. C. Levin, M. S. Lubell, R. Püttner, A. S. Schlachter, A. M. Covington, S. Schippers, A. Müller, and B. M. McLaughlin  
K-shell photoionization of Be-like carbon ions: experiment and theory for  $C^{2+}$   
*J. Phys. B* **38**, 1967 (2005).
- [197] C. Sorg, A. Scherz, H. Wende, T. Gleitsmann, Z. Li, S. Rüttinger, Ch. Litwinski, and K. Baberschke  
Co/Cu/Ni trilayers near their Curie temperature studied by XMCD  
*Physica Scripta* **T115**, 638 (2005).
- [198] A. P. Turnbull, D. Kümmel, B. Prinz, C. Holz, J. Schultchen, C. Lang, F. H. Niesen, K.-P. Hofmann, H. Delbrück, J. Behlke, E.-C. Müller, E. Jarosch, T. Sommer, and U. Heinemann  
Structure of palmitoylated human BET3: Insights into TRAPP complex assembly and membrane localization  
*EMBO J.* **24**, 875 (2005).
- [199] J. Vogel, W. Kuch, J. Camarero, K. Fukumoto, Y. Pennec, S. Pizzini, M. Bonfim, F. Petroff, A. Fontaine, and J. Kirschner  
Interplay between magnetic anisotropy and interlayer coupling in nanosecond magnetization reversal of spin-valve trilayers  
*Phys. Rev. B* **71**, 060404(R) (2005).
- [200] J. Vogel, W. Kuch, R. Hertel, J. Camarero, K. Fukumoto, F. Romanens, S. Pizzini, M. Bonfim, F. Petroff, A. Fontaine, and J. Kirschner  
Influence of domain wall interactions on nanosecond switching in magnetic tunnel junctions  
*Phys. Rev. B* **72**, 220402(R) (2005).
- [201] J. Wang, W. Kuch, L. I. Chelaru, F. Offi, and M. Kotsugi  
Influence of exchange bias coupling on the single-crystalline FeMn ultrathin film  
*Appl. Phys. Lett.* **86**, 122504 (2005).
- [202] W. H. Wang, M. Przybylski, W. Kuch, L. I. Chelaru, J. Wang, Y. F. Lu, J. Barthel, and J. Kirschner  
Spin polarization of single-crystalline  $Co_2MnSi$  films grown by PLD on GaAs(001)  
*J. Magn. Magn. Mater.* **286**, 336 (2005).
- [203] W. H. Wang, M. Przybylski, W. Kuch, L. I. Chelaru, J. Wang, Y. F. Lu, J. Barthel, H. Meyerheim, and J. Kirschner  
Magnetic properties and spin polarization of  $Co_2MnSi$  Heusler alloy thin films epitaxially grown on GaAs(001)  
*Phys. Rev. B* **71**, 144416 (2005).

- [204] H. Wende, A. Scherz, C. Sorg, Z. Li, P. Pouloupoulos, K. Baberschke, A. Ankudinov, J. J. Rehr, F. Wilhelm, N. Jaouen, A. Rogalev, D. L. Schlagel, and T. A. Lograsso  
Temperature dependence of magnetic EXAFS for rare earth elements  
*Physica Scripta* **T115**, 600 (2005).
- [205] E. Weschke, H. Ott, E. Schierle, C. Schüßler-Langeheine, G. Kaindl, V. Leiner, and H. Zabel  
Resonant magnetic x-ray scattering at the lanthanide  $M_5$  edges  
*Physica B: Condensed Matter* **357**, 16 (2005).

## Theses

### Diploma theses:

- [1] Catharina Clanner  
Decomposition and Reactivity of Gold(III)Oxide  
Diplomarbeit, Fachbereich Biologie/Chemie/Pharmazie, Freie Universität Berlin, 2000.
- [2] Andreas Möller  
Elektronische und magnetische Eigenschaften sauerstoff- und stickstoffbedeckter Lanthanidmetalloberflächen  
Diplomarbeit, Fachbereich Physik, Freie Universität Berlin, 2000.
- [3] Andreas Scherz  
Magnetischer Röntgenzirkulardichroismus (XMCD) an ultradünnen magnetischen Filmen der 3d-Übergangsmetalle Kobalt und Nickel: Temperaturabhängige Messungen an Ein- und Dreischichtsystemen  
Diplomarbeit, Fachbereich Physik, Freie Universität Berlin, 2000.
- [4] Enrico Schierle  
Der Einfluss des magnetischen finite-size-Effektes auf elektronische Struktur und Gitterparameter schwerer Lanthanidmetalle: Gadolinium und Holmium  
Diplomarbeit, Fachbereich Physik, Freie Universität Berlin, 2001.
- [5] Tobias Gleitsmann  
Einfluss des Surfactants Sauerstoff auf die elektronischen und magnetischen Eigenschaften ultradünner Nickelfilme  
Diplomarbeit, Fachbereich Physik, Freie Universität Berlin, 2002.
- [6] Christian Litwinski  
SEXAFS-Untersuchungen an  $(2 \times 1)O/Cu(110)$   
Diplomarbeit, Fachbereich Physik, Freie Universität Berlin, 2002.
- [7] Steffen Rüttinger  
EXAFS-Messungen an dünnen Kobaltfilmen auf gestuftem Platin  
Diplomarbeit, Fachbereich Physik, Freie Universität Berlin, 2002.
- [8] Andreas Schöler  
Strukturanalyse manganhaltiger Ablagerungen auf der Süßwasseralge *Chara corallina*  
Diplomarbeit, Fachbereich Physik, Freie Universität Berlin, 2004.
- [9] Matthias Bernien  
Spinfluktuationen in gekoppelten, magnetischen Schichten: eine temperaturabhängige Röntgenzirkulardichroismus-Studie  
Diplomarbeit, Fachbereich Physik, Freie Universität Berlin, 2005.
- [10] Florian Lovis  
Wechselwirkungen von Stickstoff mit einer Au(110)-Oberfläche bei Physisorption und Ionenimplantation  
Diplomarbeit, Fachbereich Biologie/Chemie/Pharmazie, Freie Universität Berlin, 2005.
- [11] Volker von Moeller  
Präparation, Kristallisation und Röntgenstrukturanalyse verschiedener Varianten des Proteins Conjugated Bile Acid Hydrolase aus *C. perfringens*  
Diplomarbeit, Fachbereich Biologie/Chemie/Pharmazie, Freie Universität Berlin, 2005.

**PhD theses:**

- [1] Fabrice Wilhelm  
Magnetic Properties of Ultrathin Films, Coupled Trilayers and 3d/5d Multilayers studied by X-ray Magnetic Circular Dichroism  
Dissertation, Fachbereich Physik, Freie Universität Berlin, 2000.
- [2] Alexei Yu. Grigoriev:  
Interaction of Si with 4f metals  
Dissertation, Univ. St. Petersburg, 2001.
- [3] Anton Meinhart  
Kristallstrukturanalyse des  $\epsilon$ , $\zeta$ -Proteinkomplexes, kodiert vom Plasmid pSM19035 aus *Streptococcus pyogenes*  
Dissertation, Fachbereich Biologie/Chemie/Pharmazie, Freie Universität Berlin, 2001.
- [4] Denis V. Vyalikh  
Quantum-well states in thin films of d transition metals  
Dissertation, Univ. St. Petersburg, 2001.
- [5] Heinrich Delbrück  
Thermostabilität und funktionelle Vielfalt ubiquitärer Proteinfaltungsdomänen  
Dissertation, Fachbereich Biologie/Chemie/Pharmazie, Freie Universität Berlin, 2002.
- [6] Michael Gottfried  
CO Oxidation over Gold  
Dissertation, Fachbereich Biologie/Chemie/Pharmazie, Freie Universität Berlin, 2002.
- [7] Franziskus Heigl  
X-ray magneto-optics in lanthanides  
Dissertation, Fachbereich Physik, Freie Universität Berlin, 2002.
- [8] Klaus J. Schmidt  
Elektronenspektroskopische Untersuchungen zur Wechselwirkung von Atomen und einfachen Molekülen mit einer Ruthenium(10-10)-Oberfläche  
Dissertation, Fachbereich Biologie/Chemie/Pharmazie, Freie Universität Berlin, 2002.
- [9] Norbert Weiher  
Combined in situ and ex situ Studies of an Electrochemical Interface: Investigation of Anodic Oxide Layers on Gold  
Dissertation, Fachbereich Biologie/Chemie/Pharmazie, Freie Universität Berlin, 2002.
- [10] Erik Werner  
Zwei Wege, Nukleotide zu binden: Kristallstrukturen der Nicotinamid-Mononukleotid-Adenylyltransferase von *Homo sapiens* und der Domäne I der Homing Endonuklease PI-SceI von *Saccharomyces cerevisiae*  
Dissertation, Fachbereich Biologie/Chemie/Pharmazie, Freie Universität Berlin, 2002.
- [11] Hai Xu  
Biochemical and Structural Studies on the Function of RepA DNA Helicase from Plasmid RSF1010  
Dissertation, Fachbereich Biologie/Chemie/Pharmazie, Freie Universität Berlin, 2002.
- [12] Astrid Heiland  
Die Wechselwirkung von 1,4-Dioxan und 1,3,5-Trioxan mit einer Silber(110)-Oberfläche  
Dissertation, Fachbereich Biologie/Chemie/Pharmazie, Freie Universität Berlin, 2003.
- [13] Jacinta Lodge  
The Crystal Structure of  $\alpha$ -glucosidase A, AglA, from *Thermotoga maritime*  
Dissertation, Fachbereich Biologie/Chemie/Pharmazie, Freie Universität Berlin, 2003.
- [14] Dheeraj Khare  
Crystallographic and Functional Study on DNA Binding Proteins: Repressor and Partitioning Protein KorB from RP4 Plasmid and the Transposase 'Sleeping Beauty' of Vertebrate Origin  
Dissertation, Fachbereich Biologie/Chemie/Pharmazie, Freie Universität Berlin, 2004.
- [15] Oleg Krupin  
Diffraction Effects in Magnetic Dichroism and Rashba Effect of Magnetized Lanthanide Systems  
Dissertation, Fachbereich Physik, Freie Universität Berlin, 2004.
- [16] Timm Maier  
Röntgenstrukturanalyse von Proteinen des humanen Sphingolipid-Stoffwechsels:  $\beta$ -Hexosaminidase B und Sphingolipid-Aktivatorproteine  
Dissertation, Fachbereich Biologie/Chemie/Pharmazie, Freie Universität Berlin, 2004.

- [17] Holger Ott  
Magnetic Structures and Phase Transitions in Ultrathin Films of Heavy Lanthanide Metals Investigated by Resonant Magnetic X-Ray Diffraction  
Dissertation, Fachbereich Physik, Freie Universität Berlin, 2004.
- [18] Yvette Roske  
Kristallstrukturanalyse des kohlenhydratbindenden Moduls 27-1 der  $\beta$ -Mannanase 26 aus *Caldicellulosiruptor saccharolyticus* im Komplex mit Mannoheptaose und Kristallisation der ATPase HP0525 aus *Helicobacter pylori*  
Dissertation, Charité-Universitätsmedizin Berlin, 2004.
- [19] Andreas Scherz  
Spin-dependent X-ray Absorption Spectroscopy of 3d Transition Metals: Systematics and Applications  
Dissertation, Fachbereich Physik, Freie Universität Berlin, 2004.
- [20] Keiki Fukumoto  
Magnetization reversal dynamics in magnetically coupled trilayer systems  
Dissertation, Fachbereich Physik, Freie Universität Berlin, 2005.
- [21] Markus Grabolle  
Die Donorseite des Photosystems II der Pflanzen: Rekombinationsfluoreszenz und Röntgenabsorptionsstudien  
Dissertation, Fachbereich Physik, Freie Universität Berlin, 2005.
- [22] Andrei Halavaty  
The "Shuttle" Mechanism of the Electron Transport by the Ruthenium(II) Bipyridyl Complex-Modified Bovine Adrenodoxin in the Steroid Hydroxylase: Crystal Structure and Intramolecular Electron Transfer  
Dissertation, Fachbereich Biologie/Chemie/Pharmazie, Freie Universität Berlin, 2005.
- [23] Peter Liebisch  
Der Mangankomplex der Photosynthese im katalytischen Zyklus: Neue röntgenspektroskopische Untersuchungen von Struktur und Mechanismus  
Dissertation, Fachbereich Physik, Freie Universität Berlin, 2005.
- [24] Bernhard Loll  
Röntgenographische Studien des Photosystems II  
Dissertation, Fachbereich Biologie/Chemie/Pharmazie, Freie Universität Berlin, 2005.
- [25] Robert Schultz-Heienbrok  
Die Domänenrotation der 5'-Mukleotidase aus *E. coli*.  
Dissertation, Fachbereich Biologie/Chemie/Pharmazie, Freie Universität Berlin, 2005.
- [26] Claudia Sorg  
Magnetic Properties of 3d and 4f Ferromagnets Studied by X-ray Absorption Spectroscopy  
Dissertation, Fachbereich Physik, Freie Universität Berlin, 2005.
- [27] Wilhelm Weihofen  
Kristallisation und Röntgenstrukturanalyse von Omega-Repressor: DNA Komplexen  
Dissertation, Fachbereich Biologie/Chemie/Pharmazie, Freie Universität Berlin, 2005.

### Habilitations:

- [1] Eugen Weschke  
Structural, Electronic and Magnetic Properties of Monocrystalline Lanthanide-Metal Films  
Habilitation, Fachbereich Physik, Freie Universität Berlin, 2000.
- [2] Norbert Sträter  
Katalyse-Mechanismen binuclearer Metalloproteasen  
Habilitation, Fachbereich Biologie/Chemie/Pharmazie, Freie Universität Berlin, 2002.
- [3] Michael Haumann  
Spectroscopic Investigations on Structure, Dynamics, and Function of Cofactors in the Catalytic Cycle of Metalloenzymes  
Habilitation, Fachbereich Physik, Freie Universität Berlin, 2004.
- [4] Heiko Wende  
Recent advances in X-ray absorption spectroscopy  
Habilitation, Fachbereich Physik, Freie Universität Berlin, 2004.



